QUANTUM PHASE TRANSITIONS IN DISORDERED MAGNETS

by

DAVID NOZADZE

A DISSERTATION

Presented to the Faculty of the Graduate School of the

MISSOURI UNIVERSITY OF SCIENCE AND TECHNOLOGY

In Partial Fulfillment of the Requirements for the Degree

DOCTOR OF PHILOSOPHY

in

PHYSICS

2013

Approved by

Dr. Thomas Vojta, Advisor
Dr. Paul Parris
Dr. Julia E. Medvedeva
Dr. Gerald Wilemski
Dr. Ribhu Kaul

DEDICATION

I dedicate this dissertation to my mother Eteri Lebanidze. Her support and encouragement have sustained me throughout my life.

Also, this dissertation is dedicated to the memory of my deceased father Vladimer Nozadze. Gone now but never forgotten. I will miss him always and love him forever.

PUBLICATION DISSERTATION OPTION

This dissertation has been prepared in the form of six papers. Paper I, pages 46–64 had been published as *Composition-tuned smeared phase transitions*, Physical Review B **83**, 224402 (2011) with Fawaz Hrahsheh, and Thomas Vojta. Paper II, pages 65–80 had been published as *Disorder correlations at smeared phase transitions*, Europhysics Letters **97**, 20007 (2012) with Christopher Svoboda, Fawaz Hrahsheh, and Thomas Vojta. Paper III, pages 81–90 had been published as *Disorder promotes ferromagnetism: Rounding of the quantum phase transition in* $Sr_{1-x}Ca_xRuO_3$, Physical Review Letters **108**, 185701 (2012) with L. Demkó, S. Bordács, T. Vojta, F. Hrahsheh, C. Svoboda, B. Dóra, H. Yamada, M. Kawasaki, Y. Tokura, and I. Kézsmárki. Paper IV, pages 91–110 had been published as *Quantum Griffiths singularities in ferromagnetic metals*, Physical Review B **85**, 174202 (2012) with Thomas Vojta, selected as an Editor's Suggestion. Paper V, pages 111–130 had been submitted as *Numerical method for disordered quantum phase transitions in the large−N limit* to Computer Physics Communications (2013) with Thomas Vojta. Paper VI, pages 131–142 had been published as *Transport properties in antiferromagnetic quantum Griffiths phases*, Europhysics Letters **95**, 57010 (2011) with Thomas Vojta.

ABSTRACT

We study the effects of quenched weak disorder on quantum phase transitions in disordered magnets. The presence of disorder in the system can lead to a variety of exotic phenomena, *e.g.*, the smearing of transitions or quantum Griffiths singularities.

Phase transitions are smeared if individual spatial regions can order independently of the bulk system. In paper I, we study smeared quantum phase transitions in binary alloys $A_{1-x}B_x$ that are tuned by changing the composition x. We show that in this case the ordered phase is extended over all compositions $x < 1$. We also study the composition dependence of observables. In paper II, we investigate the influence of spatial disorder correlations on smeared phase transitions. As an experimental example, we demonstrate in paper III, that the composition-driven ferromagnetic-to-paramagnetic quantum phase transition in $Sr_{1-x}Ca_xRuO_3$ is smeared.

When individual spatial regions cannot order but fluctuate slowly, the phase transition is characterized by strong singularities in the quantum Griffiths phase. In paper IV, we develop a theory of the quantum Griffiths phases in disordered ferromagnetic metals. We show that the quantum Griffiths singularities are stronger than the usual power-law quantum Griffiths singularities in insulating magnets. In paper V, we present an efficient numerical method for studying quantum phase transitions in disordered systems with $\mathcal{O}(N)$ order parameter symmetry in the large-N limit. Our algorithm solves iteratively the large-N self-consistent equations for the renormalized distances from criticality.

Paper VI is devoted to the study of transport properties in the quantum Griffiths phase associated with the antiferromagnetic quantum phase transition in a metal. We find unusual behavior of transport properties which is in contrast to the normal Fermi-liquid behavior.

ACKNOWLEDGMENTS

I would like especially to give my thanks to my advisor Dr. Thomas Vojta for his help, great interest and assistance in the pursuit of these studies and preparation of this thesis.

In addition, I would like to thank my fellow graduate student Fawaz Hrahsheh for his collaboration on projects. Also, I would like to thank Christopher Svoboda, an undergraduate student at Missouri S&T, who was involved in two of these projects. I wish to thank Dr. Vojta's other research group members. It was very interesting to interact with them.

I would like to thank our chairman, Dr. George D. Waddill, and staffs: Ellen Marie Kindle, Pamela J. Crabtree, Janice Gargus and Russell L. Summers for all their help. I wish to thank my dear friends especially students at Missouri S&T for enjoyable and great memories. It has been great to know all of you during my time here at Missouri S&T Also, I wish to thank all my friends in Gerogia for their support and encouragement.

I wish to thank my committee members, Dr. Gerald Wilemski, Dr. Paul Parris, Dr. Julia Medvedeva, and Dr. Ribhu Kaul for their input, valuable discussions and accessibility.

In the end, I would like to express my eternal appreciation towards my mother who has always been there for me no matter where I am, for all the unconditional support and patience. Thank you for being ever so understanding and supportive. Also, I would like to thank my brother George and all my relatives, especially my uncle Dr. Gogi Ishkhneli and aunts LaLi Ishkhneli and Ciala Lebanidze in Georgia for their support and encouragement.

TABLE OF CONTENTS

Page

LIST OF ILLUSTRATIONS

Paper II

Paper III

Paper IV

Paper V

Paper VI

LIST OF TABLES

1. INTRODUCTION

1.1. PHASE TRANSITIONS AND CRITICAL PHENOMENA

A phase transition is the abrupt transformation of a thermodynamic system from one phase to another. Examples are the phase transitions of water [2]. The water can exist as a gas, liquid, or solid depending on temperature and pressure as shown in Fig. 1.1. The solid and gas phases are connected along the line AC, where they coexist and are in equilibrium. The liquid and solid phases are connected along the line AD, they also coexist and are in equilibrium on the coexistence line AD. Similarly, liquid and gas can also coexist. These two phases are separated by the liquid-gas coexistence line AB. At point A, at which the three lines intersect, solid, liquid, and gas all exist in equilibrium. This point is known as the *triple point*.

The phase transitions occurring when crossing coexistence lines are characterized by discontinuities in the *first* derivatives of the Gibbs free energy across the coexistence lines. They are called *first-order* phase transitions. First order phase transitions involve *latent heat* which is absorbed or released during the crossing of the coexistence lines. The point B at which the liquid and gas phases of a water become identical is called the *critical point*. It is characterized by a *critical* temperature T_c and a *critical* pressure P_c. At temperatures above T_c and pressures higher than P_c, there is only one fluid phase. The transition occuring at the critical point is called a *second-order* or *continuous* phase transition. At continuous phase transitions, no latent heat is released or absorbed and the *first* derivatives of the Gibbs free energy are continuous.

Another example of phase transitions are magnetic phase transitions. Just as a fluid can exist as a liquid, or a gas, a magnetic system can exist as a ferromagnet

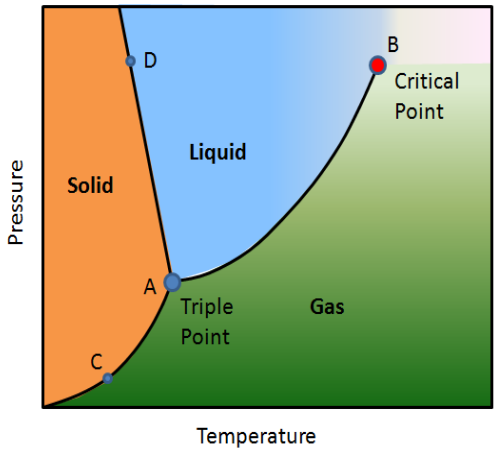

Figure 1.1: Schematic phase diagram of water.

or paramagnet. But, just as liquid and gas are not the only phases of a fluid system, the ferromagnetic and paramagnetic phases are also not the only two possible phases of magnetic systems.

The most basic model of magnetic systems is the Ising model. The Ising model consists of a lattice in $d \geqslant 1$ dimensional space. The classical spin variable $S_i = \pm 1$ is attached to the i-th lattice site. In the presence of an external magnetic field, the model is described by the following Hamiltonian

$$H = -J \sum_{i,j} S_i S_j - h \sum_i S_i \,, \tag{1.1}$$

where J is the interaction between spins and h is a uniform external magnetic field. In the absence of the magnetic field $h = 0$, for $J > 0$ and at temperatures $T < T_c$, where T_c is the critical temperature, spins prefer to align in parallel; the corresponding phase is called the ferromagnetic phase (Fig. 1.2a). For $J < 0$ and low temperatures, the spins are antiparallel, and the system is in the antiferromagnetic phase (Fig. 1.2b). At temperatures $T > T_c$, the system shows paramagnetic behavior (Fig. 1.2c), *i.e.*, the spins fluctuate between up and down. Different phases can be distinguished by an *order parameter*, a quantity that is zero in one phase (the disordered phase) and

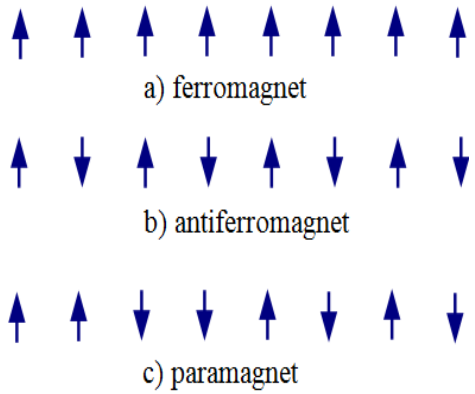

Figure 1.2: Magnetic systems. a) ferromagnet, b) antiferromagnet, c) paramagnet, spins fluctuate in time.

non-zero in the other, ordered phase. In a ferromagnetic system, the order parameter is the magnetisation per site $m = \langle S_i \rangle$. $m = 0$ in the paramagnetic phase and $m \neq 0$ in the ferromagnetic phase as shown in Fig. 1.3a.

At low temperatures $T < T_c$, the ferromagnet has two equivalent thermodynamic states with magnetizations $m > 0$ and $m < 0$. In the presence of an external magnetic field $h \neq 0$, the field energy will tend to align the spins with h. Therefore, as h changes from being negative to positive, the sign of the magnetizarion, m, will also change abruptly. So, for $T \leq T_c$ the field-driven transition between two up and down phases is first order. It turns into a continuous transition at $T = T_c$ (Fig. 1.3b).

1.1.1. Landau Mean-Field Theory. Landau theory postulates that for a given phase transition, the free energy F (known as the Landau free energy) is an analytic function of the order parameter m and can be expanded in a power series

$$F = F_0 + tm^2 + vm^3 + um^4 + \mathcal{O}(m^5) - hm\,, \tag{1.2}$$

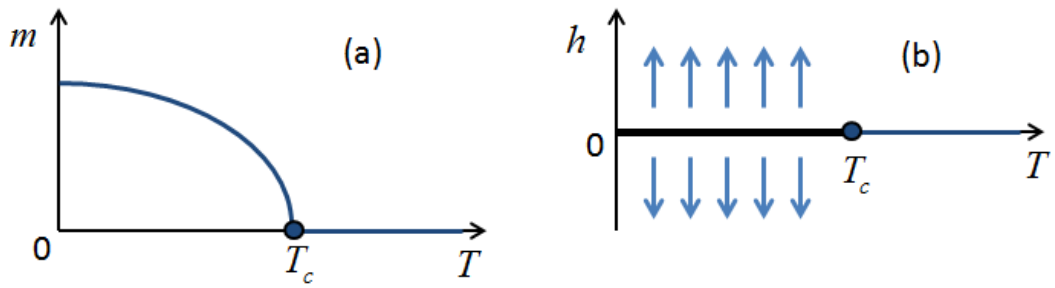

Figure 1.3: Phase transition in a ferromagnet. a) Magnetisation as a function of temperature in the ferromagnetic Ising model, b) Phase diagram of the ferromagnetic Ising model.

where t, v, u are system parameters that may depend on external parameters such as temperature, pressure and chemical composition *etc.*. h is an external field. The correct physical value of the order parameter can be determined by minimizing the free energy. Landau theory only uses the average value of m, thus it can be understood as a sophisticated mean-field theory.

If $v \neq 0$, Landau theory describes first-order phase transitions. In the absence of the external field, for $t > t^*$, where $t^* = 9v^2/32u$, there is a minimum only at $m = 0$ (Fig. 1.4a). For $t < t^*$, a secondary minimum and maximum appear in addition to the minimum at $m = 0$ (Fig. 1.4b). As t is lowered further to the value t' both minima have the same value (Fig. 1.4c). Below t', the secondary minimum is now the global minimum, and the value of the order parameter m which minimizes the Landau free energy F jumps discontinuously from $m = 0$ to a non-zero value (Fig. 1.4d).

For $v = 0$, Landau theory describes continuous phase transitions. In the absence of external field, and for $t > 0$, the Landau free energy has a single minimum at $m = 0$ (Fig. 1.5a). For $t \leq 0$, the minima of F are at (Fig. 1.5b,c)

$$m = \pm\sqrt{\frac{-t}{2u}} \sim (-t)^{\beta} . \tag{1.3}$$

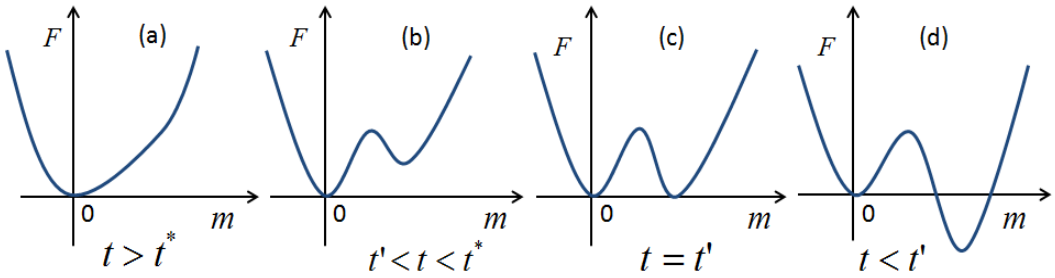

Figure 1.4: First-order phase transition. The Landau free energy as a function of order parameter for various temperatures.

Thus, according to Landau theory, criticality in the order parameter is characterized by a critical exponent $\beta = 1/2$. The singularity in Eq. (1.3) is an example of critical singularities. Singularities also occur in the vicinity of the critical point in the following observables

$$C \sim |t|^{-\alpha}\,, \tag{1.4}$$

$$\chi \sim |t|^{-\gamma}\,, \tag{1.5}$$

and

$$m_c(h) \sim h^{1/\delta}\,. \tag{1.6}$$

Here, C is the specific heat, χ is the order parameter susceptibility, and m_c is the order parameter at the critical point. α, γ and δ are called critical exponents. The values of critical exponents within Landau theory are given in the Table 1.1. They are identical to the usual mean-field values.

1.1.2. Breakdown of Landau Theory. Landau theory uses the average order-parameter while neglecting fluctuations about this average. The effects of these

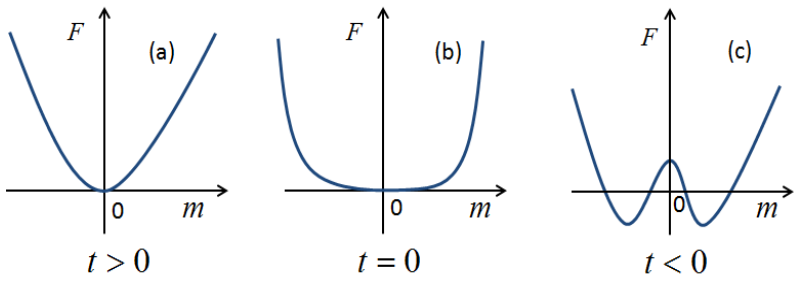

Figure 1.5: Second-order phase transition. The Landau free energy as a function of order parameter for various temperatures.

fluctuations can become important near the critical point and cause the Landau theory to fail . The fluctuations are described by the correlation function

$$G(\vec{r}_1, \vec{r}_2) = \langle m(\vec{r}_1) m(\vec{r}_2) \rangle \; - \langle m(\vec{r}_1) \rangle \, \langle m(\vec{r}_2) \rangle \, . \tag{1.7}$$

For translationally invariant system $G(\vec{r}_1, \vec{r}_2) = G(\vec{r}_1 - \vec{r}_2) = G(\vec{r})$. Near the the critical point, $G(\vec{r})$ has the form [2]

$$G(\vec{r}) \sim \frac{1}{r^{d-2+\eta}} \exp(-r/\xi) \, . \tag{1.8}$$

The critical exponent is $\eta = 0$ in the Landau theory. The correlation length ξ diverges at the critical point as

$$\xi \sim |t|^{-\nu} \, , \tag{1.9}$$

implying long-range correlations in space. Here, ν is the correlation length exponent.

In addition to the long-range correlations in space, there are analogous long-range correlations of the order parameter fluctuations in time. Close to the critical

Table 1.1: Critical exponents in the Landau mean field theory.

crit. exp.	β	γ	δ	α	η	ν
	1/2	1	3	0	0	1/2

point, the correlation time diverges as

$$\tau_c \sim |t|^{-\nu z}\,, \tag{1.10}$$

where z is the dynamical critical exponent.

The relative strength of the order-parameter fluctuations can be estimated by

$$P_{\rm LG} = \frac{|\int d^d\vec{r} G(\vec{r})|}{\int d^d\vec{r} m^2(\vec{r})}\,. \tag{1.11}$$

The criterion that $P_{\rm LG}$ be small ($P_{\rm LG} \ll 1$) for the validity of Landau theory is called the Ginzburg criterion [3]. Substituting Eqs. (1.3,1.8,1.9) into Eq. (1.11), the Ginzburg criterion takes the form

$$t^{\nu d - 2\beta - 2\nu} \ll 1\,. \tag{1.12}$$

Thus, the Landau theory is valid in the limit $t \to 0$, if

$$d > \frac{2\beta + 2\nu}{\nu} \equiv d^+\,, \tag{1.13}$$

where d^+ is the upper critical dimension. Inserting mean-field values $\beta = 1/2$ and $\nu = 1/2$ gives $d^+ = 4$. Thus, according the Ginzburg criterion the Landau theory breaks down for $d < 4$. Another critical dimension is the so-called lower critical dimension d^-. Below d^-, no phase transition is observed in the system. In such a

case, no long range order is possible due to strong fluctuations. $d^- = 1$, or 2 for Ising and O(3) Heisenberg symmetries, respectively.

1.1.3. Landau-Ginzburg-Wilson Theory. As we have seen in the last subsection, Landau theory breaks down below the upper critical dimension $d^+ = 4$ because of the strong order parameter fluctuations. In order to describe phase transitions more adequately one needs to generalize the Landau free energy function (1.2) to a functional that depends on a spatially varying order parameter field $\phi(\mathbf{r})$. Expanding in both $\phi(\mathbf{r})$ and its gradient yields the Landau-Ginzburg-Wilson (LGW) functional (for the case $v = 0$)

$$S[\phi(\mathbf{r})] = \frac{1}{T}\int d^d\mathbf{r}\left\{t\phi^2(\mathbf{r}) + c[\nabla\phi(\mathbf{r})]^2 + u\phi^4(\mathbf{r})\right\}, \tag{1.14}$$

The LGW theory is a nontrivial many-body problem which cannot be solved in closed form. Wilson solved this problem for which he was awarded a Nobel Prize in Physics in 1982 [4, 5]. He treated the Landau-Ginzburg-Wilson theory by means of a renormalization group (RG) [2] which is based on the Kadanoff scaling. We will discuss both scaling theory and RG in details below.

1.1.4. The Scaling Hypothesis. In this subsection, we will discuss the scaling theory [2, 6]. The scaling hypothesis is based on the idea [7] that close to the critical point, the only relevant length is the correlation length. Let us consider a system with a lattice constant a_0 close to ferromagnetic phase transition. The neighboring spins are mostly parallel. Therefore we can replace a block of neighboring spins of size ba_0 by a single "renormalized" spin. If we do this everywhere in the lattice, we get a system with a new lattice constant ba_0. If we now rescale all lengths by a factor b, the distance from criticality t and field h will be renormalized as $t_b = b^{y_t}t$ and $h_b = b^{y_h}h$. Rescaling length by b leads to the change of the free energy density

f by a factor of b^{-d}. f therefore fulfills the homogeneity relation

$$f(t,h) = b^{-d} f(b^{y_t} t, b^{y_h} h)\,. \tag{1.15}$$

Because the length scale is reduced by the factor of b, correlation length is changed by the same factor, $\xi' = \xi/b$. Therefore, the scaling form for the correlation length has the form

$$\xi(t,h) = b\xi(b^{y_t} t, b^{y_h} h)\,. \tag{1.16}$$

Using scaling forms Eq. (1.15,1.16), we can find the scaling behavior of thermodynamic functions and derive scaling relations.

As the rescaling factor b is arbitrary, we can choose it such that $b^{y_t} t = 1$. This leads to the scaling forms

$$f(t,h) \sim t^{d/y_t} g_f(h/t^{y_h/y_t})\,, \tag{1.17}$$

and

$$\xi(t,h) \sim t^{-1/y_t} g_\xi(h/t^{y_h/y_t})\,. \tag{1.18}$$

Thus, in zero magnetic field, the correlation length diverges as

$$\xi(t) = |t|^{-\nu}\,, \tag{1.19}$$

with $\nu = 1/y_t$.

The zero-field magnetization can be found as

$$m(t) = -\left(\frac{\partial f}{\partial h}\right)_T \sim t^{(d-y_h)/y_t}\,. \tag{1.20}$$

Comparing the above equation with Eq. (1.3) gives the scaling relation

$$\beta = (d - y_h)\nu\,, \tag{1.21}$$

The magnetization at the critical point $t = 0$, with the choice of $b = h^{-1/y_h}$ in Eq. (1.15), has the form

$$m \sim h^{(d-y_h)/y_h}\,, \tag{1.22}$$

which gives Widom's scaling relation [8]

$$\delta = \frac{y_h}{d - y_h}\,. \tag{1.23}$$

Similarly, the susceptibility $\chi(t) = \partial m/\partial h \sim |t|^{-(2y_h-d)\nu}$ and gives Fisher's scaling law [9],

$$\gamma = (2y_h - d)\nu\,, \tag{1.24}$$

and the specific heat $C(t) = -T\partial^2 f/\partial t^2 \sim |t|^{\nu d-2} \sim |t|^{-\alpha}$ leads to Joshephson's identity [10]

$$\alpha = 2 - \nu d\,. \tag{1.25}$$

Joshephson's scaling law is valid only below the upper critical dimension.

Finally, using scaling relations derived above, we can obtain Rushbrooke's identity [11]

$$\alpha + 2\beta + \gamma = 2\,, \tag{1.26}$$

and Widom's identity

$$\alpha + \beta(\delta + 1) = 2\,. \tag{1.27}$$

Scaling theory was originally developed on a purely heuristic basis. Today it can be derived by means of the renormalization group. It is an extremely powerful tool for analyzing experiments and numerical data.

1.1.5. Renormalization Group Theory. The renormalization group (RG) method [2, 6] is based on the idea that close to the critical point, the correlation length, ξ, is the only important length scale, and that microscopic length scales are irrelevant. The fact that at the critical point the correlation length diverges causes the critical behavior to be dominated by long-wavelength fluctuations. If we integrate over fluctuations having wavelength $a \lesssim \lambda \lesssim ba$, a a being lattice constant, the behavior of the correlation function for distances $r > ba$ will not be changed. The integration over short-wavelength fluctuations assigns to the original system another corresponding system having the same behavior at long distances. The transformation between these systems is called a renormalization-group transformation (RGT). It leads to a system with a new Hamiltonian with new coupling constants which can be obtained from the old one by the RG recursion relations. RGT can be iterated by integrating over fluctuations having wavelenghts $ba \lesssim \lambda \lesssim b^2a$ etc..

The crucial ingredient of the RG method is existence of *fixed points.* A fixed point is a point where the Hamiltonian is mapped onto itself under the RGT. Correspondingly, at fixed points the correlation length ξ does not change under the RGT

and thus it can be 0 or ∞. The fixed point with $\xi = \infty$ is referred to as a *critical fixed point*, and a fixed point with $\xi = 0$ as a *trivial fixed point*. The behavior of the RG flows, (*i.e.* the change of the Hamiltonian parameters under the RGT) determine the phase diagrams. A fixed point can be attractive, repulsive, or mixed. If the system starts close to an attractive fixed point, then the iterations bring it back to the fixed point. On the other hand, if the system starts close to a repulsive fixed point, it is driven away from that by the iterations. The fixed point is mixed if the system is repulsive in one direction and attractive in another direction. At the critical point, the RG fixed point is repulsive in one direction and attractive in all other directions.

Renormalization Group in the momentum space. As an example, let us construct explicitly the RG transformations in the simple case of the *Gaussian model*. The model is described by the Landau functional in the momentum space

$$\beta H = -hm(0)\beta + \frac{1}{2}\int_{|\mathbf{q}|<\Lambda} d^d\mathbf{q}\ [t + |\mathbf{q}|^2]|m(\mathbf{q})|^2\,, \tag{1.28}$$

in the presence of external magnetic field h. Here, $\beta = 1/T$ *. Λ is a high momentum cut off. This model is defined only for $t \geqslant 0$, since there is no m^4 term to insure stability for $t < 0$. However, the partition function is still singular at $t = 0$. So, the model represents approaching a phase transition from the disordered side. To do RG calculations, we need to implement three following steps:

(1) *Coarse grain:* We divide the fluctuations into two components as:

$$m(\mathbf{q}) = \begin{cases} m(\mathbf{q}) & \text{for} \quad 0 < q < \Lambda/b \\ \sigma(\mathbf{q}) & \text{for} \quad \Lambda/\mathrm{b} < \mathrm{q} < \Lambda \end{cases} \tag{1.29}$$

*We set Planck's constant and Boltzmann constant to unity ($\hbar = k_B = 1$) in what follows.

Then, we integrate out the short-wavelength fluctuations $\sigma(\mathbf{q})$ (Fig. 1.6). The functional integral in the partition function involves only integrations over independent modes. We obtain

$$Z = Z_0 \int \mathcal{D}m(\mathbf{q}) \exp\left\{ -hm(0) + \frac{1}{2}\int_{|\mathbf{q}|<\Lambda/b} d^d\mathbf{q}\ [t + |\mathbf{q}|^2]|m(\mathbf{q})|^2 \right\}, \tag{1.30}$$

where Z_0 is the non-singular part resulting from integration over σ.

(2) *Rescale:* Next, we need to rescale momentum $\mathbf{q} = b^{-1}\mathbf{q}'$. This leads to

$$H' = -hm(0) + \frac{1}{2}\int_{|\mathbf{q}|<\Lambda} d^d\mathbf{q}'\ b^{-d}\ [t + b^{-2}|\mathbf{q}'|^2]|m(\mathbf{q}'/b)|^2\,, \tag{1.31}$$

(3) *Renormalize:* Finally, we rescale $m = zm'$ such that coefficient in the above Hamiltonian in front of $|\mathbf{q}'|^2$ is recovered to $1/2$. This leads to the renormalized Hamiltonian

$$H' = -h'm(0) + \frac{1}{2}\int_{|\mathbf{q}|<\Lambda} d^d\mathbf{q}'\ \ [t' + |\mathbf{q}'|^2]|m(\mathbf{q}')|^2\,, \tag{1.32}$$

with the renormalized parameters

$$h' = hb^{1+d/2}, \quad t' = tb^2\,. \tag{1.33}$$

These are the recursion relations.

There is a unique fixed point at $t^* = h^* = 0$, called Gaussian fixed point. Comparing Eq. (1.33) to Eq. (1.15), we can identify the exponents $y_t = 2$ and $y_h = 1 + d/2$. Using these exponents in Sec. 1.1.4, one can find the critical exponents $\nu = 1/2$ and $\alpha = 2 - d/2$.

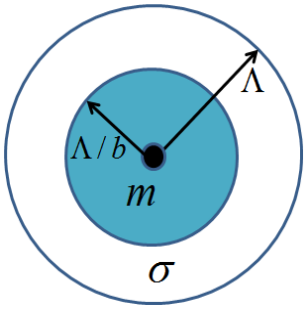

Figure 1.6: The reduction of momentum by a factor b in the RG scheme.

RG methods for more complex models follow the same basic steps. Just the technical implementation is different.

1.1.6. Quantum Phase Transitions. Quantum phase transitions [12] occur by varying a non-thermal parameter such as magnetic field, pressure or chemical composition at absolute zero temperature. The macroscopic order can be destroyed by quantum fluctuations which are in accordance with Heisenberg's uncertainty principle. The critical point associated with a continuous quantum phase transition is called quantum critical point. Quantum phase transitions may seem like an abstract theoretical idea of little practical consequence because absolute zero cannot be reached. However, they are the key to explain a wide variety of experiments. The quantum fluctuations dominate the material's properties in the vicinity of the quantum critical point not just at absolute zero but also at low but non-zero temperatures. In metallic systems, they can cause strong deviations from the conventional Fermi-Liquid behavior of normal metals [13].

An experimental example of a quantum phase transition was found in the compound $LiHoF_4$ by Bitko *et al.* in 1996 [1]. The phase diagram of this compound is shown in Fig. 1.7. The phase transition between the ferromagnetic and paramagnetic phases can be achieved in two different ways: (*i*) *thermal* (classical) phase transition, by varying the temperature at fixed small external magnetic field and (*ii*) *quantum*

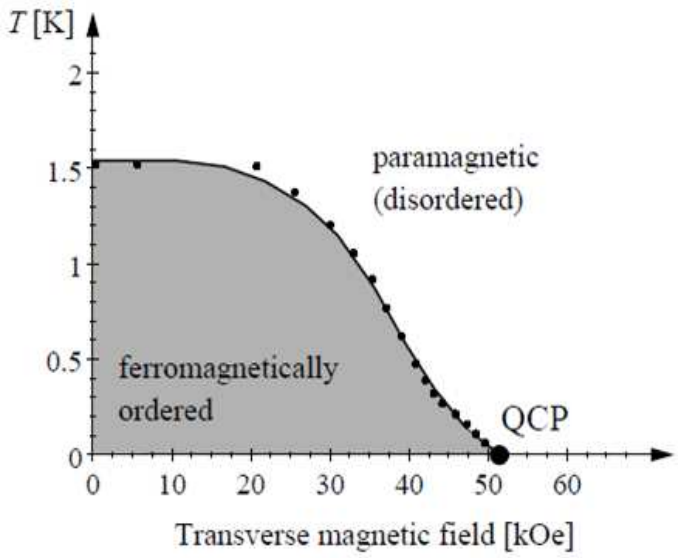

Figure 1.7: Temperature-transverse magnetic field phase diagram of $LiHoF_4$ after [1].

phase transition, by changing external field at absolute zero temperature $T = 0$. As pointed out above, quantum phase transitions are caused by quantum fluctuations. In $LiHoF_4$ compound, these fluctuations are caused by the transverse magnetic field, they increase with increasing field and destroy the ferromagnetic order at the quantum critical point.

To understand relations between classical and quantum phase transitions, let us look at the quantum-to-classical mapping. In classical statistical mechanics, static and dynamic behaviors decouple. The kinetic and potential parts of the Hamiltonian commute, resulting in factorization of the partition function

$$Z = \int \Pi_i dp_i e^{-\beta H_{\rm kin}} \int \Pi_i dq_i e^{-\beta H_{\rm pot}} = Z_{\rm kin} Z_{\rm pot} \,. \tag{1.34}$$

The kinetic contribution to the free energy will usually not display any singularities, since it derives from the product of simple Gaussian integrals. Therefore, one can study classical phase transitions using a time independent Landau-Ginzburg-Wilson theory such as equation (1.14).

In contrast, in quantum mechanics the kinetic and potential parts of the Hamiltonian do not commute. Thus, the partition function does not factorize and one must solve for the dynamics together with the thermodynamics. Therefore, quantum mechanical analogs of the Landau-Ginzburg-Wilson theory need to be formulated in terms of space and time dependent fields. A simple example of such a quantum Landau-Ginzburg-Wilson functional has the form [14, 15]

$$S[\phi] = \int_0^\beta d\tau \int d^d\mathbf{r} \left[[\partial_\tau \phi(\mathbf{r},\tau) + [\nabla\phi(\mathbf{r},\tau)]^2 + r\phi^2(\mathbf{r},\tau) + \frac{1}{2}\phi^4(\mathbf{r},\tau) \right] , \qquad (1.35)$$

where τ and $\phi(\mathbf{r},\tau)$ are imaginary time and the order parameter field, respectively. r measures distance to the quantum critical point. At quantum phase transitions, the imaginary time acts as an additional coordinate. In addition to the correlation length ξ, quantum system is characterized by the correlation length in imaginary time direction ξ_τ. As the transition is approached both the order parameter correlation length ξ and correlation time ξ_τ diverge:

$$\xi \sim |r|^{-\nu}, \qquad \xi_\tau \sim \xi^z \,, \qquad (1.36)$$

where z is the dynamical critical exponent.

At non-zero temperatures, the extension of the extra dimension is finite and close to the critical point where $\xi_\tau > \beta$, the extra dimension cannot affect the critical behavior. In contrast, at $T = 0$, the extension in imaginary time direction is infinite, and the critical behavior is described by a theory in higher dimension. The quantum phase transition in d dimensions is equivalent to some classical phase transition in higher $d + z$ dimensional space. If space and imaginary time enter the theory symmetrically the dynamical exponent $z = 1$, but in general, it can be larger than one.

Let us now discuss properties of the system near a quantum critical point qualitatively [16]. The schematic phase diagram is shown in Fig. 1.8. The disordered phase at finite temperatures T can be divided into different regimes. For low T and $r > 0$, the extension in imaginary time direction $\xi_\tau < \beta$, equivalently $T < r^{\nu z}$. In this regime quantum mechanics is important and excitations are well-defined quasiparticles. Correspondingly, the regime is called "quantum disordered". For magnetic transitions in metallic systems, this regime will be the usual Fermi-liquid regime. For $T > T_c$ and $r < 0$, but $\beta > \xi_\tau$, the order is destroyed by thermal fluctuations. The corresponding regime is called "thermally disordered" regime (excitations are well-defined quasiparticles). In the "quantum critical" regime, bounded by crossover lines $T \sim |r|^{\nu z}$, properties are determined by unconventional excitation spectrum of the quantum critical ground state, where quasiparticle excitations are replaced by a critical continuum of excitations.

In the quantum critical regime, this continuum is thermally excited leading to unconventional power-law temperature dependencies of observables. Quantum critical behavior is cutoff at high temperatures when T exceeds a characteristic microscopic energy scale of the system. In a magnet this cutoff is the typical exchange energy.

For any transition occurring at a finite temperature T_c, quantum mechanics is unimportant for $|t| \lesssim T_c^{1/\nu z}$ "because $\hbar\omega_c \leq k_{\rm B}T$", where $t = (T - T_c)/T_c$ and $\hbar\omega_c$ is the quantum energy scale. Correspondingly, the critical behavior is described by the classical theory.

Let us now discuss briefly scaling at quantum phase transitions. Because a quantum phase transition in d spatial dimensions is related to a classical transition in $d + z$ dimensions, the scaling form can be generalized as

$$f(r, h, T) = b^{-(d+z)} f(rb^{1/\nu}, hb^{y_h}, Tb^z)\,. \tag{1.37}$$

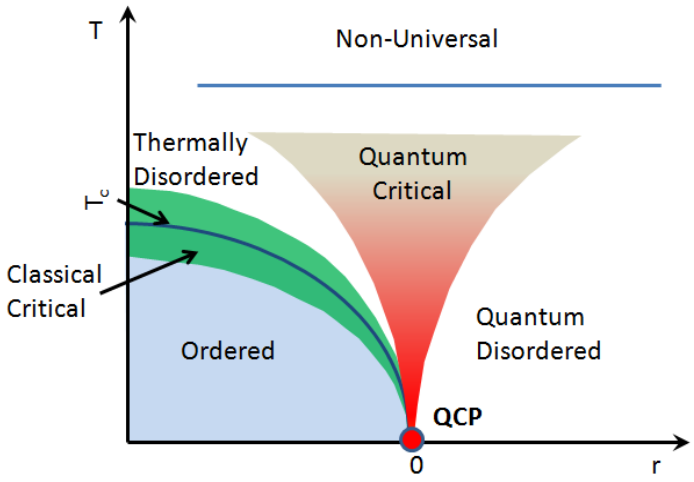

Figure 1.8: Schematic phase diagram in the vicinity of a quantum critical point. The horizontal axis represents the quantum control parameter r, the vertical axis is the temperature T. T_c is the phase boundary.

Using this homogeneity relation, we can see how quantum fluctuations result in unconventional power-law temperature dependencies of physical observables. In the absence of field $h = 0$, if we choose $b = r^{-\nu}$, we find

$$f = r^{\nu(d+z)} f(1, Tr^{-\nu z}) \,, \tag{1.38}$$

or if we substitute $b = T^{-1/z}$, we obtain

$$f = T^{(d+z)/z} g(rT^{-1/\nu z}) \,. \tag{1.39}$$

Then, for the specific heat $C = T\partial S/\partial T$ at $r = 0$, we obtain the unconventional relation

$$C(r = 0, T) \sim T^{d/z} \,, \tag{1.40}$$

in the quantum critical regime.

1.2. PHASE TRANSITIONS IN THE PRESENCE OF DISORDER

Realistic materials always contain impurities, defects or other kinds of disorder. Therefore, significant attention has been attracted by phase transitions in the presence of quenched disorder [17, 18]. In the following, we consider weak quenched disorder i.e., time independent-disorder which does not qualitatively modify the two bulk phases separated by the transition. The question of how quenched disorder influences phase transitions has a long history. Initially, it was thought that any kind of disorder destroy continuous transitions, because in the presence of disorder, the system divides itself up into spatial regions which independently undergo the phase transition at different temperatures. Correspondingly, there would not be singularities in observables (see Ref. [19] for a historical discussion). However, later, it became clear that phase transitions can remain sharp in the presence of disorder in the system.

1.2.1. Harris Criterion. Harris [20] found a simple heuristic criterion that governs whether weak disorder changes the critical behavior of a given clean critical point. Here, we sketch the derivation of the Harris criterion. Let us consider a system with quenched disorder which undergoes a second order phase transition at a temperature T_c^0. Due to the presence of the disorder, the effective transition temperature $T_c(\mathbf{r})$ may be position dependent ($T_c(\mathbf{r})$ is not a true phase transition temperature but marks the point where the order parameter at $\mathbf{r}$ orders locally). The deviation from the critical temperature T_c^0 can be written as

$$\delta T_c(\mathbf{r}) = T_c(\mathbf{r}) - T_c^0 \,. \tag{1.41}$$

The typical value of the fluctuations $\delta T_c(\mathbf{r})$, over a large volume with linear size L can be estimated using the central limit theorem, yielding

$$\Delta T_c(\mathbf{r}) \sim L^{-d/2}\,. \tag{1.42}$$

Harris observed that a sharp phase transition can only occur if the fluctuations $\delta T_c(\mathbf{r})$ over a correlation volume ξ^d are much smaller than the global distance from the critical point T_c^0. At the clean critical point $\xi \sim |T - T_c^0|^{-\nu}$, therefore the criterion for the stability of the clean critical point becomes

$$|T - T_c^0|^{-d\nu/2} < |T - T_c^0|\,, \tag{1.43}$$

which is fulfilled if

$$d\nu > 2\,. \tag{1.44}$$

The last inequality is called the Harris criterion. Thus, if the Harris criterion is fulfilled, weak disorder does not change the clean critical behaviors. However, non-universal quantities such as the critical temperature can be changed.

1.2.2. Strong-Disorder Renormalization Group Theory. We now discuss the strong-disorder renormalization group methods used for studies of the critical behavior of disordered systems. These methods are defined only for disordered systems and are performed in real space. Strong-disorder renormalization group cannot be defined for pure systems which do not feature spatial heterogeneities.

The strong-disorder renormlization group was introduced by Ma, Dasgupta and Hu [21] for the random antiferromagnetic quantum spin chain. The idea of the strong-disorder renormalization group is to identify the strongest coupling in the system. One then finds the ground state of the corresponding part of the Hamiltonian,

and treats the coupling to the rest of the system perturbatively. Finally, one then throws out the excited states involving the strong coupling, yielding a new effective Hamiltonian. This renomalization procedure is repeated ad infinitum.

We now sketch the strong-disorder renormalization group procedure in the random transverse-field Ising model developed by Fisher [22]. The Hamiltonian of the transverse-field Ising model is given by

$$H = -\sum_i J_i \sigma_i^z \sigma_{i+1}^z - \sum_i h_i^x \sigma_i^x \,. \tag{1.45}$$

Here, $J_i > 0$ are the nearest neighbor interactions and h_i^x are random transverse fields. σ_i^x and σ_i^z are Pauli matrices representing the spin at site i,

$$\sigma^x = \begin{pmatrix} 0 & 1 \\ 1 & 0 \end{pmatrix}, \quad \sigma^y = \begin{pmatrix} 0 & -i \\ i & 0 \end{pmatrix}, \quad \sigma^z = \begin{pmatrix} 1 & 0 \\ 0 & -1 \end{pmatrix}.$$

The orthogonal eigenstates corresponding to the operator σ^z are

$$|\uparrow\rangle = \begin{pmatrix} 1 \\ 0 \end{pmatrix} \quad \text{and} \quad |\downarrow\rangle = \begin{pmatrix} 0 \\ 1 \end{pmatrix}.$$

For the operator σ^x, the orthogonal eigenstates are

$$|\rightarrow\rangle = \frac{|\uparrow\rangle + |\downarrow\rangle}{\sqrt{2}} \quad \text{and} \quad |\leftarrow\rangle = \frac{|\uparrow\rangle - |\downarrow\rangle}{\sqrt{2}}.$$

The renormalization group procedure is as follows:

(1) Find the strongest coupling

$$\Omega \equiv \max\{J_i, h_i^x\}. \tag{1.46}$$

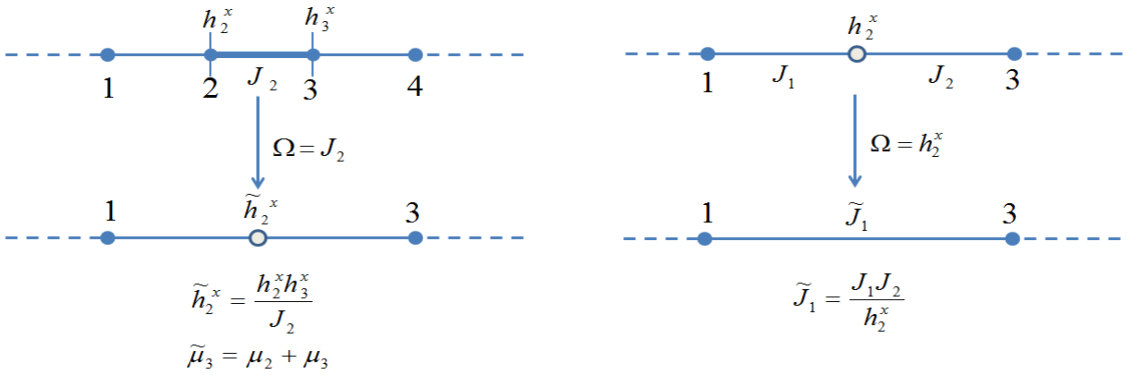

Figure 1.9: Schematic of strong-disorder renormalization group decimation for spin chain.

If the largest coupling is an interaction, for example $\Omega = J_3$, then neighboring transverse fields h_2^x and h_3^x can be treated as a perturbation to the term $-J_3\sigma_2^z\sigma_3^z$, which has two degenerate ground states $|\downarrow\downarrow\rangle$ and $|\uparrow\uparrow\rangle$. The two spins involved are joined together into a spin cluster with an effective transverse field (Fig. 1.9)

$$\tilde{h_2^x} \approx \frac{h_2^x h_3^x}{J_2}\,. \tag{1.47}$$

We now throw away the excited states $|\uparrow\downarrow\rangle$ and $|\downarrow\uparrow\rangle$ of the spin cluster and treat the cluster as an effective spin whose moment is

$$\tilde{\mu_3} = \mu_2 + \mu_3\,. \tag{1.48}$$

If instead the strongest coupling is a transverse field, for instance $\Omega = h_2^x$, then the associate part of H is $-h_2^x\sigma_2^x$ which has a ground state $|\rightarrow\rangle$ and excited state $|\leftarrow\rangle$. The coupling of σ_2 to the rest of the system $-J_1\sigma_1^z\sigma_2^z - J_2\sigma_2^z\sigma_3^z$ is treated in second-order perturbation theory. This yields an effective interaction

$$\tilde{J}_1 \approx \frac{J_1 J_2}{h_2^x} \,. \tag{1.49}$$

Throwing out σ_2 by neglecting its excited state leads to a new spin chain with one fewer spin and new coupling $\tilde{J}_1$.

The strong-disorder renormalization steps explained above are sketched in Fig. 1.9. Under the repeated use of the decimation transformations, Eqs. (1.47, 1.49), the energy scale Ω is gradually decreased accompanied by an aggregation and annihilation process of spin clusters. These steps are repeated ad infinitum.

When the strongest coupling is a field, the corresponding cluster is annihilated. In contrast, if the largest one is an interaction, the clusters that it connects are aggregated into one cluster. In the paramagnetic phase, annihilation dominates as $\Omega \to 0$, and large clusters are not created. In the ferromagnetic phase, the aggregation dominates as $\Omega \to 0$. A cluster of infinite size is formed at $\Omega = 0$. At the quantum critical point annihilation and aggregation balance and an infinite cluster first appears.

Because the J_i and h_i^x are random quantities, we need to study their probability distributions. At each strong-disorder renormalization group step these probability distributions of $\log J$ and $\log h$ change. The corresponding flow equations for the distribution functions were derived by Fisher [22]. The renormalization flow equations display very interesting behavior. At the critical point, given by $[\log J]_{\rm av} = [\log h^x]_{\rm av}$, here $[...]_{\rm av}$ denotes disorder average, the widths of the distributions diverge as $\Omega \to 0$. Therefore, the critical fixed point is called an infinite randomness fixed point.

This type of critical point has unusual properties. For example, it displays activated scaling rather than conventional power-law scaling. At the critical point

the length of the clusters or renormalized bonds scales as

$$L^{\psi} \sim \log\left(\frac{\Omega_0}{\Omega}\right). \tag{1.50}$$

Here, Ω_0 is a microscopic energy scale and $\psi = 1/2$ is known as the tunneling critical exponent. The relation between time-scale and length-scale is thus logarithmic

$$\log \xi_\tau \sim \xi^{\psi}, \tag{1.51}$$

This implies that the dynamical exponent z is formally ∞. The magnetic moment of a cluster scales as

$$\mu \sim \log\left(\frac{\Omega_0}{\Omega}\right)^{\phi}, \tag{1.52}$$

with $\phi = (1+\sqrt{5})/2$ equal to the golden mean.

The correlation length is found to scale like

$$\xi \sim r^{-\nu}, \tag{1.53}$$

where the exponent $\nu = 2$. Here, the distance r from criticality is defined as

$$r = \frac{[\log h^x]_{\text{av}} - [\log J]_{\text{av}}}{\text{var}(\log h^x) + \text{var}(\log J)}, \tag{1.54}$$

where var(...) denotes the variance.

The strong-disorder renormalization group can also be used to analyse thermodynamic observables off criticality. Fisher [22] found strong power-law quantum Griffiths behaviors of thermodynamic observables in the so-called Griffiths region. In the next subsections, we discuss the Griffiths phase in more detail.

1.2.3. Classification of Critical Points. We emphasize that the Harris criterion is only a necessary condition for the stability of a clean critical point. It is not a sufficient condition because it only deals with average disorder behavior at large length scale. Possible qualitative effects at finite length scales are not covered by the Harris criterion. Using the Harris criterion and strong-disorder renormalization group analysis, we can classify critical points (Motrunich et al. [23]):

The first class includes systems whose clean correlation length critical exponents ν fulfil the Harris criterion. At the critical point, when the length scale increases (coarse graining), the effective disorder becomes smaller and smaller without bound. At large length scales, the system becomes asymptotically homogeneous. Thus, disorder is renormalization group irrelevant at the critical point. The system is then controlled by a pure fixed point. An example is the classical three-dimensional Heisenberg model with the clean critical exponent $\nu \approx 0.698$ [24], which fulfills the Harris criterion.

The second class contains systems whose clean critical exponent ν does not fulfil the Harris criterion. Under coarse graining, the effective disorder strength converges, towards a finite level, and the system is then controlled by a finite-disorder fixed point. The critical behavior is of conventional power-law type but with a different critical exponent which fulfills the Harris criterion. An example is the three-dimensional classical Ising model with the clean critical exponent $\nu \approx 0.627$ [25] which does not fulfill the Harris criterion. In the presence of disorder, the critical exponent is $\nu \approx 0.684$ [26].

In the third class, the clean critical exponent also does not fulfil the Harris criterion. At the critical point, under coarse graining, the effective disorder becomes larger and larger without bound. The system is controlled by an infinite-randomness fixed point. At the infinite-randomness critical point, the dynamical scaling is activated (logarithmic) rather than power-law. Examples in this class are:

the one-dimensional random quantum spin chain, and one and two-dimensional random quantum Ising systems [27, 28, 29].

1.2.4. Rare Region Effects. We now discuss the effect of rare strong disorder fluctuations on phase transitions. Let us consider a randomly diluted classical magnet (Fig. 1.10). The dilution reduces the transition temperature from its clean value T_c to the new value $T_c(p)$, where p is the vacancy concentration. However, there will always be large spatial regions (rare regions) that are devoid of impurities. For temperatures $T_c(p) < T < T_c$, they can show local order even if the bulk system is in the disordered phase. The locally ordered rare regions are not static but they fluctuate slowly. Griffiths showed that the rare regions can lead to a singularity in the free energy in a whole parameter region $T_c(p) < T < T_c$, which is now known as the Griffiths phase [30]. The effect of the rare regions depends on the effective dimension of the rare regions. Three cases can be distinguished [31]:

(i) If the rare regions are below the lower critical dimensionality d_c^- of the problem, an isolated rare region cannot undergo the phase transition by itself. As will be shown in Sec. 1.2.5, the Griffiths singularity is only an essential one and the resulting rare-region contributions to observables are small. This case is realized in generic classical systems (where the rare regions are finite in all directions and thus effectively zero-dimensional). It also happens at some quantum phase transitions such as the transition in the diluted bilayer Heisenberg quantum antiferromagnet [32, 33]. Here, the rare regions are equivalent to one-dimensional classical Heisenberg models which are below $d_c^- = 2$.

(ii) In the second class, the rare regions are exactly at the lower critical dimension. In this case, the system shows strong power-law quantum Griffiths singularities (see Secs. 1.2.6, 1.2.7). This case is realized, e.g., in classical Ising models with linear defects [34] and random quantum Ising models (each rare regions corresponds to a one-dimensional classical Ising model in imaginary time direction) [28] as well as in

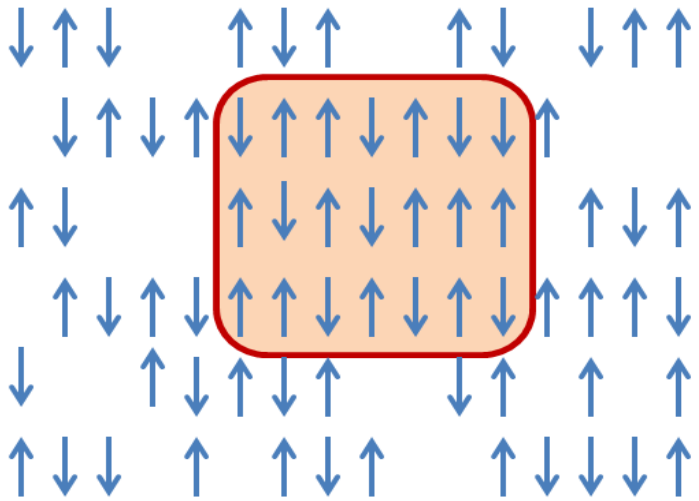

Figure 1.10: Schematic plot of a diluted magnet. Circled shaded area (rare region) is devoid of impurities.

the disordered itinerant quantum Heisenberg magnets (the rare regions are equivalent to classical one-dimensional Heisenberg models with $1/\tau^2$ interaction) [31].

(iii) Finally, in the third class, the rare regions are above the lower critical dimension, i.e., they can undergo the phase transition independently from the bulk system. This leads to a smeared phase transition (see Sec. 1.2.8). Examples are: classical Ising magnets with planar defects [35] (the rare regions are effectively two-dimensional) and itinerant quantum Ising magnets [36, 37] where the rare regions are equivalent to classical one-dimensional Ising models with $1/\tau^2$ interaction.

1.2.5. Classical Griffiths Effects. Uncorrelated disorder at classical phase transitions leads to exponentially weak classical Griffiths singularities (the singularity in the free energy is only an essential one). The singularities in thermodynamic observables can be estimated using optimal fluctuation theory [38, 39].

Let us consider the diluted classical magnet (Fig. 1.10). The probability for the finding an impurity-free region of linear size L_{RR} is

$$\mathcal{P}(L_{\rm RR}) \sim \exp(-bL_{\rm RR}^d)\,, \tag{1.55}$$

with b a constant that depends on the disorder strength. For temperatures $T_c(p) < T < T_c$, the system is in the Griffiths phase. In an external magnetic field h, a rare region of linear size $L_{\rm RR}$ can be polarized if $\mu h > k_{\rm B}T$, where $\mu \sim L_{\rm RR}^d$ is the magnetic moment of a rare region. Using this condition, one can define a minimum volume of a rare region that can be polarized, $L_m^d \sim k_{\rm B}T/h$. The rare-region contribution to the magnetization-field curve can be estimated by summing over all polarized rare regions

$$m_{\rm RR}(h) \sim \int_{L_m}^{\infty} dL_{\rm RR}\mathcal{P}(L_{\rm RR})L_{\rm RR}^d \sim \exp(-bk_{\rm B}T/h)\,. \tag{1.56}$$

Thus, the rare-region contribution is singular, however it is exponentially weak.

The contribution of the rare regions to the magnetic susceptibility can be estimated easily. The order parameter susceptibility $\chi(L_{\rm RR})$ is proportional to $L_{\rm RR}^{2d}$. Thus, the rare region contribution to the susceptibility grows as a power of its linear size $L_{\rm RR}$. The rare region contribution to the total susceptibility can be obtained by summing over all rare regions,

$$\chi_{\rm RR} \sim \int dL_{\rm RR}\mathcal{P}(L_{\rm RR})\chi(L_{\rm RR})\,. \tag{1.57}$$

The power law increase of the susceptibility cannot overcome the exponential drop in the rare region density $\mathcal{P}(L_{\rm RR})$. Thus, the rare region contribution to the order parameter susceptibility is exponentially weak [40].

1.2.6. Quantum Griffiths Effects. We have seen in the subsection (1.2.5) that the rare-region effects are exponentially weak at classical phase transitions. In

this subsection, we discuss the rare-region effects at quantum phase transitions. At quantum phase transitions quenched disorder is perfectly correlated in the imaginary time direction which becomes infinitely extended at zero temperature. This leads to enhanced rare-region effects [17, 18].

For definiteness, we consider the random transverse-field Ising model with random interactions and homogeneous field. Let us assume that the interactions are binary distributed random variables, so the interaction can take values J_l or J_h ($J_h > J_l$). Because of the disorder, the critical field h_c will be between $h_{c,h}$ and $h_{c,l}$, critical fields of hypothetical systems with $J_i \equiv J_h$ or $J_i \equiv J_l$. The probability for finding a rare region of linear size L_{RR}, which has only strong bonds is exponentially small in its volume

$$\mathcal{P} \sim \exp(-bL_{\mathrm{RR}}^d)\,. \tag{1.58}$$

In the Griffiths phase $h_{c,l}^x < h^x < h_{c,h}^x$, these rare regions are locally ordered. The energy gap of a rare region is given by [41]

$$\varepsilon \sim \exp(-cL_{\mathrm{RR}}^d)\,, \tag{1.59}$$

where $c = \log(h/J)$. Combining the last two Eqs. (1.58, 1.59) leads to the power-law density of states of the rare-region excitations in the low-energy regime,

$$\rho(\varepsilon) \sim \varepsilon^{\lambda-1}\,. \tag{1.60}$$

Here, $\lambda = b/c$ is the non-universal Griffiths exponent. It varies systematically within the Griffiths phase and vanishes at the critical point.

The power-law density of states $\rho(\varepsilon)$ leads to non-universal power-law quantum Griffiths singularities of several thermodynamic observables. The rare regions are

equivalent to two-level systems with gap ε. The rare regions with energy gap $\varepsilon > T$ are in their quantum ground states while rare regions with gap $\varepsilon < T$ are free. The number n of free rare regions at temperature T can be found as

$$n(T) \sim \int d\epsilon \rho(\epsilon) e^{-\epsilon/T}/(1+e^{-\epsilon/T}) \sim T^{\lambda}\,. \tag{1.61}$$

The uniform static susceptibility can be estimated by summing Curie susceptibilities for all free rare regions, yielding

$$\chi(T) = n(T)/T \sim T^{\lambda-1}\,. \tag{1.62}$$

The specific heat C can be obtained from

$$\Delta E \sim \int d\epsilon \rho(\epsilon) \epsilon\ e^{-\epsilon/T}/(1+e^{-\epsilon/T}) \sim T^{\lambda+1}\,, \tag{1.63}$$

which gives

$$C \sim T^{\lambda}\,. \tag{1.64}$$

Knowing the specific heat, we can find the rare region contribution to the entropy as

$$\Delta S \sim T^{\lambda}\,. \tag{1.65}$$

To determine the zero-temperature magnetization in a small ordering field h, we note that rare regions with $\epsilon < h$ are (almost) fully polarized while the rare regions

with $\epsilon > h$ have very small magnetization. Thus,

$$m \sim \int_0^h d\epsilon \rho(\epsilon) \sim h^\lambda \,. \tag{1.66}$$

The power-law singularities (1.61 - 1.66) are called the quantum Griffiths singularities [17, 18].

1.2.7. Quantum Griffiths Singularities in Metals. Let us now discuss rare-region effects at quantum phase transitions in a disordered metal. The standard model that describes quantum phase transitions in metals was introduced by Hertz [14]. He derived the model from a microscopic Hamiltonian of interacting electrons (Hubbard model) by integrating out the fermionic degrees of freedom in the partition function. As the result, he obtained Landau-Ginzburg-Wilson order parameter field theories for the ferromagnetic and antiferromagnetic quantum phase transitions.

An important difference between systems of localized spins and metallic magnets is that magnetic excitations are undamped in the localized spin systems while they are damped in the itinerant magnets. This is the result of the coupling between magnetic degrees of freedom and the gapless particle-hole excitations in the metal. The damping is reflected in the frequency-dependent term in the Landau-Ginzburg-Wilson action. The Landau-Ginzburg-Wilson action of the clean transition is given by [14]

$$S = \int d\tau \int d^d\mathbf{x} \Big[\phi(\mathbf{x},\tau)\Gamma(\mathbf{x},\tau)\phi(\mathbf{x},\tau) + u\phi^4(\mathbf{x},\tau) \Big] \,. \tag{1.67}$$

where $\phi(\mathbf{x},\tau)$ is the order parameter field, magnetization for a ferromagnet and staggered magnetization for an antiferromagnet. It is a scalar for Ising symmetry, while it has three components (ϕ_1, ϕ_2, ϕ_3) for a Heisenberg magnet. $\Gamma(\mathbf{x},\tau)$ is the Gaussian

vertex whose Fourier transform is

$$\Gamma(\mathbf{q}, \omega_n) = r + \mathbf{q}^2 + \gamma(\mathbf{q})|\omega_n| \,. \tag{1.68}$$

Here, ω_n is a bosonic Matsubara frequency. The linear frequency dependence corresponds to the overdamped dynamic of the system. This so-called Landau damping is Ohmic. In contrast, for undamped dynamics the leading frequency dependence in (1.68) would be ω_n^2. The form of $\gamma(\mathbf{q})$ depends on the type of the transition. For antiferromagnetic transitions it is a constant $\gamma(\mathbf{q}) = \gamma_0$ for $\mathbf{q} \to 0$ while for ferromagnetic transitions $\gamma(\mathbf{q}) \sim 1/|\mathbf{q}|^a$. In the former case, the lifetime of the spin-fluctuations (*paramagnons*) is $\mathbf{q}-$independent reflecting the fact that the order parameter is not a conserved quantity and paramagnons can decay locally. In the latter case, the lifetime is $\mathbf{q}-$dependent. This is due to the fact that the order parameter, the total magnetization, is a conserved quantity in the ferromagnet. Relaxation of a low$-\mathbf{q}$ excitations thus requires transporting the order parameter over a large distance which takes a long time and has to diffuse over a large distance, in long times. The value of a depends on the character of the electron motion in the system and equals 1 or 2 for ballistic and diffusive ferromagnets, respectively. The effect of long-range interactions created by soft modes in the itinerant ferromagnet modifies the rare-region effects [42]. We will discuss dirty ferromagnetic metals in detail in Paper IV. Here, we discuss antiferromagnetic metals.

Consider for example, an itinerant antiferromagnetic Heisenberg model. The randomness can be introduced by making r a random function of position, $r \to r + \delta r(\mathbf{x})$. The rare regions are finite in the d space dimensions and infinitely large in imaginary time. Let us consider a single large rare region which is locally ordered, while the bulk system is in the disordered phase. In the presence of damping, the action (1.67) contains the linear dependence of the frequencies which is equivalent

to a long-range interaction in imaginary time of the form $1/(\tau - \tau')^2$. Thus, each rare region is equivalent to an one-dimensional Heisenberg model with a long-range interaction $1/\tau^2$. This model is known to be exactly at its lower critical dimension. Correspondingly, the characteristic energy ε of a rare region decreases exponentially with its volume $L_{\rm RR}^d$, resulting in power-law Griffiths singularities analogous to those in the random transverse-field Ising model (1.61 - 1.66). Without damping, the interaction in imaginary time direction would be short-ranged and the corresponding one-dimensional Heisenberg model is below its lower critical dimension. Thus, the characteristic energy ε decreases as a power-law with its volume, leading to the exponentially small contributions to the thermodynamic observables.

In recent years, indications of quantum Griffiths phases have been observed in experiments on a number of metallic systems such as magnetic semiconductors [43, 44, 45], Kondo lattice ferromagnets [46, 47] and transition metal ferromagnets [48, 49]. The phase diagram of $Ni_{1-x}V_x$ is shown in Fig. 1.11. Pure Nickel undergoes a ferromagentic phase transition at 630K. By doping vanadium atoms, the critical temperature decreases. At constant temperature, the transition can be tuned by changing the concentration of vanadium atoms. At zero temperature, the $Ni_{1-x}V_x$ compound under goes a quantum phase transition at vanadium concentration of $x_c \approx 11.4\%$. As shown in Fig. 1.12a , for concentrations slightly above x_c $(11 - 15\%)$ the temperature dependence of the magnetic susceptibility is described by non-universal quantum Griffiths power laws for temperatures 30–300K. As shown in Fig. 1.12b, the magnetization-field curves show non-linear behaviors above 3000 Gauss. These behaviors are in very good agreement with the Griffiths singularities (1.62) and (1.66).

1.2.8. Smeared Phase Transitions. In the last subsection, we have seen that at lower temperatures, i.e., when damping is sufficiently strong, itinerant Heisenberg magnets display power-law Griffiths singularities. Millis et al. [36, 37] showed that metallic Ising magnets show qualitatively different behavior.

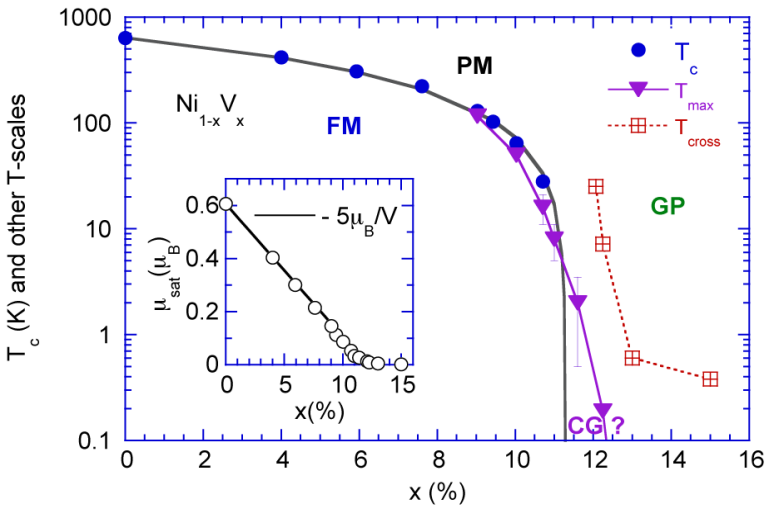

Figure 1.11: Temperature-composition magnetic phase diagram of $Ni_{1-x}V_x$ (see Ref. [48] for more details).

At zero temperature, each rare region is equivalent to a one-dimensional classical Ising model finite in the d space dimensions and infinite in imaginary time. The interaction in the imaginary time direction is short-range without damping, while Ohmic damping leads to a long-range $1/\tau^2$ interaction. The one-dimensional Ising model with $1/\tau^2$ long-range interaction is known to have a phase transition [50]. Thus, each rare region undergoes the phase transition independently, *i.e.*, individual rare regions stop tunneling, leading to the smearing of the global phase transition. At higher temperatures but below a microscopic cutoff scale, the damping is unimportant, *i.e.*, the interaction is short range. In this case, the Ising model is exactly at its lower critical dimension $d_c^- = 1$. Correspondingly, the energy gap ϵ decreases exponentially with its volume. Thus, the dissipationless quantum Ising model can show quantum Griffiths singularities.

We now sketch the theory of smeared phase transitions in disordered metallic Ising systems proposed by Vojta [17, 51]. Using optimal fluctuation theory, we can study the thermodynamics for small order parameter M. Let us again assume that

the disorder is introduced via dilution. The probability for finding a rare region of width L_{RR} is given by

$$\mathcal{P} \sim \exp(-bL_{\mathrm{RR}}^{d})\,. \tag{1.69}$$

Such rare regions develop static order if the local distance from criticality fulfills $r < r_c(L_{\mathrm{RR}}) < 0$. Since rare regions are finite in space, using finite size-scaling [52, 53], we can find

$$r_c(L_{\mathrm{RR}}) = A/L_{\mathrm{RR}}^{\phi}\,, \tag{1.70}$$

with $A < 0$, Here, ϕ is the finite-size scaling shift exponent. Thus, the probability for finding a rare region which becomes locally ordered at r_c is exponentially small

$$\mathcal{P}(t_c) \sim \exp(-\tilde{b}|r_c|^{-d/\phi})\,, \tag{1.71}$$

where $\tilde{b}$ is a constant. The total order parameter can be obtained by summing over all rare regions showing local orders i.e. $r_c > r$. This yields an exponential tail towards the clean critical point

$$M(t) \sim \exp(-\tilde{b}|r|^{-d/\phi})\,. \tag{1.72}$$

Thus, the global phase transition is destroyed by rounding, because static order can develop on isolated rare regions.

At non-zero temperatures, the static magnetic order on the rare regions is destroyed, and a finite interaction of the order of the temperature is necessary to align them. This means that the sharp phase transition is recovered. To estimate the critical temperature T_c that bounds the ferromagnetic phase we note that the

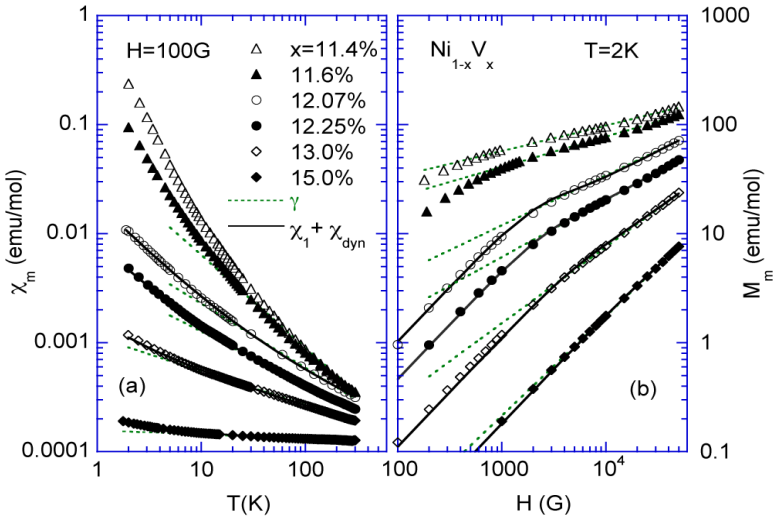

Figure 1.12: Behavior of observables in the quantum Griffiths phase. (a) The temperature dependence of magnetic susceptibility of $Ni_{1-x}V_x$ for different Vanadium concentrations. Dotted lines represent fits to Eq. (1.62). The solid lines represent a model that sums a quantum Griffiths law and a Curie term (see Ref. [48] for more details). (b) Magnetization versus field. The dashed lines represents fits to Eq. (1.66).

interaction between two rare regions drops off exponentially with their distances x, $E_{\rm int} \sim e^{-x/\xi}$ [51], where ξ is the bulk correlation length. The typical distance $x_{\rm typ}$ between neighboring locally ordered rare regions can be estimated from their density, ρ, as $x_{\rm typ} \sim \rho^{-1/d} \sim M^{-1/d}$. Therefore, the critical temperature dependence on r is thus

$$\log(1/T_c) \sim \exp(-\tilde{b}|r|^{-d/\phi})\,. \tag{1.73}$$

If we take a Ruderman-Kittel-Kasuya-Yosida type interaction into account which decays as $1/x^d$ with distance but is not contained in Hertz's theory, the $r-$dependence of T_c changes to a simple exponential [51].

Let us now consider classical smeared phase transitions. A classical system with uncorrelated disorder cannot show a smeared phase transition because all rare

regions are of finite size and cannot undergo true phase transition at non-zero temperatures. However, if quenched disorder is perfectly correlated in one or more dimensions then rare regions are infinitely extended. If the number of correlated dimensions $d_{\rm cor}$ is high enough then large rare regions can undergo the phase transition independently of the bulk system. This leads to a destruction of the sharp transition by smearing [17].

Let us consider a classical random Ising model (Fig. 1.13). Assume that the disorder is correlated in a sufficiently large dimension $d_{\rm cor} = 2$ and it is distributed randomly in $d_{\rm ran} = d - d_{\rm cor}$ dimension, so that the system undergoes a smeared phase transition. Optimal fluctuation theory for the behavior of the observable in the tail can be developed along the same lines as the theory above. The only difference is that the randomness is restricted in $d_{\rm ran}$ dimension. The dimensionality d in Eqs. (1.72, 1.73) therefore needs to be replaced by $d_{\rm ran}$, yielding

$$M(r) \sim e^{-\tilde{b}|r|^{-d_{\rm ran}/\phi}} . \tag{1.74}$$

and

$$\log(1/T_c) \sim \exp(-\tilde{b}|r|^{-d_{\rm ran}/\phi}) . \tag{1.75}$$

1.3. FERMI LIQUIDS AND NON FERMI LIQUIDS

1.3.1. Landau Fermi-Liquid Theory. The Fermi-liquid theory is a phenological model of interacting fermions that describes the normal state of most metals at low temperatures [54]. The theory of Fermi-liquids was developed by Landau in 1956, and later refined by Abrikosov *et al.* (see e.g. [55]). According to the Fermi-liquid theory, a gas of interacting fermionic particles is equivalent to a system of almost non-interacting *quasiparticles*.

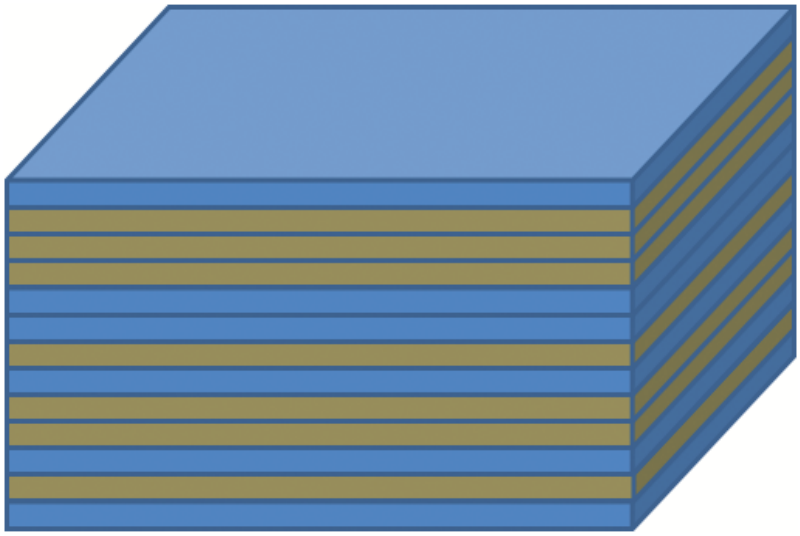

Figure 1.13: Randomly layered magnet: disorder is correlated in two dimensions.

Based on the idea of turning on the interactions between particles adiabatically, Landau suggested that the excited states of the interacting system correspond one-to-one to the excited states of the noninteracting system, so that the total particle number, spin, and momentum are conserved. However, dynamical properties, such as mass, magnetic moment etc. are renormalized to new values. Imagine, starting with a noninteracting system with one particle in state $\mathbf{k}, \sigma$ added to the ground state Fermi sea. Turning on the interactions, the particle becomes "dressed" by interactions; this results in a state with the characteristics of a particle in an excited state with definite momentum $\mathbf{k}$, and spin σ. However, it is not a true eigenstate of the interacting Hamiltonian. It is called a quasiparticle.

The Fermi-liquid theory is valid if the typical excitation energy *i.e.* T, is much larger then the rate of the change of the Hamiltonian ζ (because of adiabatic turning on of the interactions), and the lifetime of the quasiparticle τ_{life} is long compared to ζ^{-1}, otherwise it will decay away during its birth. Thus, there is an energy window

where the Fermi-liquid theory makes sense,

$$\tau_{\text{life}}^{-1} \ll \zeta \ll T\,. \tag{1.76}$$

Within Fermi-liquid theory, the lifetime is inversely proportional to the square of the temperature, $\tau_{\text{life}}^{-1} \propto T^2$. Thus, there is always a temperature range at low temperatures where Eq. (1.76) is fulfilled. Within the Fermi-liquid theory the behavior of observables shows universal temperature dependencies (see Table 1.2) [56].

1.3.2. Metals Near a Quantum Critical Point. The Fermi-liquid theory has been very successfully in describing the low-temperature behavior of normal metals. However, some experimental measurements show strong deviations from Fermi-liquid behavior (e.g. [13]). Non Fermi-liquid behavior is often observed to occur near a quantum critical point. For example, such non Fermi-liquid behavior was observed experimentally in the $CeCu_{6-x}Au_x$ compounds [57]. In these compounds, the phase transition is tuned by changing the gold concentration. The quantum critical point is found at a concentration $x_c \approx 0.1$. For concentrations $x < x_c$, the system is in a non-magnetic phase, while for $x > x_c$, the system is in the antiferromagentic phase. Fig. (1.14a) shows specific heat data in the vicinity of the quantum critical point plotted as C/T. The specific heat shows a $T\log(T)$ form between 0.06 K and 2.5 K, indicating non Fermi-liquid behavior. Non Fermi-liquid behavior is observed also in resistivity data shown in Fig. (1.14b). Far away from critical point, for concentrations $x = 0.5$ and $x = 1$ system shows Fermi-Liquid behavior, *i.e.*, resistivity $\rho \sim T^2$. At the critical point, non Fermi-liquid behavor is observed with $\rho \sim T$.

1.3.3. Semi-Classical Boltzmann Theory. In this subsection, we discuss transport phenomena in metals [58] within the semi-classical Boltzmann transport formalism.

Table 1.2: Behaviors of observables in the Fermi-liquid.

Specific heat	$C \sim T$
Entropy	$S \sim T$
Pauli susceptibility	$\chi \sim$ const.
Electrical resistivity	$\rho \sim T^2$

In semi-classical approximation, an electron wavepacket is constructed from a superposition of plane wave states, so that its size dr in space is much smaller then its *mean free path* l, *i.e.*, the length traveled by electrons between successive collisions. This allows us to consider electrons as point-like quasiparticles. In order to assign a mean wave number k, to the wave packet, electrons should be localized in k space, i.e. $dk \ll k$. According to the Heisenberg uncertainty principle $dkdr \approx 1$, which implies that the mean wave length of the electron $\lambda = 2\pi/k$ should be much smaller than the mean free path l: $\lambda \ll l$.

A macroscopic system contains of the order of 10^{23} electrons; therefore it is impossible to solve the equations of motion for each electron and a statistical treatment is needed. It is useful to know what electrons do "on average" and less important what each particular electron does. The Boltzmann transport equation describes the time evolution of the electron distribution function $f(r, k, t)$, *i.e.*, the occupancy of state k at position r and time t. The distribution function can change due to three reasons: diffusion, drift and collisions. The diffusion is caused by any gradient in electron concentration, e.g $\partial f/\partial r$, whereas the drift (diffusion in k space) is caused by external forces. The collisions are due to "internal" forces between electrons. The time evolution of the electron distribution function is given by Boltzmann transport equation

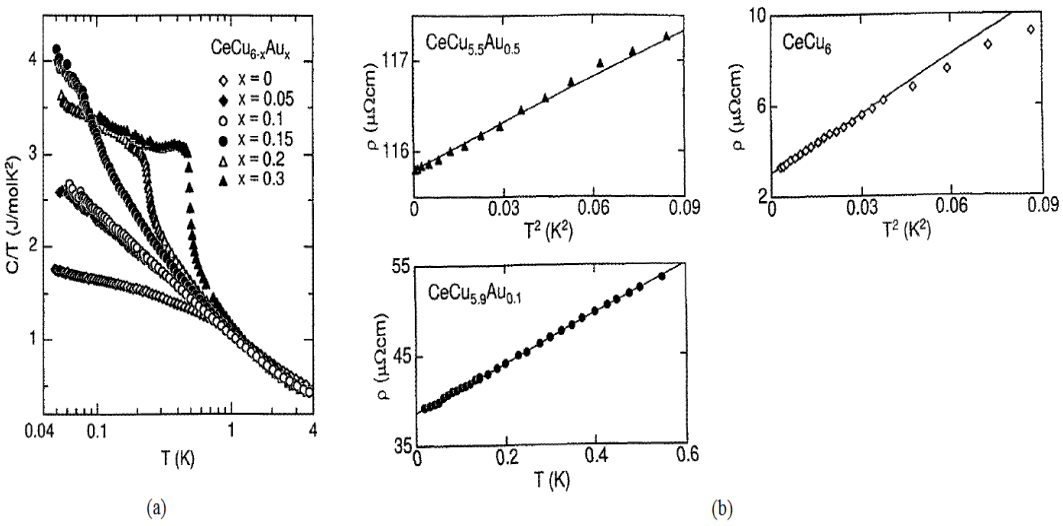

Figure 1.14: Low-temperature begavior of the $CeCu_{6-x}Au_x$ compound. (a) Specific heat, plotted as C/T versus $\log(T)$ for different concentrations of Au atoms. (b) The resistivity ρ as a function of temperature T for the concentrations of Au: $x = 0.5$, $x = x_c = 0.1$ and $x = 1$. Data taken from Ref. [57].

$$\frac{\partial f}{\partial t} = -\mathbf{v}_\mathbf{k} \cdot \frac{\partial f}{\partial \mathbf{r}} - \dot{\mathbf{k}} \cdot \frac{\partial f}{\partial \mathbf{k}} + \left.\frac{\partial f}{\partial t}\right|_{\text{coll}} . \tag{1.77}$$

Here, on the right hand side, the first and second terms correspond to the changes of the electron distribution function f due to the diffusion and drift, respectively. The last one is the collision term, which depends on the microscopic scattering mechanism. The total local rate of change of the distribution must vanish in a steady state.

Assume there is elastic scattering only, from state $|\mathbf{k}\rangle$ to state $|\mathbf{k}'\rangle$. The scattering probability $\mathcal{P}_{\mathbf{k}\mathbf{k}'} d\mathbf{k}'$ is given by

$$\mathcal{P}_{\mathbf{k}\mathbf{k}'} d\mathbf{k}' = f_\mathbf{k}(1 - f_{\mathbf{k}'}) \mathcal{Z}_{\mathbf{k}\mathbf{k}'} d\mathbf{k}' . \tag{1.78}$$

Here, $\mathcal{Z}_{\mathbf{k}\mathbf{k}'}$ is transition amplitude. Summing over all states $\mathbf{k}'$ from which the particle may come and into which it may go, we obtain

$$\left.\frac{\partial f}{\partial t}\right|_{\text{coll}} = \int [f_{\mathbf{k}'}(1-f_{\mathbf{k}}) - f_{\mathbf{k}}(1-f_{\mathbf{k}'})]\mathcal{Z}_{\mathbf{k}\mathbf{k}'}d\mathbf{k}' \,. \tag{1.79}$$

Combining the two Eqs. (1.77, 1.79) gives a nonlinear integrodifferential equation for the distribution function

$$-\mathbf{v}_{\mathbf{k}} \cdot \frac{\partial f}{\partial \mathbf{r}} - \dot{\mathbf{k}} \cdot \frac{\partial f}{\partial \mathbf{k}} + \int [f_{\mathbf{k}'}(1-f_{\mathbf{k}}) - f_{\mathbf{k}}(1-f_{\mathbf{k}'})]\mathcal{Z}_{\mathbf{k}\mathbf{k}'}d\mathbf{k}' = 0 \,. \tag{1.80}$$

It is clear that finding a complete solution of this equation must be beyond feasibility in most cases. Hence, approximations must be made. A very common simplification is the linearization for small deviations from equilibrium, *i.e.*, $f_{\mathbf{k}} = f^0_{\mathbf{k}} + \delta f_{\mathbf{k}}$, where $f^0_{\mathbf{k}}$ is the equilibrium Fermi-Dirac distribution function. Substituting the approximated $f_{\mathbf{k}}$ into Eq. (1.81), and keeping terms to leading order in $\delta f_{\mathbf{k}}$, gives the linearized Boltzmann equation in the form

$$-\mathbf{v}_{\mathbf{k}} \cdot \frac{\partial f^0}{\partial T}\nabla T - \dot{\mathbf{k}} \cdot \frac{\partial f^0}{\partial \mathbf{k}} = -\int [(f_{\mathbf{k}} - f^0_{\mathbf{k}}) - (f_{\mathbf{k}'} - f^0_{\mathbf{k}'})]\mathcal{Z}_{\mathbf{k}\mathbf{k}'}d\mathbf{k}' \,. \tag{1.81}$$

While we discussed only elastic scattering above, a similar equation with modified transition rates $\mathcal{Z}_{\mathbf{k}\mathbf{k}'}$ is obtained for inelastic scattering. Transition rates $\mathcal{Z}_{\mathbf{k}\mathbf{k}'}$ can be calculated from the microscopic Hamiltonian using Fermi's golden rule.

The task of finding a solution of a linearized inhomogeneous integral Boltzmann equation is a typical problem of applied mathematics. It is well known that the solution can be formally constructed be applying a variational principle to a general trial function [58]. For this approach it is convenient to introduce a new function $\Phi_{\mathbf{k}}$

defined by

$$f_{\mathbf{k}} = f^0_{\mathbf{k}} - \Phi_{\mathbf{k}} \frac{\partial f^0_{\mathbf{k}}}{\partial \varepsilon_{\mathbf{k}}} \,. \tag{1.82}$$

$\Phi_{\mathbf{k}}$ is a measure of the deviation of the electron distribution from equilibrium. By defining the scattering operator $\hat{\mathcal{P}}$

$$\hat{\mathcal{P}}(...) = \int d\mathbf{k}'(...)\mathcal{P}_{\mathbf{k}\mathbf{k}'} \,, \tag{1.83}$$

one can write the right side of the Boltzmann Eq. (1.81) as $\hat{\mathcal{P}}\Phi_{\mathbf{k}}/T$. In the same way, $\mathcal{X}$ is defined such that $\mathcal{X}/T$ matches the left side of the Eq. (1.81). This leads to the new alternative formulation of the Boltzmann equation in the form

$$\mathcal{X} = \hat{\mathcal{P}}\Phi_{\mathbf{k}} \,. \tag{1.84}$$

Defining an inner product by

$$\langle \Phi, \Psi \rangle = \int d\mathbf{k} \Phi_{\mathbf{k}} \Psi_{\mathbf{k}} \,. \tag{1.85}$$

leads to

$$\langle \Phi, \mathcal{X} \rangle = \langle \Phi, \hat{\mathcal{P}}\Phi \rangle \,. \tag{1.86}$$

The variational principle states that among all functions which satisfy this condition, the solution of the integral equation maximizes $\langle \Phi, \hat{\mathcal{P}}\Phi \rangle$. Alternatively, it can be formulated as follow: the solution of the integral Eq. (1.86) gives the minimal

value to the functional

$$\frac{\langle \Phi, \hat{\mathcal{P}}\Phi \rangle}{\langle \Phi, \mathcal{X} \rangle^2} \,. \tag{1.87}$$

The variational principle can be formulated in thermodynamics and in transport properties as well. In the thermodynamics, the variational principle states that in the steady state the currents in the sample are such that the entropy production takes its maximum value [58].

According to the variational principle, the electrical resistivity in the steady state is given by as minimum of a functional of $\Phi_{\mathbf{k}}$

$$\rho = \frac{\langle \Phi, \hat{\mathcal{P}}\Phi \rangle}{\langle \Phi, \mathcal{X}(E=1) \rangle^2} \,, \tag{1.88}$$

where $\mathbf{E}$ is the external electrical field which is related to the change of the $\mathbf{k}$ vector as $\dot{\mathbf{k}} = \mathbf{E}$.

Thus, the electrical resistivity is the extremal value of the variational function in unit electric field. Similarly, the variational principle can be applied to other transport properties such as the thermal conductivity, the Peltier coefficient and the thermopower [58].

1.4. SUMMARY

In this section, an introduction was given to classical and quantum phase transitions (Section. 1.1). We derived the critical behavior of observable quantities near the phase transition within the Landau mean-field approach. We also showed that for dimensions $d < 4$ the Landau theory breaks down; and we discussed the Landau-Ginzburg-Wilson theory which works for dimensions $d < 4$. In addition, we discussed the scaling theory to characterize critical behavior and gave an introduction

to the renormalization group method in momentum space which can be used to solve the Landau-Ginzburg-Wilson theory.

Section 1.2 was devoted to a discussion of how disorder can affect phase transitions. We saw that disorder can have much more dramatic effects on quantum phase transitions than on classical phase transitions. The impurities and defects may lead to strong-disorder phenomena including power-law quantum Griffiths singularities, infinite-randomness critical points and the smearing of the phase transition. Quantum Griffiths singularities are caused by rare spatial configurations of the disorder (rare regions) that fluctuate very slowly. As a consequence, observables display singular behavior not just at criticality but in a whole parameter region near the critical point which is called the quantum Griffiths phase. If rare regions show static order, *i.e.,* they undergo the phase transition independently of the bulk system, they lead to a smearing of the global phase transition. We also briefly discussed the strong-disorder renomalization group which can be used to study the critical behavior of the observable quantities on disordered system.

In the Section 1.3, we considered the Fermi-liquid theory which describes the behavior of observable quantities in normal metals at low temperatures. We showed that the strong quantum fluctuations near quantum phase transitions can cause significant deviations from the Fermi-liquid behavior of normal metals. In addition, we introduced the semi-classical Boltzmann transport theory which can be used to study the transport properties near quantum phase transitions in metals. We also discussed the solution of the Boltzmann transport equation by means of a variational principle.

PAPER

I. COMPOSITION-TUNED SMEARED PHASE TRANSITIONS

Fawaz Hrahsheh, David Nozadze, and Thomas Vojta

[1] *Department of Physics, Missouri University of Science & Technology, Rolla, MO 65409*

ABSTRACT*

Phase transitions in random systems are smeared if individual spatial regions can order independently of the bulk system. In this paper, we study such smeared phase transitions (both classical and quantum) in substitutional alloys $A_{1-x}B_x$ that can be tuned from an ordered phase at composition $x = 0$ to a disordered phase at $x = 1$. We show that the ordered phase develops a pronounced tail that extends over all compositions $x < 1$. Using optimal fluctuation theory, we derive the composition dependence of the order parameter and other quantities in the tail of the smeared phase transition. We also compare our results to computer simulations of a toy model, and we discuss experiments.

*Published in Physical Review B **83** 224402 (2011).

1. INTRODUCTION

When a phase transition occurs in a randomly disordered system, one of the most basic questions to ask is whether the transition is still sharp, i.e., associated with a singularity in the free energy. Naively, one might expect that random disorder rounds or smears any critical point because different spatial regions undergo the transition at different values of the control parameter. This expectation turns out to be mistaken, as classical (thermal) continuous phase transitions generically remain sharp in the presence of weak randomness. The reason is that a finite-size region cannot undergo a true phase transition at any nonzero temperature because its partition function must be analytic. Thus, true static long-range order can only be established via a collective phenomenon in the entire system

Recent work has established, however, that some phase transitions are indeed smeared by random disorder. This can happen at zero-temperature quantum phase transitions when the order parameter fluctuations are overdamped because they are coupled to an (infinite) heat bath.[51, 59] As the damping hampers the dynamics, sufficiently large but finite-size regions can undergo the phase transition independently from the bulk system. Once several such regions have developed static order, their local order parameters can be aligned by an *infinitesimally small* mutual interaction. Thus, global order develops gradually, and the global phase transition is smeared. Classical thermal phase transitions can also be smeared provided the disorder is perfectly correlated in at least two dimensions. In these cases, individual "slabs" of finite thickness undergo the phase transition independently of the bulk system.[35, 60]

The existing theoretical work on smeared phase transitions focuses on situations in which a sample with some fixed degree of randomness is tuned through the transition by changing the temperature (for classical transitions) or the appropriate quantum control parameter such as pressure or magnetic field (for quantum phase

transitions). However, many experiments are performed on substitutional alloys such as $CePd_{1-x}Rh_x$ or $Sr_{1-x}Ca_xRuO_3$. These materials can be tuned from an ordered phase (ferromagnetic for the two examples) at composition $x = 0$ to a disordered phase at $x = 1$ while keeping the temperature and other external parameters fixed, i.e., they undergo a phase transition as a function of composition. The composition parameter x actually plays a dual role in these transitions. On the one hand, x is the control parameter of the phase transition. On the other hand, changing x also changes the degree of randomness. If such a composition-tuned phase transition is smeared, its behavior can therefore be expected to be different than that of smeared transitions occurring at fixed randomness.

In this paper, we investigate the properties of composition-tuned smeared phase transitions in substitutional alloys of the type $A_{1-x}B_x$. We show that the ordered phase extends over the entire composition range $x < 1$, and we derive the behavior of the system in the tail of the smeared transition. Our paper is organized as follows. In Sec. 2, we consider a smeared quantum phase transition in an itinerant magnet. We use optimal fluctuation theory to derive the composition dependence of the order parameter, the phase boundary, and other quantities. In Section 3 we briefly discuss how the theory is modified for smeared classical transitions in systems with correlated disorder. Section 4 is devoted to computer simulations of a toy model that illustrate and confirm our theory. We conclude in Sec. 5 by comparing composition-tuned smeared transitions with those occurring at fixed randomness. We also discuss experiments.

2. SMEARED QUANTUM PHASE TRANSITION

2.1. Model and Phase Diagram. In this section we investigate the ferromagnetic or antiferromagnetic quantum phase transition of itinerant electrons with

Ising order parameter symmetry. In the absence of quenched randomness, the Landau-Ginzburg-Wilson free energy functional of this transition in d space dimensions reads [14, 15]

$$S = \int dydz\ \psi(y)\Gamma(y,z)\psi(z) + u\int dy\ \psi^4(y)\,. \tag{1.1}$$

Here, ψ is a scalar order parameter field, $y \equiv (\mathbf{y},\tau)$ comprises imaginary time τ and d-dimensional spatial position $\mathbf{y}$, $\int dy \equiv \int d\mathbf{y}\int_0^{1/T} \mathrm{d}\tau$, and u is the standard quartic coefficient. $\Gamma(y,z)$ denotes the bare inverse propagator (two-point vertex) whose Fourier transform reads

$$\Gamma(\mathbf{q},\omega_n) = r + \xi_0^2\mathbf{q}^2 + \gamma_0(\mathbf{q})\,|\omega_n|\ . \tag{1.2}$$

Here, r is the distance from criticality,[†] ξ_0 is a microscopic length scale, and ω_n is a Matsubara frequency. The dynamical part of $\Gamma(\mathbf{q},\omega_n)$ is proportional to $|\omega_n|$. This overdamped dynamics reflects the Ohmic dissipation caused by the coupling between the order parameter fluctuations and the gapless fermionic excitations in an itinerant system. The damping coefficient $\gamma_0(\mathbf{q})$ is $\mathbf{q}$-independent for an antiferromagnetic transition but proportional to $1/|\mathbf{q}|$ or $1/|\mathbf{q}|^2$ for ballistic and diffusive ferromagnets, respectively.

We now consider two materials A and B. Substance A is in the magnetic phase, implying a negative distance from criticality, $r_A < 0$, while substance B is nonmagnetic with $r_B > 0$. By randomly substituting B-atoms for the A-atoms to form a binary alloy $\mathrm{A}_{1-x}\mathrm{B}_x$, we can drive the system through a composition-driven magnetic quantum phase transition.

A crucial role in this transition is played by rare A-rich spatial regions. They can be locally in the magnetic phase even if the bulk system is nonmagnetic. In

[†]Strictly, one needs to distinguish the bare distance from criticality that appears in (1.2) from the renormalized one that measures the distance from the true critical point. We suppress this difference because it is unimportant for our purposes.

the presence of Ohmic dissipation, the low-energy physics of each such region is equivalent to that of a dissipative two-level system which is known to undergo, with increasing dissipation strength, a phase transition from a fluctuating to a localized phase.[61] Therefore, the quantum dynamics of sufficiently large rare regions completely freezes,[36] and they behave as classical superspins. At zero temperature, these classical superspins can be aligned by an *infinitesimally small* residual interaction which is always present as they are coupled via the fluctuations of the paramagnetic bulk system. The order parameter is thus spatially very inhomogeneous, but its average is nonzero for any $x < 1$ implying that the global quantum phase transition is smeared by the disorder inherent in the random positions of the A and B atoms.[17, 18, 51]

At small but nonzero temperatures, the static magnetic order on the rare regions is destroyed, and a finite interaction of the order of the temperature is necessary to align them. This restores a sharp phase transition at some transition temperature $T_c(x)$ which rapidly decreases with increasing x but reaches zero only at $x = 1$. If the temperature is raised above T_c, the locally ordered rare regions act as independent classical moments, leading to super-paramagnetic behavior. A sketch of the resulting phase diagram is shown in Fig. 1.

2.2. Optimal Fluctuation Theory. In this section, we use optimal fluctuation theory [62, 63, 64] to derive the properties of the tail of the smeared quantum phase transition. This is the composition range where a few rare regions have developed static magnetic order but their density is so small that they are very weakly coupled.

A crude estimate of the transition point in the binary alloy $A_{1-x}B_x$ can be obtained by simply averaging the distance from criticality, $r_{\rm av} = (1-x)r_A + xr_B$. The transition point corresponds to $r_{\rm av} = 0$. This gives the critical composition in

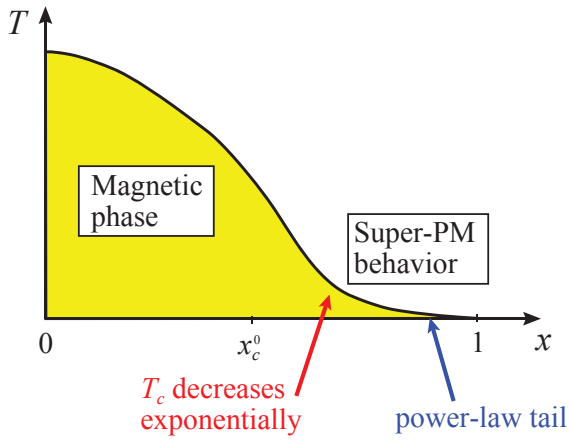

Figure 1: (Color online) Schematic temperature-composition phase diagram of a binary alloy $A_{1-x}B_x$ displaying a smeared quantum phase transition. In the tail of the magnetic phase, which stretches all the way to $x = 1$, the rare regions are aligned. Above T_c, they act as independent classical moments, resulting in super-paramagnetic (PM) behavior. x_c^0 marks the critical composition in average potential approximation defined in (1.3).

"average potential approximation,"

$$x_c^0 = -r_A/(r_B - r_A) \ . \tag{1.3}$$

Let us now consider a single A-rich rare region of linear size L_{RR} embedded in a nonmagnetic bulk sample. If the concentration $x_{\rm loc}$ of B atoms in this region is below some critical concentration $x_c(L_{RR})$, the region will develop local magnetic order. The value of the critical concentration follows straightforwardly from finite-size scaling,[52, 53]

$$x_c(L_{RR}) = x_c^0 - DL_{RR}^{-\phi} \ , \tag{1.4}$$

where ϕ is the finite-size shift exponent and D is a constant. Within mean-field theory (which should be qualitatively correct in our case because the clean transition is above its upper critical dimension[14]), one finds $\phi = 2$ and $D = \xi_0^2/(r_B - r_A)$.

Since $x_c(L_{RR})$ must be positive, (1.4) implies that a rare region needs to be larger than $L_{\min} = (D/x_c^0)^{1/\phi}$ to develop local magnetic order.

As the last ingredient of our optimal fluctuation theory, we now analyze the random distribution of the atoms in the sample. For simplicity, we assume that the lattice sites are occupied *independently* by either A or B atoms with probabilities $1-x$ and x, respectively. Modifications due to deviations from a pure random distribution (i.e., clustering) will be discussed in the concluding section 5. The probability of finding $N_B = N x_{\rm loc}$ sites occupied by B atoms in a spatial region with a total of $N \sim L_{RR}^d$ sites is given by the binomial distribution

$$P(N, x_{\rm loc}) = \binom{N}{N_B} (1-x)^{N-N_B} x^{N_B} \ . \tag{1.5}$$

We are interested in the regime $x > x_c^0$ where the bulk system will not be magnetically ordered but $x_{\rm loc} = N_B/N < x_c(L_{RR})$ such that local order is possible in the region considered.

To estimate the total zero-temperature order parameter M in the tail of the smeared transition (where the rare regions are very weakly coupled), we can simply sum over all rare regions displaying local order

$$M \sim \int_{L_{\min}}^{\infty} dL_{RR} \int_0^{x_c(L_{RR})} dx_{\rm loc}\, m(N, x_{\rm loc}) P(N, x_{\rm loc}) \ . \tag{1.6}$$

Here, $m(N, x_{\rm loc})$ is the order parameter of a single region of N sites and local composition $x_{\rm loc}$; and we have suppressed a combinatorial prefactor. We now analyze this integral in two parameter regions, (i) the regime where x is somewhat larger than x_c^0 but not by too much, and (ii) the far tail of the transition at $x \to 1$.

If x is not much larger than x_c^0, the rare regions are expected to be large, and we can approximate the binomial distribution (1.5) by a Gaussian,

$$P(N, x_{\rm loc}) = \frac{1}{\sqrt{2\pi N(1-N)}} \exp\left[-N\frac{(x_{\rm loc}-x)^2}{2x(1-x)}\right] \tag{1.7}$$

To exponential accuracy in x, the integral (1.6) can now be easily performed in saddle point approximation. Neglecting $m(N, x_{\rm loc})$, which only modifies power-law prefactors, we find that large rare regions of size $L_{RR}^{\phi} = D(2\phi - d)/[d(x - x_c^0)]$ and maximum possible B-concentration $x_{\rm loc} = x_c^0 - DL_{RR}^{-\phi}$ dominate the integral. Inserting these saddle point values into the integrand yields the composition dependence of the order parameter as[‡]

$$M \sim \exp\left[-C\frac{(x-x_c^0)^{2-d/\phi}}{x(1-x)}\right] \tag{1.8}$$

where $C = 2(D/d)^{d/\phi}(2\phi - d)^{d/\phi - 2}\phi^2$ is a non-universal constant.

Let us now analyze the far tail of the smeared transition, $x \to 1$. In this regime, the binomial distribution cannot be approximated by a Gaussian. Nonetheless, the integral (1.6) can be estimated in saddle-point approximation. We find that for $x \to 1$, the integral is dominated by pure-A regions of the minimum size that permits local magnetic order. This means $L_{RR} = L_{\rm min} = (D/x_c^0)^{1/\phi}$ and $x_{\rm loc} = 0$. Inserting these values into the integrand of (1.6), we find that the leading composition dependence of the order parameter in the limit $x \to 1$ is given by a non-universal power law,

$$M \sim (1-x)^{L_{\rm min}^d} = (1-x)^{(D/x_c^0)^{d/\phi}} \ . \tag{1.9}$$

We thus find that M is nonzero in the entire composition range $0 \le x < 1$, illustrating the notion of a smeared quantum phase transition.

[‡]This result is valid for $d < 2\phi$ which is fulfilled for our transition. In the opposite case, the integral over L_{RR} is dominated by its lower bound, resulting in a purely Gaussian dependence of M on $x - x_c^0$.

So far, we have focused on the zero-temperature order parameter. Other quantities can be found in an analogous manner. Let us, for example, determine the phase boundary, i.e., the composition dependence of the critical temperature T_c. As was discussed in Sec. 2.1, the static magnetism of the rare regions is destroyed at nonzero temperatures. Consequently, magnetic long-range order in the sample can only develop, if the rare regions are coupled by an interaction of the order of the temperature. The typical distance between neighboring locally ordered rare regions can be estimated from their density, ρ, as $r_{\rm typ} \sim \rho^{-1/d} \sim M^{-1/d}$. Within the Landau-Ginzburg-Wilson theory (1.1,1.2), the interaction between two rare regions drops off exponentially with their distance r, $E_{\rm int} \sim \exp(-r/\xi_b)$, where ξ_b is the bulk correlation length. This leads to a double-exponential dependence of T_c on x for compositions somewhat above x_c^0, i.e., $\ln(1/T_c) \sim \exp\{C(x-x_c^0)^{2-d/\phi}/[dx(1-x)]\}$. For $x \to 1$, we find $\ln(1/T_c) \sim (1-x)^{-L_{\rm min}^d/d}$. However, in a real metallic magnet, the locally ordered rare regions are coupled by an RKKY-type interaction that decays as a power law with distance, $E_{\rm int} \sim r^{-d}$, rather than exponentially.[65] (This interaction is not contained in the long-wavelength expansion implied in (1.2).) Therefore, the composition dependence of the critical temperature takes the same form as that of the magnetization,

$$T_c \sim \exp\left[-C\frac{(x-x_c^0)^{2-d/\phi}}{x(1-x)}\right] \tag{1.10}$$

for compositions somewhat above x_c^0 and

$$T_c \sim (1-x)^{L_{\rm min}^d} = (1-x)^{(D/x_c^0)^{d/\phi}} \tag{1.11}$$

in the far tail of the smeared transition, $x \to 1$.

We now turn to the order parameter susceptibility. It consists of two different contributions, one from the paramagnetic bulk system and one from the locally ordered rare regions. The bulk system provides a finite, non-critical background

throughout the tail of the smeared transition. Let us discuss the rare region contribution in more detail. At zero temperature, the total order parameter M is nonzero for all $x < 1$. The rare regions therefore always feel a symmetry-breaking effective field which cuts off any possible divergence of their susceptibilities. We conclude that the zero-temperature susceptibility does not diverge anywhere in the tail of the smeared transition. If the temperature is raised above T_c, the relative alignment of the rare regions is lost, and they behave as independent large (classical) moments, leading to a super-paramagnetic temperature dependence of the susceptibility, $\chi \sim 1/T$ (see Fig. 1). At even higher temperatures, when the damping of the quantum dynamics becomes unimportant, we expect the usual non-universal quantum Griffiths power-laws, $\chi \sim T^{\lambda-1}$, where λ is the Griffiths exponent.[17, 18, 66]

3. SMEARED CLASSICAL PHASE TRANSITION

Classical (thermal) phase transitions with uncorrelated disorder cannot be smeared because all rare regions are of finite size and can thus not undergo a true phase transition at any nonzero temperature. However, perfect disorder correlations in one or more dimensions lead to rare regions that are infinitely extended in the thermodynamic limit. If the number of correlated dimensions is high enough, these infinitely large rare regions can undergo the phase transition independently of the bulk system, leading to a smearing of the global phase transition.[60] This happens, for example, in a randomly layered Ising magnet, i.e., an Ising model with disorder correlated in two dimensions.[35]

In this section, we discuss how the theory of Sec. 2 is modified for these smeared classical phase transitions. For definiteness, we consider a classical Landau-Ginzburg-Wilson free energy in d dimensions,

$$S = \int d\mathbf{y}\ \psi(\mathbf{y})[r - \partial_{\mathbf{y}}^2]\psi(\mathbf{y}) + u \int d\mathbf{y}\ \psi^4(\mathbf{y})\,. \tag{1.12}$$

As in the quantum case, we now consider a binary "alloy" $A_{1-x}B_x$ of two materials A and B. The atoms are arranged randomly in $d_\perp$ dimensions, while they are perfectly correlated in $d_\parallel = d - d_\perp$ dimensions. For example, if $d_\perp = 1$ and $d_\parallel = 2$, the system would consist of a random sequence of layers, each made up of only A atoms or only B atoms.

If the correlated dimension $d_\parallel$ is sufficiently large, the "alloy" undergoes a smeared classical phase transition as the composition x is tuned from 0 to 1 at a (fixed) temperature at which material A is magnetically ordered, $r_A < 0$, while material B is in the nonmagnetic phase, $r_B > 0$. The optimal fluctuation theory for the behavior in the tail of the smeared transition can be developed along the same lines as the theory in Sec. 2. The only important difference stems from the fact that the randomness is restricted to $d_\perp$ dimensions. The dimensionality d in eqs. (1.8) and (1.9) therefore needs to be replaced by $d_\perp$, leading to

$$M \sim \exp\left[-C\frac{(x - x_c^0)^{2-d_\perp/\phi}}{x(1-x)}\right] \tag{1.13}$$

for compositions somewhat above x_c^0 and

$$M \sim (1-x)^{L_{\min}^{d_\perp}} = (1-x)^{(D/x_c^0)^{d_\perp/\phi}} \tag{1.14}$$

for $x \to 1$. The same substitution of d by $d_\perp$ was also found for smeared classical transitions tuned by temperature rather than composition.[60]

4. COMPUTER SIMULATIONS

To verify the predictions of the optimal fluctuation theory in Sec. 2 and to illustrate our results, we have performed computer simulations of a toy model, viz., a classical Ising model with d space-like dimensions and one time-like dimension. The interactions are between nearest neighbors in the space-like directions but infinite-ranged in the time-like ones. This $(d+1)$-dimensional toy model retains the possibility of static order on the rare regions (which is crucial for the transition being smeared) but permits system sizes large enough to study exponentially rare events. The Hamiltonian reads

$$H = -\frac{1}{L_\tau} \sum_{\langle \mathbf{y},\mathbf{z}\rangle,\tau,\tau'} S_{\mathbf{y},\tau} S_{\mathbf{z},\tau'} - \frac{1}{L_\tau} \sum_{\mathbf{y},\tau,\tau'} J_{\mathbf{y}} S_{\mathbf{y},\tau} S_{\mathbf{y},\tau'} \tag{1.15}$$

Here $\mathbf{y}$ and $\mathbf{z}$ are d-dimensional space-like coordinates and τ is the time-like coordinate. L_τ is the system size in time direction and $\langle \mathbf{y},\mathbf{z}\rangle$ denotes pairs of nearest neighbors on the hyper-cubic lattice in space. $J_{\mathbf{y}}$ is a quenched random variable having the binary distribution $P(J) = (1-x)\ \delta(J-J_h) + x\ \delta(J-J_l)$ with $J_h > J_l$. In this classical model L_τ plays the role of the inverse temperature in the corresponding quantum system and the classical temperature plays the role of the quantum tuning parameter. Because the interaction is infinite-ranged in time, the time-like dimension can be treated in mean-field theory. For $L_\tau \to \infty$, this leads to a set of coupled mean-field equations for the local magnetizations $m_{\mathbf{y}} = (1/L_\tau) \sum_\tau S_{\mathbf{y},\tau}$. They read

$$m_{\mathbf{y}} = \tanh \beta\ [J_{\mathbf{y}} m_{\mathbf{y}} + \sum_{\mathbf{z}} m_{\mathbf{z}} + h]\ , \tag{1.16}$$

where the sum is over all nearest neighbors of site $\mathbf{y}$ and $h \to 0$ is a very small symmetry-breaking magnetic field which we typically set to 10^{-12}. If all $J_{\mathbf{y}} \equiv J_h$, the system undergoes a (sharp) phase transition at $T_h = J_h + 2d$, and if all $J_{\mathbf{y}} \equiv J_l$, it

undergoes the transition at $T_l = J_l + 2d$. In the temperature range $T_h > T > T_l$, the phase transition can therefore be tuned by composition x.

The mean-field equations (1.16) can be solved efficiently in a self-consistency cycle. Using this approach, we studied systems in one, two, and three space dimensions. The system sizes were up to L=10000 in 1d, and up to $L = 100$ in 2d and 3d. For each parameter set, the data were averaged over a large number of disorder realizations. Details will be given with the individual results below.

Figure 2 shows an overview over the magnetization M as a function of composition x for a $(3+1)$-dimensional system at several values of the classical temperature in the interval $T_h > T > T_l$.

The figure clearly demonstrates that the magnetic phase extends significantly beyond the "average potential" value $x_c^0 = (T_h - T)/(T_h - T_l)$. In this sense, the magnetic phase in our binary alloy benefits from the randomness. In agreement with the smeared phase transition scenario, the data also show that $M(x)$ develops a pronounced tail towards $x = 1$. (By comparing different system sizes, we can exclude that the tail is due to simple finite-size rounding.[60]) We performed similar simulations for systems in one and two space dimensions, with analogous results.

To verify the theoretical predictions of the optimal fluctuation theory developed in Sec. 2, we now analyze the tail of the smeared phase transition in more detail. Figure 3 shows a semi-logarithmic plot of the magnetization M vs. the composition x for a $(1 + 1)$-dimensional system, a $(2 + 1)$-dimensional system, and a $(3 + 1)$-dimensional one. In all examples, the data follow the theoretical prediction (1.8) over at least 2 orders of magnitude in M in a transient regime of intermediate compositions x.

We also check the behavior of the magnetization for compositions very close to $x = 1$. Since (1.9) predicts a non-universal power law, we plot $\log(M)$ vs. $\log(1 - x)$ for a $(3 + 1)$-dimensional system in Fig. 4. The figure shows that the

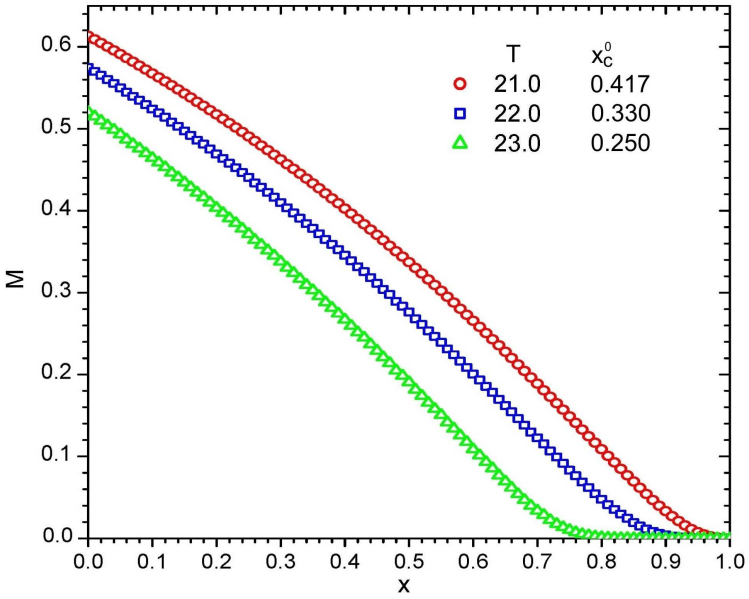

Figure 2: (Color online) Magnetization M vs composition x for a $(3+1)$-dimensional system having $J_h = 20$, $J_l = 8$ and several values of the classical temperature T. The data represent averages over 100 samples of size $L = 100$. The values of the critical concentration in "average potential approximation," x_c^0, are shown for comparison.

magnetization tail indeed decays as a power of $(1 - x)$ with $x \to 1$. The exponent increases with increasing temperature in agreement with the prediction that it measures the minimum size $N_{\min} \sim L_{\min}^d$ a rare regions needs to have to undergo the transition independently. The inset of Fig. 4 shows a fit of the exponent to $L_{\min}^d \sim [x_c^0(T)]^{-3/2} = [(T_h - T)/(T_h - T_l)]^{-3/2}$. The equation describes the data reasonably well; the deviations at small exponents can be explained by the fact that our theory assumes the rare-region size to be a continuous variable which is not fulfilled for rare regions consisting of just a few lattice sites.

Our computer simulation thus confirm the theoretical predictions in both composition regions in the tail of the transition. In a transient regime above x_c^0, we observe the exponential dependence (1.8) while the magnetization for $x \to 1$ follows the non-universal power law (1.9).

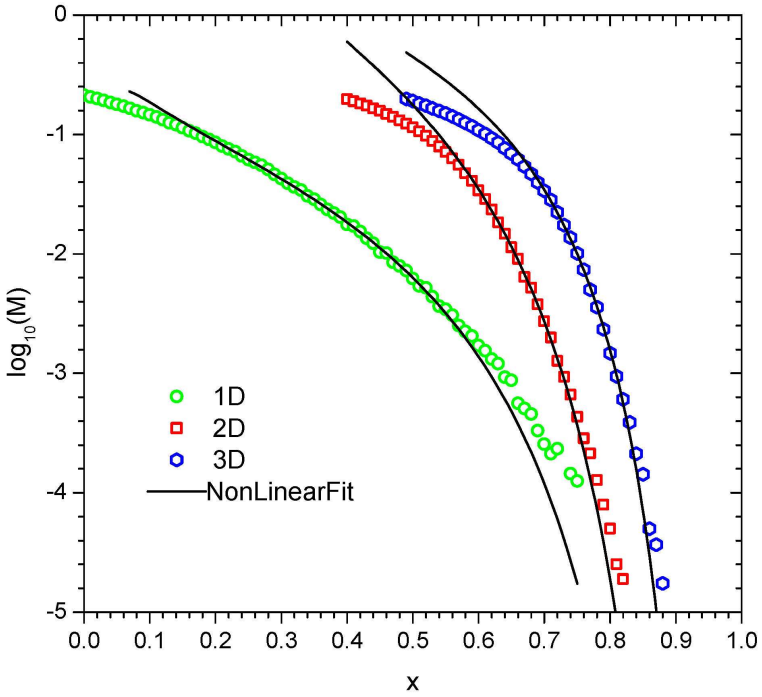

Figure 3: (Color online) $\log(M)$ vs x in the tail of the transition for three example systems: (i) $(3+1)$-dimensional system with $L = 100, J_h = 20, J_l = 8$, and $T = 23$, (ii) $(2+1)$-dimensional system with $L = 100, J_h = 15, J_l = 8$, and $T = 18$, and (iii) $(1+1)$-dimensional system with $L = 10000, J_h = 11, J_l = 8$, and $T = 12.8$. All data are averages over 100 disorder configurations. The solid lines are fits to (1.8), with the fit intervals restricted to $x \in (0.25, 0.55)$ in (1+1) dimensions, (0.6,0.72) in (2+1) dimensions and (0.7,0.82) for the (3+1)-dimensional example.

5. CONCLUSIONS

In summary, we have investigated phase transitions that are tuned by changing the composition x in a random binary alloy $A_{1-x}B_x$ where pure A is in the ordered phase while pure B is in the disordered phase. If individual, rare A-rich spatial regions develop true static order, they can be aligned by an infinitesimal residual interaction. This results in the smearing of the global phase transition, in agreement with the classification put forward in Ref.

As an example, we have studied the quantum phase transition of an itinerant Ising magnet of the type $A_{1-x}B_x$. At zero temperature, the ordered phase in this

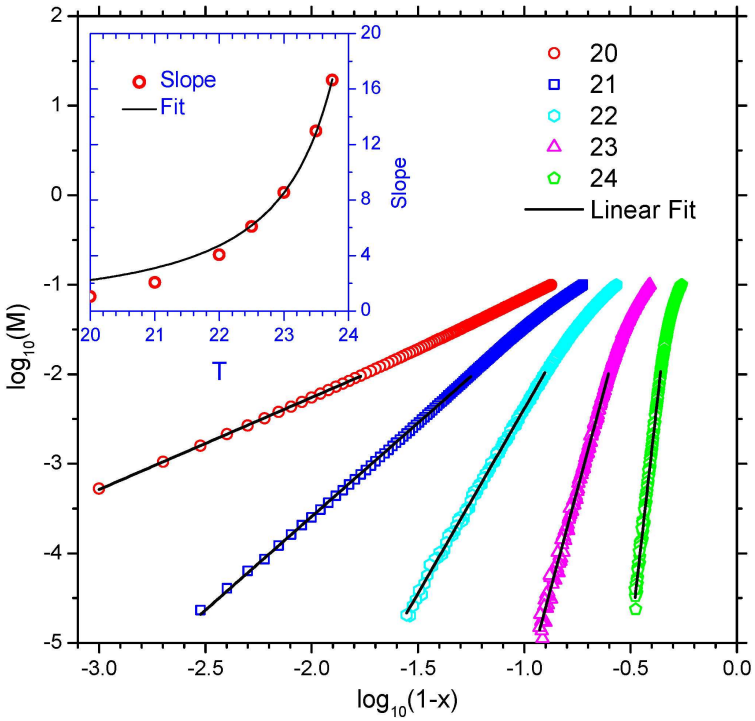

Figure 4: (Color online) $\log(M)$ vs $\log(1-x)$ for a $(3+1)$-dimensional system with $L = 100, J_h = 20, J_l = 8$ and several temperatures. All data are averages over 100 disorder configurations. The solid lines are fits to the power-law (1.9). The inset shows the exponent as a function of temperature, with the solid line being a fit to $[x_c^0(T)]^{-3/2}$.

binary alloy extends over the entire composition range $x < 1$, illustrating the notion of a smeared quantum phase transition. Upon raising the temperature, a sharp phase transition is restored, but the transition temperature $T_c(x)$ is nonzero for all $x < 1$ and reaches zero only right at $x = 1$ (see Fig. 1). Using optimal fluctuation theory, we have derived the functional forms of various thermodynamic observables in the tail of the smeared transition. We have also briefly discussed smeared classical phase transitions that can occur in systems with correlated disorder, and we have performed computer simulations of a toy model that confirm and illustrate the theory.

Although our results are qualitatively similar to those obtained for smeared phase transitions occurring at fixed randomness as a function of temperature or an

appropriate quantum control parameter, the functional forms of observables are not identical. The most striking difference can be found in the far tail of the transition. In the case of composition-tuning, the order parameter vanishes as a non-universal power of the distance from the end of the tail ($x = 1$), reflecting the fact that the minimum rare region size required for local magnetic order is finite. In contrast, if the transition occurs at fixed composition as a function of temperature or some quantum control parameter, the order parameter vanishes exponentially,[51, 60] because the minimum size of an ordered rare region diverges in the far tail. These differences illustrate the fact that the behavior of observables at a smeared phase transition is generally *not* universal in the sense of critical phenomena; it depends on details of the disorder distribution and how the transition is tuned. Only the question of whether or not a particular phase transition is smeared is universal, i.e., determined only by symmetries and dimensionalities.

Let us briefly comment on the relation of our theory to percolation ideas. The optimal fluctuation theory of Sec. 2.2 applies for compositions x larger than the percolation threshold of the A-atoms. Because the A-clusters are disconnected in this composition range, percolation of the A atoms does not play a role in forming the tail of the ordered phase at large x. Instead, distant rare regions are coupled via the fluctuations of the paramagnetic bulk phase and, in metallic magnets, via the RKKY interaction. Percolation does play a role, though, in the crossover between the inhomogeneous order in the tail of the transition and the bulk order at lower x.

We note in passing that the behavior of a diluted system (where B represents a vacancy) with *nearest-neighbor* interactions is not described by our theory. In this case, the A-clusters are not coupled at all for compositions x larger than the A percolation threshold. Therefore they cannot align, and long-range order is impossible. As a result, the super-paramagnetic behavior of the locally ordered clusters extends

all the way down to zero temperature. This was recently discussed in detail on the example of a diluted dissipative quantum Ising model.[67]

In the present paper, we have assumed that the A and B atoms are distributed independently over the lattice sites, i.e., we have assumed that there are no correlations between the atom positions. It is interesting to ask how the results change if this assumption is not fulfilled, for example because like atoms tend to cluster. As long as the correlations of the atom positions are short-ranged (corresponding to a finite, microscopic length scale for clustering), our results will not change *qualitatively*. All arguments in the optimal fluctuation theory still hold using a typical cluster of like atoms instead of a single atom as the basic unit. However, such clustering will lead to significant *quantitative* changes (i.e., changes in the non-universal constants in our results), as it greatly increases the probability of finding large locally ordered rare regions. We thus expect that clustering of like atoms will enhance the tail and move the phase boundary $T_c(x)$ towards larger x. A quantitative analysis of this effect requires explicit information about the type of correlations between the atom positions and is thus relegated to future work.

Let us finally turn to experiment. Tails of the ordered phase have been observed at many quantum phase transitions. However, it is often not clear whether these tails are an intrinsic effect or due to experimental difficulties such as macroscopic concentration gradients or other macroscopic sample inhomogeneities. Recent highly sensitive magneto-optical experiments on $Sr_{1-x}Ca_xRuO_3$ have provided strong evidence for a smeared ferromagnetic quantum phase transition.[§] The behavior of the magnetization and critical temperature in the tail of the smeared transition agree well with the theory developed here. Moreover, the effects of clustering discussed above may explain the wide variation of the critical composition between about 0.5 and 1 reported in earlier studies.[68, 69, 70] We expect that our smeared quantum

[§]L. Demko et al., unpublished.

phase transition scenario applies to a broad class of itinerant systems with quenched disorder.

6. ACKNOWLEDGEMENTS

We thank I. Kezsmarki for helpful discussions. This work has been supported in part by the NSF under grant no. DMR-0906566.

II. DISORDER CORRELATIONS AT SMEARED PHASE TRANSITIONS

Christopher Svoboda, David Nozadze, Fawaz Hrahsheh, and Thomas Vojta

[1] *Department of Physics, Missouri University of Science & Technology, Rolla, MO 65409*

ABSTRACT*

We investigate the influence of spatial disorder correlations on smeared phase transitions, taking the magnetic quantum phase transition in an itinerant magnet as an example. We find that even short-range correlations can have a dramatic effect and qualitatively change the behavior of observable quantities compared to the uncorrelated case. This is in marked contrast to conventional critical points, at which short-range correlated disorder and uncorrelated disorder lead to the same critical behavior. We develop an optimal fluctuation theory of the quantum phase transition in the presence of correlated disorder, and we illustrate the results by computer simulations. As an experimental application, we discuss the ferromagnetic quantum phase transition in $Sr_{1-x}Ca_xRuO_3$.

*Published in Europhysics Letters **97**, 20007 (2012).

1. INTRODUCTION

Quenched disorder has various important consequences in condensed matter. For example, disorder can change the universality class of a critical point [71, 72] or even change the order of a phase transition [73, 74, 75].

In theoretical studies, the disorder is often assumed to be uncorrelated in space even though many sample preparation techniques will produce some degree of correlations between the impurities and defects. As long as the correlations are short-ranged, i.e., characterized by a finite correlation length $\xi_{\rm dis}$, this assumption is usually justified if one is interested in the universal properties of critical points. (There are exceptions for special, fine-tuned local correlations [76]). The reason why short-range correlated disorder leads to the same behavior as uncorrelated disorder can be easily understood within the renormalization group framework. Under repeated coarse graining, a nonzero disorder correlation length $\xi_{\rm dis}$ decreases without limit. The disorder thus becomes effectively uncorrelated on the large length scales that determine the critical behavior.

A formal version of this argument follows from the Harris criterion [20]. It states that a clean critical point is stable against weak *uncorrelated* disorder if its correlation length critical exponent ν fulfills the inequality $d\nu > 2$ where d is the space dimensionality. If the inequality is violated, the disorder is relevant and changes the critical behavior. According to Weinrib and Halperin [77], *spatially correlated* disorder leads to the same inequality as long as its correlations decay faster than r^{-d} with distance r. Thus, short-range correlated disorder and uncorrelated disorder have the same effect on the stability of a clean critical point.

In this letter, we demonstrate that spatial disorder correlations are much more important at *smeared* phase transitions, a broad class of classical and quantum phase transitions characterized by a gradual, spatially inhomogeneous onset of the ordered

phase [17]. Specifically, we show that short-range correlated disorder and uncorrelated disorder lead to qualitatively different behaviors. The disorder correlations do not only influence quantities usually considered non-universal such as the location of the phase boundary, they also change the functional dependence of the order parameter and other quantities on the tuning parameters of the transition, as indicated in Fig. 1. We propose that this mechanism may be responsible for the unusually wide variations reported in the literature on the properties of the ferromagnetic quantum phase transition (QPT) in $Sr_{1-x}Ca_xRuO_3$.

In the following, we sketch the derivation of our theory, compute observables, and illustrate them by simulations. We also discuss the generality of our findings, and we compare them to experiment.

2. SMEARED QUANTUM PHASE TRANSITION

For definiteness, we consider a magnetic QPT in a metallic system with Ising order parameter symmetry. In the absence of quenched disorder, the Landau-Ginzburg-Wilson free energy functional of this transition is given by [14, 15]

$$S = \int dydz\ \psi(y)\Gamma(y,z)\psi(z) + u\int dy\ \psi^4(y)\,, \tag{2.1}$$

where ψ is the order parameter field, $y \equiv (\mathbf{y},\tau)$ comprises d-dimensional spatial position $\mathbf{y}$ and imaginary time τ, the integration means $\int dy \equiv \int d\mathbf{y}\int_0^{1/T} \mathrm{d}\tau$, and u is the standard quartic coefficient. The Fourier transform of the Gaussian vertex $\Gamma(y,z)$ reads

$$\Gamma(\mathbf{q},\omega_n) = r + \xi_0^2\mathbf{q}^2 + \gamma_0(\mathbf{q})\,|\omega_n|\ . \tag{2.2}$$

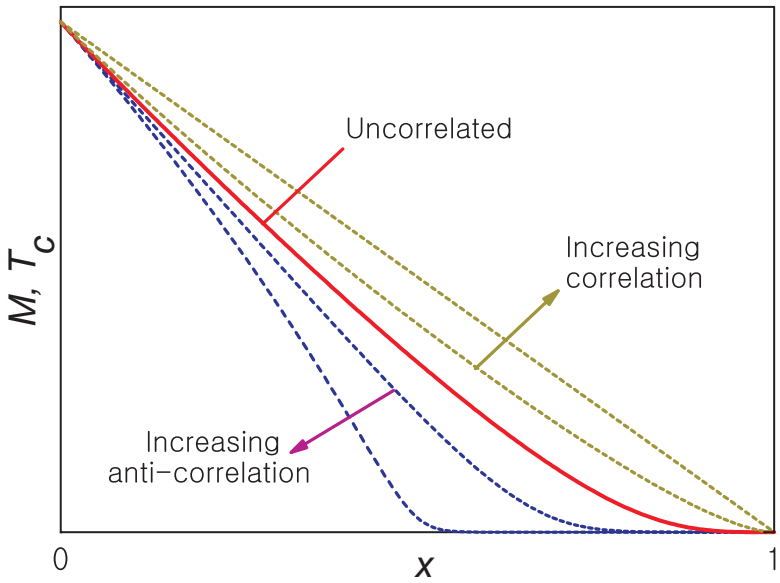

Figure 1: (Color online) Schematic of the zero-temperature magnetization-composition curve (M vs x) and the finite-temperature phase boundary (T_c vs x) at a smeared quantum phase transition in a random binary alloy $A_{1-x}B_x$. The cases of uncorrelated, correlated, and anti-correlated disorder are contrasted.

Here, r is the distance from criticality,[†] ξ_0 is a microscopic length, and ω_n is a Matsubara frequency. The dynamical part of $\Gamma(\mathbf{q}, \omega_n)$ is proportional to $|\omega_n|$. This reflects the Landau damping of the order parameter fluctuations by gapless electronic excitations in a metallic system. The coefficient $\gamma_0(\mathbf{q})$ is $\mathbf{q}$-independent for an antiferromagnetic transition but proportional to $1/|\mathbf{q}|$ or $1/|\mathbf{q}|^2$ for ballistic and diffusive ferromagnets, respectively.

We now consider a random binary alloy $A_{1-x}B_x$ consisting of two materials A and B. Pure substance B has a non-magnetic ground-state, implying a positive distance from quantum criticality, $r_B > 0$. Substance A has a magnetically ordered ground state with $r_A < 0$. By randomly substituting B atoms for A atoms, one can drive the system through a QPT from a magnetic to a nonmagnetic ground state.

[†]Strictly, one needs to distinguish the bare distance from criticality that appears in (2.2) from the renormalized one that measures the distance from the true critical point. We suppress this difference because it is unimportant for our purposes.

Due to statistical fluctuations, the distribution of A and B atoms in the alloy will not be spatially uniform. Some regions may contain significantly more A atoms than the average. If the local A-concentration is sufficiently high, such regions will be locally in the magnetic phase even if the bulk system is nonmagnetic. Because the magnetic fluctuations are overdamped, the quantum dynamics of sufficiently large such locally magnetic spatial regions completely freezes (for Ising symmetry [36]). At zero temperature, these rare regions thus develop static magnetic order independently of each other. This destroys the sharp QPT by smearing [17, 18, 51] and is manifest in a pronounced tail in the zero-temperature magnetization-composition curve [78].

At any nonzero temperature, the static magnetic order on individual, independent rare regions is destroyed because they can fluctuate via thermal excitations. Therefore, a finite interaction between the rare regions of the order of the thermal energy is necessary to align them. This restores a conventional sharp phase transition at any nonzero temperature. However, the smeared character of the underlying QPT leads an unusual concentration dependence of the critical temperature T_c which displays a tail towards large x [51, 78].

The effects of disorder correlations can be easily understood at a qualitative level. For positive correlations, like atoms tend to cluster. This increases, at fixed composition, the probability of finding large A-rich regions compared to the uncorrelated case. The tail of magnetization-composition curve therefore becomes larger (see Fig. 1). In contrast, like atoms repel each other in the case of negative correlations (anti-correlations). This decreases the probability of finding large A-rich regions and thus suppresses the tail.

3. OPTIMAL FLUCTUATION THEORY

To quantify the influence of the disorder correlations, we now develop an optimal fluctuation theory [51, 78]. We focus on the "tail" of the smeared transition (large x) where a few rare regions show magnetic order but their interactions are weak because they are far apart.

We roughly estimate the transition point in the alloy $A_{1-x}B_x$, by setting the average distance from criticality to zero, $r_{\rm av} = (1-x)r_{\rm A} + x r_{\rm B} = 0$. This defines the critical composition in "average-potential" approximation,

$$x_c^0 = -r_{\rm A}/(r_{\rm B} - r_{\rm A})\,. \tag{2.3}$$

For compositions $x > x_c^0$, static magnetic order can only develop on rare, atypical spatial regions with a higher than average A-concentration. Specifically, a single A-rich rare region of linear size $L_{\rm RR}$ can show magnetic order, if the local concentration $x_{\rm loc}$ of B atoms is below some critical value x_c. Because the rare region has a finite size, the critical concentration is shifted from the bulk value x_c^0. According to finite-size scaling [52, 53]

$$x_c(L_{\rm RR}) = x_c^0 - D L_{\rm RR}^{-\phi}\,, \tag{2.4}$$

where ϕ is the finite-size shift exponent and D is a non-universal constant. In a three-dimensional itinerant magnet, ϕ takes the mean-field value of 2 because the clean transition is above its upper critical dimension. As $x_c(L_{\rm RR})$ must be positive, a rare region must be larger than $L_{\rm min} = (D/x_c^0)^{1/\phi}$ to show magnetic order.

In the tail of the smeared transition, the magnetically ordered rare regions are far apart and interact only weakly. To find the total magnetization M one can thus

simply sum over all magnetically ordered rare regions. This gives

$$M \sim \int_{L_{\min}}^{\infty} dL_{RR} \int_{0}^{x_c(L_{\rm RR})} dx_{\rm loc} P(N, x_{\rm loc}) m(N, x_{\rm loc}) \,, \tag{2.5}$$

where $P(N, x_{\rm loc})$ is the probability for finding a region of N sites and local composition $x_{\rm loc}$ (i.e., a region containing $N_B = N x_{\rm loc}$ atoms of type B), and $m(N, x_{\rm loc})$ is its magnetization

Let us analyze the spatial distribution of atoms in the sample to determine the probability $P(N, x_{\rm loc})$. Specifically, let us assume that the random positions of the A and B atoms are positively correlated such that like atoms form clusters of typical correlation volume (number of lattice sites) $V_{\rm dis} \approx 1 + a\xi_{\rm dis}^d$ where $\xi_{\rm dis}$ is the disorder correlation length and a is a geometric prefactor. The probabilities for finding A and B clusters in the sample are $1 - x$ and x, respectively. The number $n_{\rm cl}$ of correlation clusters contained in a large spatial region of N sites ($N \gg V_{\rm dis}$) is approximately

$$n_{\rm cl} \approx N/V_{\rm dis} = N/(1 + a\xi_{\rm dis}^d) \ . \tag{2.6}$$

The probability $P(N, x_{\rm loc})$ for finding a region of N sites and local composition $x_{\rm loc}$ is therefore equal to the probability $P_{\rm clus}(n_{\rm cl}, n_{\rm B})$ for finding $n_{\rm B} = x n_{\rm cl}$ clusters of B atoms among all the $n_{\rm cl}$ clusters contained in the region. It can be modeled by a binomial distribution

$$P_{\rm clus}(n_{\rm cl}, n_{\rm B}) = \binom{n_{\rm cl}}{n_{\rm B}} (1-x)^{n_{\rm cl} - n_{\rm B}} x^{n_{\rm B}} \ . \tag{2.7}$$

We now distinguish two cases, (i) the regime where x is not much larger than x_c^0, and (ii) the far tail of transition at $x \to 1$.

(i) If x is just slightly larger than x_c^0, rare regions are large and the probability (2.7) can be approximated by a Gaussian

$$P_{\rm clus} \approx \frac{1}{\sqrt{2\pi x(1-x)/n_{\rm cl}}} \exp\left[-n_{\rm cl}\frac{(x_{\rm loc}-x)^2}{2x(1-x)}\right] . \tag{2.8}$$

We estimate the integral (2.5) in saddle point approximation. Neglecting subleading contributions from $m(N, x_{\rm loc})$, we find that rare regions of size $L_{\rm RR}^{\phi} = D(2\phi-d)/[d(x-x_c^0)]$ and composition $x_c(L_{\rm RR})$ dominate the integral. The resulting $M(x)$ dependence reads

$$M \sim \exp\left[-\frac{C}{(1+a\xi_{\rm dis}^d)}\frac{(x-x_c^0)^{2-d/\phi}}{x(1-x)}\right] , \tag{2.9}$$

where $C = 2(D/d)^{d/\phi}(2\phi-d)^{d/\phi-2}\phi^2$ is a non-universal constant. In this regime, varying the disorder correlation length thus modifies the non-universal prefactor of the exponential dependence of M on x.

(ii) An even more striking effect occurs in the tail of the transition for $x \to 1$. As rare regions cannot be large in this regime, the binomial distribution (2.7) cannot be approximated by a Gaussian. However, within saddle point approximation, the integral (2.5) is dominated by rare regions containing only A atoms and having the minimum size permitting local order. Inserting $L_{RR} = L_{\rm min} = (D/x_c^0)^{1/\phi}$ and $x_{\rm loc} = 0$ into (2.5), we find that the composition dependence of the magnetization is given by the power law,

$$M \sim (1-x)^{\beta} \qquad (x \to 1) , \tag{2.10}$$

with $\beta = aL_{\rm min}^d/(1+a\xi_{\rm dis}^d)$. In this regime, the disorder correlations thus modify the seeming critical exponent of the order parameter. The exponent value is given by the minimum number of correlation clusters necessary to form a magnetically ordered rare region. The results for uncorrelated disorder [78] are recovered by substituting $\xi_{\rm dis} = 0$ into (2.9) and (2.10).

So far we have assumed that a typical disorder correlation cluster of A atoms is smaller than the minimum rare region size required for magnetic order. For larger disorder correlation length $\xi_{\rm dis} \geq L_{\rm min}$, a single correlation cluster is already large enough to order magnetically. As a result, (almost) all A atoms contribute to the total magnetization. Correspondingly, the composition dependence of the order parameter is given by

$$M \sim (1-x)\,. \tag{2.11}$$

To combine the power laws (2.10) and (2.11) for different ranges of $\xi_{\rm dis}$, we construct the heuristic formula

$$\beta = (aL_{\rm min}^d + a\xi_{\rm dis}^d)/(1 + a\xi_{\rm dis}^d) \tag{2.12}$$

which can be used to fit experimental data or simulation results.

Other observables such as the finite-temperature phase boundary can be found in similar fashion. As discussed above, at $T \neq 0$, individual rare regions do not develop a static magnetization. Instead, global magnetic order arises via a conventional (sharp) phase transition at some transition temperature T_c which can be estimated from the condition that the interaction energy between the rare regions is of the order of the thermal energy. To determine the interaction energy, we note that in a metallic magnet, the rare-regions are coupled by an RKKY interaction which falls off as r^{-d} with distance r. As the typical distance between neighboring rare regions behaves as $r \sim M^{-1/d}$ [51], the composition dependence of the critical temperature is analogous to that of the magnetization. In particular,

$$T_c(x) \sim (1-x)^\beta \tag{2.13}$$

in the tail of the smeared transition, $x \to 1$.

4. SIMULATIONS

We now verify and illustrate the theoretical predictions by performing computer simulations of a toy model [51, 60]. Its Hamiltonian is motivated by the so-called quantum-to-classical mapping [12] which relates a quantum phase transitions in d space dimensions to a classical transition in $d+1$ dimensions. The extra space dimension corresponds to imaginary time in the quantum problem. Consequently, we consider a (3+1)-dimensional classical Ising model on a hypercubic lattice with three space dimensions and a single imaginary time-like dimension. The interaction in the time-like direction is long-ranged as the $|\omega_n|$ frequency dependence in (2.2) corresponds to a $1/\tau^2$ in imaginary time. In the toy model, we replace this interaction by an infinite-range interaction in time direction, both on the same site and between spatial neighbors.[‡] This correctly reproduces the smeared character of the phase transition due to static magnetic order on the rare regions. The Hamiltonian of the toy model takes the form

$$H = -\frac{1}{L_\tau} \sum_{\langle \mathbf{y},\mathbf{z}\rangle,\tau,\tau'} J_0 S_{\mathbf{y},\tau} S_{\mathbf{z},\tau'} - \frac{1}{L_\tau} \sum_{\mathbf{y},\tau,\tau'} J_{\mathbf{y}} S_{\mathbf{y},\tau} S_{\mathbf{y},\tau'} \ , \tag{2.14}$$

where $\mathbf{y}$ and $\mathbf{z}$ are space coordinates, τ is the time-like coordinate, and $S_{\mathbf{y},\tau} = \pm 1$. L_τ is the system size in time and $\langle \mathbf{y}, \mathbf{z}\rangle$ denotes pairs of nearest neighbors in space. $J_{\mathbf{y}}$ is a binary random variable whose value, J_h or J_l, is determined by the type of atom on lattice site $\mathbf{y}$. The values at different sites $\mathbf{y}$ and $\mathbf{z}$ are *not* independent, they are correlated according to some correlation function $\mathcal{C}(\mathbf{y}-\mathbf{z})$. The average concentrations of J_h-sites and J_l-sites are $1-x$ and x, respectively.

Treating the time-like dimension within mean-field theory, which is exact because of the infinite range of the interactions, a set of coupled nonlinear equations

[‡]Even though the bare action (2.1, 2.2) does not have an interaction between spatial neighbors at different imaginary times τ, such a coupling will be generated in perturbation theory (or under RG) from the short-range spatial interaction and the long-range interaction in time.

emerge for the local magnetizations $m_{\mathbf{y}} = (1/L_\tau) \sum_\tau S_{\mathbf{y},\tau}$,

$$m_{\mathbf{y}} = \tanh \frac{1}{T_{cl}} \left(J_{\mathbf{y}} m_{\mathbf{y}} + \sum_{\mathbf{z}} J_0 m_{\mathbf{z}} + h \right) . \tag{2.15}$$

Here, the $\mathbf{z}$-sum is over the nearest neighbors of site $\mathbf{y}$, and h is a tiny symmetry-breaking magnetic field. According to the quantum-to-classical mapping, the classical temperature T_{cl} is not related to the physical temperature of the underlying quantum system (which is encoded in L_τ) but rather some quantum control parameter that tunes the distance from the quantum phase transition.

The local mean-field equations (2.15) can be solved efficiently in a self-consistency cycle. In the two clean limits with either $J_{\mathbf{y}} = J_h$ or $J_{\mathbf{y}} = J_l$ for all $\mathbf{y}$, the phase transition occurs at $T_h = J_h + 6J_0$ and $T_l = J_l + 6J_0$, respectively. We choose a classical temperature between T_h and T_l and control the transition by changing the composition x.

To generate the correlated binary random variables representing the site occupations, a version of the Fourier-filtering method [79] is implemented. This method starts from uncorrelated Gaussian random numbers $u_{\mathbf{y}}$ and turns them into correlated Gaussian random numbers $v_{\mathbf{y}}$ characterized by some correlation function $\mathcal{C}(\mathbf{r})$. This is achieved by transforming the Fourier components $\tilde{u}_{\mathbf{q}}$ of the uncorrelated random numbers according to

$$\tilde{v}_{\mathbf{q}} = \left[\tilde{\mathcal{C}}(\mathbf{q}) \right]^{\frac{1}{2}} \tilde{u}_{\mathbf{q}}, \tag{2.16}$$

where $\tilde{\mathcal{C}}(\mathbf{q})$ is the Fourier transform of $\mathcal{C}(\mathbf{r})$. The $v_{\mathbf{y}}$ then undergo binary projection to determine the occupation of site $\mathbf{y}$; the site is occupied by atom A if $v_{\mathbf{y}}$ is greater than a composition-dependent threshold and by atom B if $v_{\mathbf{y}}$ is less than the threshold.

In the majority of our calculations, we focus on attractive short-range disorder correlations of the form $\mathcal{C}(\mathbf{r}) = \exp\left(-r^2/2\xi_{\text{dis}}^2\right)$. Figure 2 shows examples of the

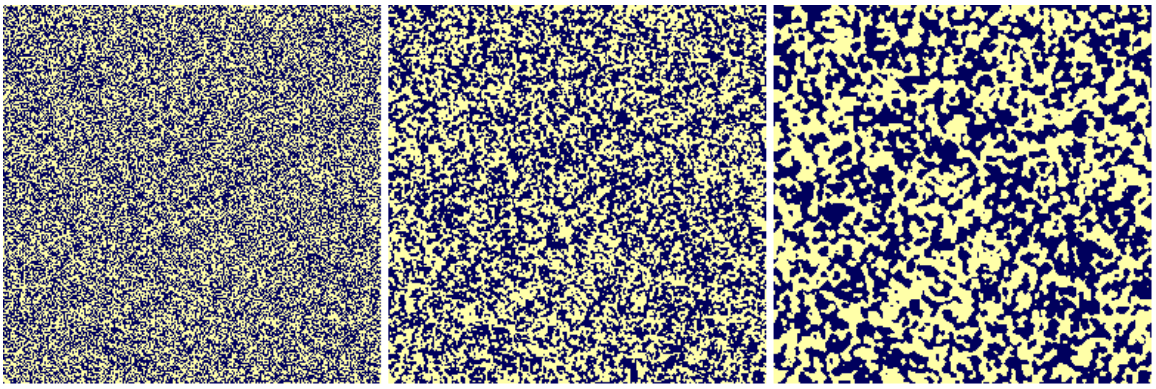

Figure 2: (Color online) Examples of the atom distribution in a plane of 256^2 sites for several values of the disorder correlation length $\xi_{\rm dis} = 0, 1.0, 2.0$ from left to right ($x = 0.5$).

resulting atom distributions for several values of the disorder correlation length $\xi_{\rm dis}$. The formation of clusters of like atoms is clearly visible.

We now discuss the results of the mean-field equations (2.15). Figure 3 presents the total magnetization M as function of composition x for several values of $\xi_{\rm dis}$ with all other parameters held constant. At a given composition x, the magnetization M increases significantly even for small $\xi_{\rm dis}$ of the order of the lattice constant. Moreover, the seeming transition point (at which M appears to reach 0) rapidly moves towards larger compositions, almost reaching $x = 1$ for a correlation length $\xi_{\rm dis} = 2$. Inset (a) of Fig. 3 shows a plot of $\log M$ versus $\log(1 - x)$ confirming the power-law behavior (2.10) in the tail of the transition. The dependence on $\xi_{\rm dis}$ of the exponents β extracted from these power laws is analyzed in inset (b) of Fig. 3. It can be fitted well with the heuristic formula (2.12).

In addition to the attractive (positive) correlations, we now briefly consider the case of anti-correlations (like atoms repel each other). We model the anti-correlations by a correlation function having values $\mathcal{C}(0) = 1$, $\mathcal{C}(\mathbf{r}) = -c$ for nearest neighbors, and $\mathcal{C}(\mathbf{r}) = 0$ otherwise. The positive constant c controls the strength of the

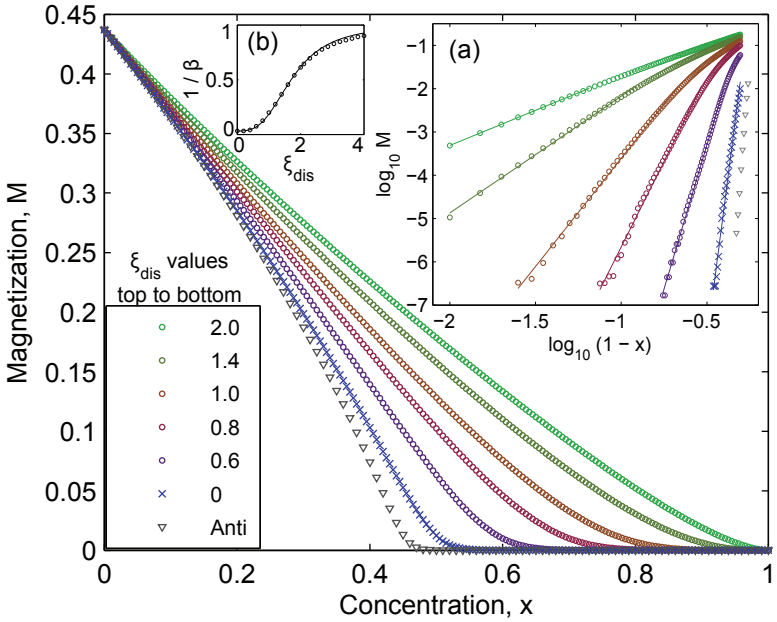

Figure 3: (Color online) Magnetization M vs. composition x for several values of the disorder correlation length $\xi_{\rm dis}$ using one disorder realization of 256^3 sites, $J_h = 20$, $J_l = 8$, $J_0 = 1$, $T_{cl} = 24.25$, and $h = 10^{-10}$. Also shown is one curve for the case of anti-correlations (128^3 sites), for details see text. Inset (a): log-log plot of M vs. $(1 - x)$ confirming the power-law behavior in the tail of the smeared transition. The tail exponent β shown in inset (b) agrees very well with (2.12) as shown by the solid fit line.

anti-correlations. A characteristic magnetization-composition curve for such anti-correlated disorder (with $c = 1/6$) is included in Fig. 3. The data show that the magnetization is reduced compared to the uncorrelated case, and the tail becomes less pronounced. Analogous simulations using different values of c show that this effect increases with increasing strength of the anti-correlations, as indicated in Fig. 1.

5. CONCLUSIONS

In summary, we have studied the effects of spatially correlated disorder on smeared phase transitions. We have found that even short-range disorder correlations

(extending over just a few lattice constants) lead to qualitative modifications of the behavior at smeared transitions compared to the uncorrelated case, including changes in the exponents that characterize the order parameter and the critical temperature. In other words, systems with uncorrelated disorder and with short-range correlated disorder behave differently

This is in marked contrast to critical points, at which uncorrelated disorder and short-range correlated disorder lead to the same critical behavior. (Long-range correlations do change the critical behavior [77, 80].) What causes this difference between critical points and smeared transitions? The reason is that critical behavior emerges in the limit of infinitely large length scales while smeared transitions are governed by a finite length scale, viz., the minimum size of ordered rare regions. This renders the renormalization group arguments underlying the generalized Harris criterion [20, 77] inapplicable.

The majority of our calculations are for the case of like atoms attracting each other. For these positive correlations, large locally ordered rare regions can form more easily than in the uncorrelated case. Thus, the tail of the smeared transition is enhanced; and the phase boundary as well as the magnetization curve move toward larger x as indicated in Fig. 1. We have also briefly considered the case of like atoms repulsing each other. These anti-correlations suppress the formation of large locally ordered rare regions compared to the uncorrelated case. As a result, the phase boundary and the magnetization curve will move toward smaller x. In addition to short-range correlations, we have also studied long-range power-law correlations which are interesting because they lead to a broad spectrum of cluster sizes. Detailed results will be published elsewhere [81].

Turning to experiment, our results imply that smeared phase transitions are very sensitive to slight short-range correlations in the spatial positions of impurities or defects. In particular, an analysis of the data in terms of critical exponents will

give values that depend on these correlations. We believe that a possible realization of the effects discussed in this paper can be found in $Sr_{1-x}Ca_xRuO_3$. This well-studied material undergoes a ferromagnetic QPT as a function of Ca concentration. Because $Sr_{1-x}Ca_xRuO_3$ is a metallic system with Ising spin symmetry, the transition is expected to be smeared [51]. Interestingly, the reported experimental phase diagrams (see Fig. 4) and magnetization curves show unusually large variations. Not only does the apparent critical composition change between $x \approx 0.5$ and 1; the functional form of the magnetization curves also varies. Although part of these discrepancies may be due to the difference between film and bulk samples [82], large variations within each sample type remain. We propose that disorder correlations, i.e., clustering or anti-clustering of like atoms may be responsible for at least part of these variations.

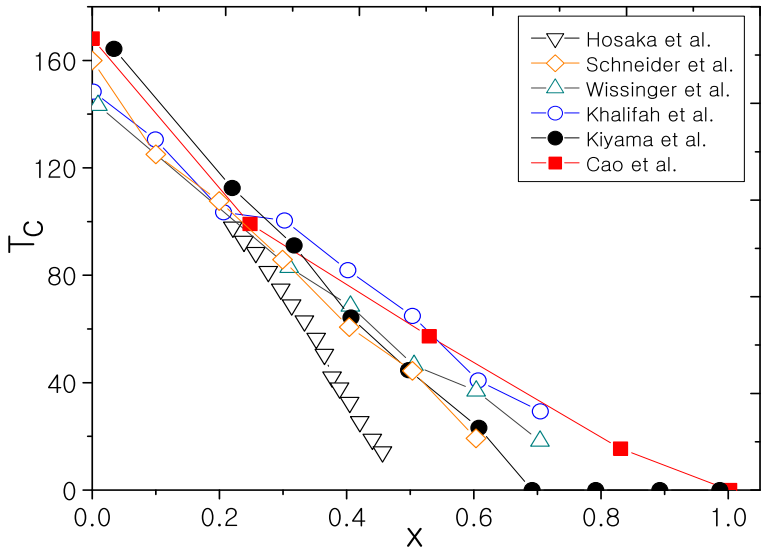

Figure 4: (Color online) Experimental temperature-composition phase diagrams of $Sr_{1-x}Ca_xRuO_3$. Data from Hosaka et al. [83], Schneider et al. [84], Wissinger et al. [82], and Khalifah et al. [85] are for thin films while those of Kiyama et al. [70], and Cao et al. [68] are for bulk samples. Published magnetization curves show similar variations.

Finally, we emphasize that even though we have considered the QPT in itinerant magnets as an example, our theory is very general and should be applicable to all phase transitions smeared by disorder including QPTs [59, 86, 87], classical transitions in layered systems [35, 60] and non-equilibrium transitions [88]

We thank I. Kezsmarki for helpful discussions. This work has been supported in part by the NSF under grant No. DMR- 0906566.

III. DISORDER PROMOTES FERROMAGNETISM: ROUNDING OF THE QUANTUM PHASE TRANSITION IN $SR_{1-X}CA_XRUO_3$

L. Demkó[1,2], S. Bordács[3,4], T. Vojta[5,6], D. Nozadze[6], F. Hrahsheh[6], C. Svoboda[6], B. Dóra[7,8], H. Yamada[9], M. Kawasaki[10,11,12], Y. Tokura[1], and I. Kézsmárki[1]

[1]*Department of Physics, Budapest University of Technology and Economics and Condensed Matter Research Group of the Hungarian Academy of Sciences, 1111 Budapest, Hungary*

[2]*Multiferroics Project, ERATO, Japan Science and Technology Agency (JST), c/o Department of Applied Physics, University of Tokyo, Tokyo 113-8656, Japan*

[3]*Department of Physics, Budapest University of Technology and Economics and Condensed Matter Research Group of the Hungarian Academy of Sciences, 1111 Budapest, Hungary*

[4]*Multiferroics Project, ERATO, Japan Science and Technology Agency (JST), c/o Department of Applied Physics, University of Tokyo, Tokyo 113-8656, Japan*

[5]*Max-Planck-Institut für Physik Komplexer Systeme, Nöthnitzer Str. 38, 01187 Dresden, Germany*

[6]*Department of Physics, Missouri University of Science and Technology, Rolla, MO 65409, USA*

[7]*Department of Physics, Budapest University of Technology and Economics and Condensed Matter Research Group of the Hungarian Academy of Sciences, 1111 Budapest, Hungary*

[8]*Max-Planck-Institut für Physik Komplexer Systeme, Nöthnitzer Str. 38, 01187 Dresden, Germany*

[9]*National Institute of Advanced Industrial Science and Technology (AIST), Tsukuba, Ibaraki 305-8562, Japan*

[10] *Cross-Correlated Materials Research Group (CMRG), RIKEN Advanced Science Institute (ASI), Wako 351-0198, Japan*

[11] *WPI-AIMR, Tohoku University, Sendai 980-8577, Japan*

[12] *Department of Applied Physics, University of Tokyo, Tokyo, 110-8656, Japan*

[13] *Department of Physics, Budapest University of Technology and Economics and Condensed Matter Research Group of the Hungarian Academy of Sciences, 1111 Budapest, Hungary*

ABSTRACT*

The subtle interplay of randomness and quantum fluctuations at low temperatures gives rise to a plethora of unconventional phenomena in systems ranging from quantum magnets and correlated electron materials to ultracold atomic gases. Particularly strong disorder effects have been predicted to occur at zero-temperature quantum phase transitions. Here, we demonstrate that the composition-driven ferromagnetic-to-paramagnetic quantum phase transition in $Sr_{1-x}Ca_xRuO_3$ is completely destroyed by the disorder introduced via the different ionic radii of the randomly distributed Sr and Ca ions. Using a magneto-optical technique, we map the magnetic phase diagram in the composition-temperature space. We find that the ferromagnetic phase is significantly extended by the disorder and develops a pronounced tail over a broad range of the composition x. These findings are explained by a microscopic model of smeared quantum phase transitions in itinerant magnets. Moreover, our theoretical study implies that correlated disorder is even more powerful in promoting ferromagnetism than random disorder.

*Published in Physical Review Letters **108**, 185701 (2012).

Classical or thermal phase transitions generally remain sharp in the presence of disorder, though their critical behavior might be affected by the randomness. On the other hand, zero-temperature quantum phase transitions [12, 16, 89] – which are induced by a control parameter such as the pressure, chemical composition or magnetic field – are more susceptible to the disorder. Nevertheless, most disordered quantum phase transitions have been found sharp as the correlation length characterizing the spatial fluctuation of the neighboring phases diverges at the transition point.

In recent years, it has become clear that the large spatial regions free of randomness, which are rare in a strongly disordered material and hereafter referred to as *rare regions*, can essentially change the physics of phase transitions [17]. Close to a magnetic transition, such rare regions can be locally in the magnetically ordered phase – with slow fluctuations leading to the famous Griffiths singularities [30] – even if the bulk system is still nonmagnetic. These rare regions are extremely influential close to quantum phase transitions. and expected to dominate the thermodynamics. They give rise to the the so-called quantum Griffiths phases [17, 18, 30] as recently observed in magnetic semiconductors [43], heavy-fermion systems [47], and transition metal alloys [48].

When the rare regions are embedded in a dissipative environment the disorder effects are further enhanced. For example, in metallic magnets, the magnetization fluctuations are coupled to electronic excitations having arbitrarily low energies. This leads to an over-damped fluctuation dynamics. Sufficiently strong damping completely freezes the dynamics of the locally ordered rare regions [36], allowing them to develop a static magnetic order. It has been predicted [51] that this mechanism destroys the sharp magnetic quantum phase transition in a disordered metal by rounding and a spatially inhomogeneous ferromagnetic phase appears over a broad range of the control parameter.

The family of perovskite-type $ARuO_3$ ruthanates (with A an alkaline earth ion) offers an ideal setting to test these predictions. $SrRuO_3$ is a ferromagnetic metal with a Curie temperature of $T_C = 165\,\mathrm{K}$. On the other hand, no long-range magnetic order develops in $CaRuO_3$ and recent studies indicate paramagnetic behavior or the presence of short-range antiferromagnetic correlations in the ground state [90]. It is demonstrated that tiny Co doping can drive the system to a low-temperature spin-glass state [91], however, the ground state of $CaRuO_3$ is still under debate. Earlier studies of the transport, thermal and magnetic properties of $Sr_{1-x}Ca_xRuO_3$ solid solutions revealed that the composition x is an efficient control parameter and the substitution of the Sr ions by the smaller Ca ions gradually suppresses the ferromagnetic character and with it the Curie temperature [68, 69, 70, 92]. However, estimates of the critical Ca concentration at which T_C vanishes show large variations depending on the way of the assignment, experimental methodology and sample synthesis (e.g. bulk crystals versus thin films with strain due to lattice mismatch with the substrate). In addition, the random distribution of Sr and Ca ions introduces strong disorder in the exchange interactions controlling the magnetic state.

To investigate the magnetic properties of $Sr_{1-x}Ca_xRuO_3$ with high accuracy, we have grown a composition-spread epitaxial film of size $10\,\mathrm{mm}\times 4\,\mathrm{mm}$ and thickness $200\,\mathrm{nm}$ ($\sim$ 500 unit cells) on a $SrTiO_3$ (001) substrate [93, 94] which sets the easy magnetization direction normal to the film plane [95]. The Ca concentration changes linearly from x=0.13 to 0.53 along the long side of the sample, as shown in Fig. 1a. The large atomically-flat area observed in the atomic force microscope image (Fig. 1a) demonstrates the high quality of this film.

The composition and temperature dependence of the magnetic properties of the $Sr_{1-x}Ca_xRuO_3$ film were probed by a home-built magneto-optical Kerr microscope equipped with a He-flow optical cryostat. Its magneto-optical Kerr rotation for visible light is dominated by the charge transfer excitations between the O 2p and

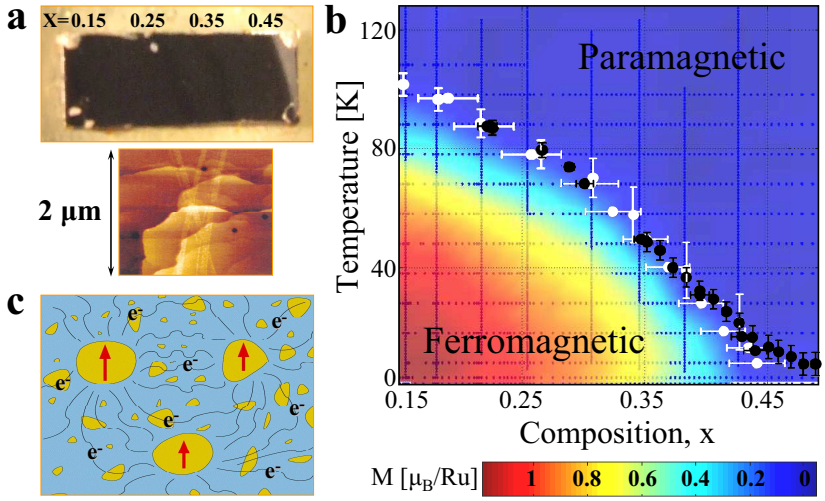

Figure 1: (Color online) Morphology and magnetic characterization of the composition-spread $Sr_{1-x}Ca_xRuO_3$ epitaxial film. **(a)** Photographic image of the $10\times4\,\mathrm{mm}^2$ film with the local concentration, x, indicated along the composition-spread direction. The large terraces of mono-atomic layers in the atomic force microscope image demonstrates the high quality of the film. **(b)** The contour plot of the remanent magnetization (M) over the composition-temperature phase diagram. The dotted mesh is the measured data set used for the interpolation of the surface. The ferromagnetic-paramagnetic phase boundary, $T_C(x)$, derived from the susceptibility and magnetization data (see text for details) is also indicated by the black and grey symbols, respectively. **(c)** Schematic of the magnetism in the tail of the smeared transition. The spins on Sr-rich rare regions (bright islands) form locally ordered "superspins". Their dynamics freezes due to the coupling to electronic excitations which also tends to align them giving rise to an inhomogeneous long-range ferromagnetic order.

Ru 4d t_{2g} states [83]. The large magnitude of the magneto-optical Kerr effect, being the consequence of strong spin-orbit coupling in ruthenates [96], was found to be proportional to the magnetization measured by a SQUID magnetometer on uniform thin films. We have performed all these experiments using a red laser diode. The resulting precisions of the magnetization (M) and susceptibility (χ) measurements were $6\cdot10^{-3}\,\mu_B$ per Ru atom and $8\cdot10^{-3}\,\mu_B\mathrm{T}^{-1}$ per Ru atom, respectively. Since the composition gradient of the sample is about $0.04\,\mathrm{mm}^{-1}$, the spatial resolution,

$\delta \lesssim 20\,\mu$m, of our microscope corresponds to a resolution of $\delta x \approx 0.001$ in the composition, allowing us to achieve an exceptionally fine mapping of the magnetization versus the control parameter of the quantum phase transition. See Supplemental Material at [97] for more details on the sample preparation, characterization, and on the experimental methodology.

An overview of the results is given in Fig. 1b which shows a color contour map of the remanent magnetization M as a function of the temperature T and the composition x. It was obtained by interpolating a large collection of $M(x)$ and $M(T)$ curves measured at constant temperatures and concentrations, respectively. The data clearly show that the area of the ferromagnetic phase and the magnitude of the low-temperature magnetization are gradually suppressed with increasing x. Figure 2 displays the temperature dependence of the magnetization and susceptibility for selected compositions. With increasing x, the upturn region in the magnetization curves significantly broadens and the width of the ac susceptibility peaks increases. This already hints at an unconventional smearing of the paramagnetic-to-ferromagnetic phase transition at higher values of the composition x. The critical temperature, $T_C(x)$ in Fig. 1b, separating the ferromagnetic and paramagnetic states in the composition-temperature phase diagram was identified with the peak positions in the susceptibility and in the first derivative of magnetization using both the temperature and the concentration sweeps.

The $T_C(x)$ line in Fig. 1b does not show a singular drop at any concentration, instead it grows a tail extending beyond $x = 0.52$ where the zero-temperature magnetization is about three orders of magnitude smaller than the saturation value for $SrRuO_3$. Similar behavior is also observed in the low-temperature magnetization M as a function of the composition, x, as shown in Fig. 3a. (We found that all $M(x)$ curves measured below T=6 K collapse onto each other without any detectable

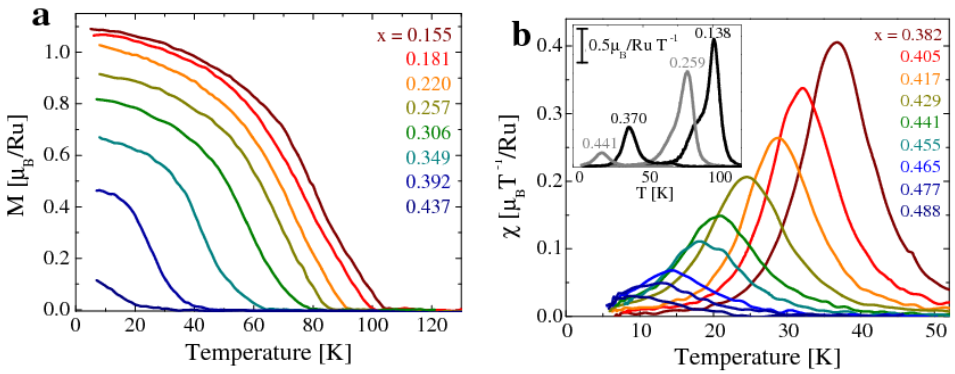

Figure 2: (Color online) Temperature dependence of **(a)** the remanent magnetization M and **(b)** ac susceptibility χ for selected compositions, x. The main panel of **(b)** focuses on the region $x \gtrsim 0.4$, and the inset displays representative susceptibility curves over the full range of x. Both the magnetization and susceptibility curves show the continuous suppression of the ferromagnetic phase with increasing x and the broadening of the transition.

temperature variation.) $M(x)$ has an inflection point at $x \approx 0.44$ followed by a pronounced tail region in which the magnetization decays slowly towards larger x. The existence of an ordered ferromagnetic moment is further confirmed by the hysteresis in the $M(B)$ loops even at $x = 0.52$ (see the inset of Fig. 3a). Thus, the evolution of both the magnetization and the critical temperature with x provide strong evidence for the ferromagnetic-to-paramagnetic quantum phase transition being smeared.

How can the unconventional smearing of the quantum phase transition and the associated tail in the magnetization be understood quantitatively? As the magnetization fluctuations in a metallic ferromagnet are over-damped, sufficiently large Sr-rich rare regions can develop true magnetic order (see Fig. 1c) even if the bulk system is paramagnetic [36, 51]. Macroscopic ferromagnetism arises because these rare regions are weakly coupled by an effective long-range interaction [42, 98]. To model this situation, we observe that the probability for finding $N_{\rm Sr}$ strontium and $N_{\rm Ca}$ calcium atoms in a region of $N = N_{\rm Sr} + N_{\rm Ca}$ unit cells (at average composition x) is given by the binomial distribution $P(N_{\rm Sr}, N_{\rm Ca}) = \binom{N}{N_{\rm Sr}}(1-x)^{N_{\rm Sr}} x^{N_{\rm Ca}}$. Such a region

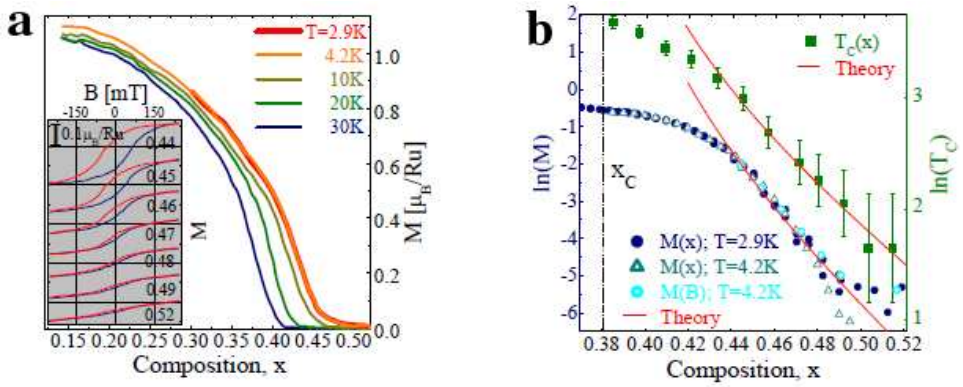

Figure 3: (Color online) The smearing of the quantum phase transition in $Sr_{1-x}Ca_xRuO_3$. **(a)** The composition dependence of the remanent magnetization M at selected temperatures. The inset shows that the hysteresis in the field loops at T=4.2 K gradually vanishes towards larger x but still present even at $x \approx 0.52$. **(b)** Semilogarithmic plots of the magnetization and the transition temperature T_C as functions of the control parameter in the tail region. The symbols represent the experimental data while solid lines correspond to the theory which predicts $x_c = 0.38$ as the location of the quantum phase transition in the (hypothetical) clean system.

orders magnetically if the local calcium concentration $x_{\rm loc} = N_{\rm Ca}/N$ is below some threshold x_c. Actually, taking finite-size effects into account [78], the condition reads $x_{\rm loc} < x_c - A/L_{RR}^2$ where L_{RR} is the size of the rare region, and A is a non-universal constant. To estimate the total magnetization in the tail of the transition ($x > x_c$), one can simply integrate the binomial distribution over all rare regions fulfilling this condition. This yields [78], up to power-law prefactors,

$$M \propto \exp\left[-C\frac{(x-x_c)^{2-d/2}}{x(1-x)}\right] \tag{3.1}$$

where C is a non-universal constant. This equation clearly illustrates the notion of "smeared" quantum phase transition: the order parameter vanishes only at $x = 1$ and develops a long, exponential tail upon approaching this point. As x_c represents the composition where the hypothetical homogeneous (clean) system having the average

ion size would undergo the quantum phase transition, the extension of the ferromagnetic phase beyond x_c is an effect of the disorder. Starting from atomic-scale disorder our theory is applicable as long as a large number of clusters are probed within the experimental resolution, so that the measured quantities represent an average over the random cluster distribution. The smooth dependence of the magnetization on x together with the small spot size of the beam ($<300\,\mu\mathrm{m}^2$) verifies that this is indeed the case. Based on the given spot size the upper bound for the typical cluster size is estimated to be 1-2 $\mu\mathrm{m}^2$ (see Supplemental Material).

As a direct test of our theory we fit the lowest-temperature $M(x)$ data with Eq. (3.1). We take the spatial dimensionality $d = 3$ due to the large thickness of the sample far beyond the spin correlation length in the system. As can be discerned in Fig. 3b, the magnetization data in the tail ($x \gtrsim 0.44$) follow the theoretical curve over about 1.5 orders of magnitude down to the resolution limit of the instrument. For the critical composition of the hypothetical clean system, we obtain $x_c = 0.38$, though the quality of the fit is not very sensitive to its precise value because the drop in M occurs over a rather narrow x interval. The composition dependence of the critical temperature T_C can be estimated along the same lines by comparing the typical interaction energies between the rare regions with the temperature and the same functional dependence on x was found [78]. The experimental data in the tail region follow this prediction with the same $x_c = 0.38$ value, as can be seen from the corresponding fit in Fig. 3b.

To summarize, we have studied the paramagnetic-to-ferromagnetic quantum phase transition of $Sr_{1-x}Ca_xRuO_3$ by means of a composition-spread epitaxial film. We found that the disorder significantly extends the ferromagnetic phase. Moreover, the phase transition in this itinerant system does not exhibit any of the singularities associated with a quantum critical point. Instead, both the magnetization and critical temperature display pronounced tails towards the paramagnetic phase. The

functional forms of these tails agree well with the predictions of our theoretical model. Our calculations also show that disorder, if correlated over a few unit cells, is even more powerful in promoting an inhomogeneous ferromagnetic phase. We thus conclude that our results provide, to the best of our knowledge, the first quantitative confirmation of a smeared quantum phase transition in a disordered metal. We expect that this scenario applies to a broad class of itinerant systems with quenched disorder.

We thank A. Halbritter and G. Mihály for fruitful discussions. This work was supported by KAKENHI, MEXT of Japan, by the Japan Society for the Promotion of Science (JSPS) through its "Funding Program for World-Leading Innovative R&D on Science and Technology (FIRST Program)", by Hungarian Research Funds OTKA PD75615, CNK80991, K73361, Bolyai program, TÁMOP-4.2.1/B-09/1/KMR-2010-0002, as well as by the NSF under grant No. DMR-0906566.

IV. QUANTUM GRIFFITHS SINGULARITIES IN FERROMAGNETIC METALS

David Nozadze and Thomas Vojta

[1]*Department of Physics, Missouri University of Science & Technology, Rolla, MO 65409*

ABSTRACT*

We present a theory of the quantum Griffiths phases associated with the ferromagnetic quantum phase transition in disordered metals. For Ising spin symmetry, we study the dynamics of a single rare region within the variational instanton approach. For Heisenberg symmetry, the dynamics of the rare region is studied using a renormalization group approach. In both cases, the rare region dynamics is even slower than in the usual quantum Griffiths case because the order parameter conservation of an itinerant ferromagnet hampers the relaxation of large magnetic clusters. The resulting quantum Griffiths singularities in ferromagnetic metals are stronger than power laws. For example, the low-energy density of states $\rho(\epsilon)$ takes the asymptotic form $\exp[-\{\tilde{\lambda}\log(\epsilon_0/\epsilon)\}^{3/5}]/\epsilon$ with $\tilde{\lambda}$ being non-universal. We contrast these results with the antiferromagnetic case in which the systems show power-law quantum Griffiths singularities in the vicinity of the quantum critical point. We also compare our result with existing experimental data of ferromagnetic alloy $Ni_{1-x}V_x$.

*Published in Physical Review B **85**, 174202 (2012), selected as an Editor's Suggestion.

1. INTRODUCTION

The low-temperature behavior of quantum many-particle systems can be sensitive to impurities, defects, or other kinds of quenched disorder. This effect is especially important near quantum phase transitions, where fluctuations in time and space become connected. The interplay between static disorder fluctuations and large-scale quantum fluctuations leads to much more dramatic effects at quantum phase transitions than at classical phase transitions, including quantum Griffiths singularities, [30, 99, 100] infinite-randomness critical points featuring exponential rather than power-law scaling, [22, 101] and the smearing of the transition.[51]

The Griffiths effects at a magnetic phase transition in a disordered system are caused by large spatial regions (rare regions) that are devoid of impurities and can show local magnetic order even if the bulk system is globally in the paramagnetic phase. The order parameter fluctuations induced by rare regions belong to a class of excitations known as *instantons*. Their dynamics is very slow because flipping the rare region requires a coherent change of the order parameter over a large volume. Griffiths showed [30] that this leads to a singular free energy, not just at the transition point but in a whole parameter region, which is now known as the Griffiths phase. In classical systems, the contribution of the rare regions to thermodynamic observables is very weak. However, due to the perfect disorder correlations in (imaginary) time, Griffiths effects at quantum phase transitions are enhanced and lead to power-law singularities in thermodynamic quantities (for reviews see, e.g., Refs. [17, 18]).

The systems in which quantum Griffiths behavior was originally demonstrated [22, 99, 100, 101] all have undamped dynamics (a dynamical exponent $z = 1$ in the clean system). However, many systems of experimental importance involve superconducting [102] or magnetic [13, 103, 104, 105] degrees of freedom coupled to conduction electrons. This leads to overdamped dynamics characterized by a clean dynamical

exponent $z > 1$. Studying the effects of the rare regions in this case is, therefore, an important issue. It has been shown that metallic Ising antiferromagnets can show quantum Griffiths behavior at higher energies, where the damping is less important. [66] In contrast, the quantum Griffiths singularities in Heisenberg antiferromagnets are caused by the dissipation and occur at lower energies. [31]

In recent years, indications of quantum Griffiths phases have been observed in experiments on a number of metallic systems such as magnetic semiconductors,[43, 44, 45] Kondo lattice ferromagnets, [46, 47] and transition metal ferromagnets.[48, 49] All these experimental observations of quantum Griffiths phases are in ferromagnets rather than in antiferromagnets. However, in contrast to antiferromagnets, a complete theory of quantum Griffiths phases in ferromagnetic metals does not yet exist.

In this paper, we therefore develop the theory of quantum Griffiths effects in ferromagnetic metals with both Ising and Heisenberg symmetries. We show that the quantum Griffiths singularities do not take power-law form, in contrast to those in antiferromagnets.[17, 18] The rare-region density of states behaves as $\rho(\epsilon) \sim \exp[-\{\tilde{\lambda}\log(\epsilon_0/\epsilon)\}^{3/5}]/\epsilon$ in the low-energy limit, where $\tilde{\lambda}$ plays a role analogous to the non-universal Griffiths exponent. This means that the Griffiths singularity is stronger than a pure power law. This kind of density of states leads to non-power-law dependencies on the temperature T of various observables, including the specific heat, $C \sim \exp[-\{\tilde{\lambda}\log(T_0/T)\}^{3/5}]$, and the magnetic susceptibility, $\chi \sim \exp[-\{\tilde{\lambda}\log(T_0/T)\}^{3/5}]/T$. The zero-temperature magnetization-field curve behaves as $M \sim \exp[-\{\tilde{\lambda}\log(H_0/H)\}^{3/5}]$.

The paper is organized as follows. In Sec. 2, we introduce the model: Landau-Ginzburg-Wilson order parameter field theories for ferromagnetic Ising and Heisenberg metals. In Sec. 3, we study the dynamics of a single rare region. For the Ising case, we use a variational instanton calculation, and for Heisenberg symmetry, we use a renormalization group theory of the quantum nonlinear sigma model with a

damping term. In Sec. 4, we average over all rare regions and calculate observables in the ferromagnetic quantum Griffiths phase. In Sec. 5, we compare our predictions with existing experimental data. Finally, we conclude in Sec. 6 by discussing the difference between ferromagnetic and antiferromagnetic quantum Griffiths singularities as well as some open questions.

2. THE MODEL

Rare region effects in disordered metallic systems are realized both in Ising magnets [66] and in Heisenberg magnets. [31] In the following, we consider both cases. Our starting point is a quantum Landau-Ginzburg-Wilson action of the itinerant ferromagnet [14, 15], [†]

$$S = S_{\rm stat} + S_{\rm diss} + S_{\rm dyn}\,, \tag{4.1}$$

where the static part has the form

$$S_{\rm stat} = E_0 \int_0^\beta d\tau \int d^3\mathbf{r} \Big[t\phi^2(\mathbf{r},\tau) + [\nabla\phi(\mathbf{r},\tau)]^2 + \frac{1}{2}\phi^4(\mathbf{r},\tau) \Big]\,. \tag{4.2}$$

Here, E_0 is a characteristic energy (assumed to be of the order of the band width in a transition metal compound or the order of the Kondo-temperature in an f-electron system). We measure lengths in units of the microscopic length scale ξ_0. $t > 0$ is the bare distance of the bulk system from criticality. $\phi(\mathbf{r},\tau)$ is the dimensionless order parameter field. It is a scalar for the Ising model, while it has three components (ϕ_1, ϕ_2, ϕ_3) for a Heisenberg magnet.

[†]We set Planck's constant and Boltzmann constant to unity ($\hbar = k_B = 1$) in what follows.

We consider disorder coupled to the square of the order parameter. The corresponding action has the form

$$S_{\rm diss} = E_0 \int_0^\beta d\tau \int d^3\mathbf{r}\; V(\mathbf{r})\phi^2(\mathbf{r},\tau)\,, \tag{4.3}$$

where $V(\mathbf{r})$ is the disorder potential.

The dynamical part of Eq. (4.1) is $S_{\rm dyn} = S^{(1)}_{\rm dyn} + S^{(2)}_{\rm dyn}$, where

$$S^{(1)}_{\rm dyn} = E_0\tau_m^2 \int_0^\beta d\tau \int d^3\mathbf{r}[\partial_\tau\phi(\mathbf{r},\tau)]^2\,, \tag{4.4}$$

corresponds to the undamped dynamics of the system with the clean dynamical exponent $z = 1$, while

$$S^{(2)}_{\rm dyn} = \frac{\gamma T}{E_0}\sum_{\omega_n} |\omega_n| \int d^3\mathbf{q}\; \frac{|\tilde{\phi}(\mathbf{q},\omega_n)|^2}{|\mathbf{q}|^a}\,, \tag{4.5}$$

describes overdamped dynamics with conserved order parameter (clean dynamical exponent $z = 2 + a$), which stems from the coupling to the conduction electrons. In Eq. (4.4), τ_m is a microscopic time, and in Eq. (4.5), γ parametrizes the strength of the dissipation. $\tilde{\phi}(\mathbf{q},\omega_n)$ is the Fourier transform of the order parameter $\phi(\mathbf{r},\tau)$ in momentum and Matsubara frequency. The value of a depends on the character of the electron motion in the system and equals 1 or 2 for ballistic and diffusive ferromagnets, respectively.

3. DYNAMICS OF A SINGLE RARE REGION

In this section, we study the dynamics of a single droplet formed on a rare region of linear size L. This means, we consider a single spherical defect of radius L

at the origin with potential $V(r) = -V$ for $r < L$, and $V(r) = 0$ otherwise. We are interested in the case $V > 0$, i.e., in defects that favor the ordered phase.

The effective dimensionality of the model defined by Eq. (4.1) is $d_{\rm eff} = 3 + z$. Thus, the clean model (4.1) is above its upper critical dimension ($d_c = 4$), implying that mean-field theory is valid. The mean-field equation for a static order parameter configuration $\phi_0(r)$ is [36]

$$\nabla^2\phi_0(r) + [t + V(r)]\phi_0(r) + \phi_0^3(r) = 0\,, \tag{4.6}$$

with solution

$$\phi_0(r) = \begin{cases} \phi_0 & \text{for} \quad r < L \\ \frac{\phi_0 L}{r} e^{-rt^{1/2}} & \text{for} \quad r > L. \end{cases} \tag{4.7}$$

This implies that the order parameter is approximately constant in the region $r < L$ and decays outside of it.

To study the dynamics of the droplet, we start from the variational instanton approach.[37] In the simplest case, the droplet maintains its shape while collapsing and reforming. In order to estimate the action associated with this process, we make the ansatz

$$\phi(r, \tau) = \phi_0'(r)\eta(\tau)\,. \tag{4.8}$$

Here, $\phi_0'(r)$ must be chosen such that $\int d^3\mathbf{r}\phi(r, \tau)$ is time independent because of order parameter conservation in an itinerant ferromagnet. This can be done by introducing $\phi_0'(r) = \phi_0(r)(1 - Ar)$ such that the $\mathbf{q} = 0$ Fourier component is canceled. A is a constant to be determined. In the limit of a large rare region, $Lt >> 1$, we find

$$\phi_0'(r) = \phi_0(r)\left(1 - \frac{4}{3}\frac{r}{L}\right)\,. \tag{4.9}$$

In the following subsections, using ansatz Eq. (4.8), we separately discuss the dynamics of the droplet in itinerant Ising and Heisenberg ferromagnets.

3.1. Itinerant Ising Model. We now calculate the tunneling rate between the "up" and "down" states of a single rare region in an itinerant Ising ferromagnet by carrying out variational instanton calculations.[37, 106] To estimate the instanton action, we use the ansatz Eq. (4.8) (which provides a variational upper bound for the instanton action) with $\eta(\tau) = \pm 1$ for $\tau \to \pm\infty$. Inserting this ansatz into the action Eq. (4.1) and integrating over the spatial variables yields, up to constant prefactors,

$$S_{\rm stat} \sim L^3 \int d\tau [-2\eta^2(\tau) + \eta^4(\tau)] \,, \tag{4.10}$$

and

$$S^{(1)}_{\rm dyn} \sim L^3 \int d\tau [\partial_\tau \eta(\tau)]^2 \,. \tag{4.11}$$

The part of the action corresponding to the overdamped dynamics becomes

$$S^{(2)}_{\rm dyn} = \frac{\alpha}{4} \int d\tau d\tau' \frac{d\eta}{d\tau} \frac{d\eta}{d\tau'} \log \frac{(\tau - \tau')^2 + \tau_m^2}{\tau_m^2} \,, \tag{4.12}$$

where the dimensionless dissipation strength $\alpha \sim \gamma L^{3+a}$. In order to estimate the action Eqs. (4.10) to (4.12), we make the variational ansatz

$$\frac{d\eta}{d\tau} = \frac{2\theta(\tau_0^2 - 4\tau^2)}{\tau_0} \,. \tag{4.13}$$

Summing all contributions, we obtain the instanton action

$$S \sim L^3/\tau_0 + L^3\tau_0 + \gamma L^{3+a} \log(\tau_0/\tau_m) \,. \tag{4.14}$$

Minimizing this action over the instanton duration gives $\tau_0 \sim L^{-a}/\gamma$. Correspondingly, the action is $S \sim \gamma L^{3+a}$. Then, the bare tunneling rate or tunnel splitting behaves as

$$\epsilon \sim \exp(-S) \sim \exp(-\text{const.} \times \gamma L^{3+a}) \,. \tag{4.15}$$

Thus, the bare tunneling rate decays exponentially with L^{3+a} in the itinerant Ising ferromagnet unlike the tunneling rate in the itinerant Ising antiferromagnet,[36, 37] which decays exponentially with L^3. The extra factor L^a can be understood as follows. To invert the magnetization of a rare region of linear size L, magnetization must be transported over a distance of the order of L, because the order parameter conservation prevents local spin flips. The rare region dynamics thus involves modes with wave vectors of the order of $q \sim 1/L$. Since the part of the action corresponding to the overdamped dynamics Eq. (4.5) is inversely proportional to momentum q^a, we obtain an extra factor L^a in the action Eq. (4.12).

Within renormalization group methods,[61] the instanton-instanton interaction renormalizes the zero-temperature tunneling rate to

$$\epsilon_{\text{ren}} \sim \epsilon^{1/(1-\alpha)} \,. \tag{4.16}$$

This implies that at zero temperature, the smaller rare regions with $\alpha < 1$ continue to tunnel with a strongly reduced rate, while the larger rare regions ($\alpha > 1$) stop to tunnel and behave classically, leading to super-paramagnetic behavior.

3.2. Itinerant Heisenberg Model. A particularly interesting case are itinerant Heisenberg ferromagnets because quantum Griffiths phases have been observed experimentally in these systems.[47, 48, 49] We now study the dynamics of a single rare region in an itinerant Heisenberg ferromagnet. We make the ansatz

$$\phi(r, \tau) = \phi_0'(r)\mathbf{n}(\tau) \,, \tag{4.17}$$

Here, $\mathbf{n}(\tau)$ is a three-component unit vector. After substituting Eq. (4.17) into the action Eq. (4.1) and integrating over the spatial variables, we obtain

$$S \sim g\tau_m^2 \int d\tau [\partial_\tau \mathbf{n}(\tau)]^2 + \frac{\alpha}{4} \int d\tau d\tau' \frac{\mathbf{n}(\tau) \cdot \mathbf{n}(\tau')}{(\tau - \tau')^2 + \tau_m^2} \,, \tag{4.18}$$

where the dimensionless coupling constant $g \sim L^3$ and $\alpha \sim \gamma L^{3+a}$ as before. Because there is no barrier in a system with continuous order parameter symmetry, the static part of the action is constant. Therefore, we cannot solve the problem within the variational instanton approach. Instead, rotational fluctuations must be taken into account.

We calculate the characteristic relaxation time of the rare region by a renormalization group analysis of the action Eq. (4.18). As shown in Sec. 7, for weak damping $\alpha \ll g$, there are two different regimes, where the behaviors of the relaxation times are different. Particularly, for energies ω larger than some crossover energy $\omega_c \sim \alpha/g$, undamped dynamics is dominant, and the relaxation time of the rare region has the form

$$\xi_g^\tau \sim L^3 \,, \tag{4.19}$$

which leads to a power-law dependence of the rare-region characteristic energy on L,

$$\epsilon \sim L^{-3} \,. \tag{4.20}$$

For energies $\omega \ll \omega_c$, overdamped dynamics dominates the system properties, and the relaxation time of the rare region behaves as

$$\xi_\gamma^\tau \sim \exp[\text{const.} \times \gamma L^{3+a}] \,. \tag{4.21}$$

This results in a characteristic energy of

$$\epsilon \sim \exp[-\text{const.} \times \gamma L^{3+a}] \,. \tag{4.22}$$

Thus, the behavior of the characteristic energy in the itinerant Heisenberg magnet is the analogous to that of the tunneling rate in the Ising model discussed above.

We can now roughly estimate the size L_c of the rare region corresponding to the crossover of the two regimes. By comparing Eqs. (4.19) and (4.21), we find for small α:

$$L_c \sim [\log(\text{const.}/\gamma)/\gamma]^{1/(3+a)} \,. \tag{4.23}$$

For small rare regions, $L < L_c$, the undamped dynamics dominates systems properties and the characteristic energy is given by Eq. (4.20), while for $L > L_c$, the damping term is dominant and the characteristic energy is determined by Eq. (4.22).

For large damping $\alpha \gg g$, the overdamped dynamics dominates the system properties for all energies ω. Correspondingly, the characteristic energy is given by Eq. (4.22).

4. OBSERVABLES

In the last section, we have seen that metallic Ising ferromagnets display modified Griffiths behavior at higher energies [Eq. (4.15)], while at asymptomatically low energies, the rare regions freeze and lead to a smeared phase transition [Eq. (4.16)]. For Heisenberg ferromagnets, we have found conventional behavior at higher energies [Eq. (4.20)], and modified Griffiths behavior at low energies [Eq. (4.22)]. Correspondingly, we expect modified Griffiths singularities in thermodynamic quantities at low energies for itinerant Heisenberg ferromagnets, while for metallic Ising ferromagnets they should occur at higher energies.

In this section, we use the single-rare-region results of Sec. 3 to study the thermodynamics in these ferromagnetic quantum Griffiths phases. To do so, we need to estimate the rare-region density of states. By basic combinatorics (see, e.g., Refs. [17, 18]), the probability for finding an impurity-free rare region of volume L^3 is $\mathcal{P} \sim \exp(-bL^3)$ with b being a constant that depends on the disorder strength. Combining this and Eq. (4.22) gives the density of states (of the Heisenberg system) in the low-energy regime as

$$\rho(\epsilon) \sim \frac{1}{\epsilon} \exp[-\{\tilde{\lambda} \log(\epsilon_0/\epsilon)\}^{3/(a+3)}] \,. \tag{4.24}$$

Here, ϵ_0 is a microscopic energy scale, and the non-universal exponent $\tilde{\lambda} \sim b^{(a+3)/3}/\gamma$ plays a role similar to the usual quantum Griffiths exponent. The same density of states follows from Eq. (4.15) for the higher-energy regime of the Ising model. Thus, in ferromagnetic metals, the rare-region density of states does not take power-law form, in contrast to the one in antiferromagnets.

We can now find observables using the rare-region density of states Eq. (4.24). The number n of free rare regions at temperature T behaves as

$$\begin{aligned} n(T) &\sim \int d\epsilon \rho(\epsilon) e^{-\epsilon/T}/(1+e^{-\epsilon/T}) \\ &\sim \exp[-\{\tilde{\lambda} \log(T_0/T)\}^{3/(a+3)}] \,, \end{aligned} \tag{4.25}$$

where T_0 is a microscopic temperature scale.

The uniform static susceptibility can be estimated by summing Curie susceptibilities for all free rare regions, yielding

$$\chi(T) = n(T)/T \sim \frac{1}{T} \exp[-\{\tilde{\lambda} \log(T_0/T)\}^{3/(a+3)}] \,. \tag{4.26}$$

The dependence of the moment μ of the rare region on its energy leads to a subleading correction only.

The contribution of the rare regions to the specific heat C can be obtained from

$$\begin{aligned} \Delta E &\sim \int d\epsilon \rho(\epsilon) \epsilon \; e^{-\epsilon/T}/(1+e^{-\epsilon/T}) \\ &\sim T \exp[-\{\tilde{\lambda} \log(T_0/T)\}^{3/(a+3)}] \,, \end{aligned} \tag{4.27}$$

which gives $\Delta C \sim \exp[-\{\tilde{\lambda} \log(T_0/T)\}^{3/(a+3)}]$. Knowing the specific heat, we can find the rare region contribution to the entropy as $\Delta S \sim \exp[-\{\tilde{\lambda} \log(T_0/T)\}^{3/(a+3)}]$.

To determine the zero-temperature magnetization in a small ordering field H, we note that rare regions with $\epsilon < H$ are (almost) fully polarized while the rare regions with $\epsilon > H$ have very small magnetization. Thus,

$$m \sim \int_0^H d\epsilon \rho(\epsilon) \sim \exp[-\{\tilde{\lambda} \log(H_0/H)\}^{3/(a+3)}] \,, \tag{4.28}$$

where H_0 is a microscopic field (again, the moment of the rare region leads to a subleading correction). The zero-temperature dynamical susceptibility can be obtained by summing the susceptibilities of the individual rare regions using the density of states Eq. (4.24),

$$\chi(\omega) = \int_0^\Lambda d\epsilon \rho(\epsilon) \chi_{\rm rr}(\omega;\epsilon) \,, \tag{4.29}$$

where the dynamical susceptibility of a single rare region in Heisenberg metals at zero temperature is given by [107]

$$\chi_{\rm rr}(\omega + i0;\epsilon) = \frac{\mu^2}{\epsilon - i\gamma\omega} \,, \tag{4.30}$$

where μ is the moment of the rare region. Substituting Eq. (4.30) into Eq. (4.29) we find

$$\chi(\omega+i0) \sim \frac{(1+i\gamma\,\mathrm{sgn}(\omega))}{|\omega|}\exp[-\{\tilde{\lambda}\log|\omega_0/\omega|\}^{3/(a+3)}]\,, \tag{4.31}$$

where ω_0 is a microscopic frequency. This result can be used to estimate the rare region contribution to the NMR spin relaxation time T_1. Inserting Eq. (4.31) into Moriya's formula [108] for the relaxation rate yields

$$1/T_1 \sim \frac{T}{\omega^2}\exp[-\{\tilde{\lambda}\log|\omega_0/\omega|\}^{3/(a+3)}]\,. \tag{4.32}$$

5. EXPERIMENT

Recently, indications of a quantum Griffiths phase have been observed in the transition metal ferromagnet $Ni_{1-x}V_x$. [48, 49] The behavior of the thermodynamics has been described well in terms of the power-low quantum Griffiths singularities predicted for an itinerant antiferromagnet (and the transverse-field Ising model). Here, we compare our new theory of ferromagnetic quantum Griffiths phases with the experimental data given in Refs. [48, 49]. The residual resistivity of $Ni_{1-x}V_x$ close to the quantum phase transition is rather high. [‡] Thus, we choose $a = 2$ for a diffusive ferromagnet. Figure 1 shows the behavior of the susceptibility as a function of temperature. The curves corresponding to the concentrations $x = 13.0\%$ and $x = 15.0\%$ (which are far away from the critical concentration $x_c \approx 11.5\%$) are described better by power laws rather than our modified quantum Griffiths behavior Eq. (4.26), at least above $T \approx 10$K (the low-temperature upturn is likely due to freezing of the rare regions). For concentrations $x = 12.07\%$ and $x = 12.25\%$, our theory fits better than power-law Griffiths singularities and extends the fit range from

[‡]A. Schroeder, private communications

30–300K down to 5–300K. The curves corresponding to the concentrations $x = 11.4\%$ and $x = 11.6\%$ can be fitted by Griffiths power-laws only in the temperature range 30 to 300 K, our new functional form Eq. (4.26) does not improve the fit of these curves.

We also compared the prediction Eq. (4.28) for a modified magnetization-field curve with the data given in Refs. [48, 49]. We found that the fits to power-laws and to the modified quantum Griffiths behavior Eq. (4.28) cannot be distinguished.

Let us also point out that the susceptibility data in the temperature range below 20K can be fitted reasonable well by Eq. (4.26); see details in Fig. 1. Further experiments may be necessary to decide whether our theory applies in this region.

Overall, our theory does not significantly improve the description of the data of Refs. [48, 49] over the temperature range where Griffiths behavior is observed. A possible reason is that the relevant rare regions are too small. At concentrations $x = 13.0\%$ and $x = 15.0\%$, they have moments of about $\mu \approx 5\mu_B$ and $\mu \approx 1\mu_B$, respectively. Correspondingly, the effect of the order parameter transport cannot play any role, whereas our functional forms arise for large rare regions where the order parameter transport limits the relaxation of the rare region. A possible reason why the curves corresponding to the concentrations $x = 11.4\%$ and $x = 11.6\%$ can not be described by our theory at $T < 30$K might be that the curves are actually slightly on the ordered side of the quantum phase transition.

6. CONCLUSIONS

In summary, we studied the dynamics of rare regions in disordered metals close to the ferromagnetic quantum phase transition, considering the cases of both Ising and Heisenberg spin symmetries. The overall phenomenology is similar to the well-studied antiferromagnetic quantum Griffiths behavior. [31, 37, 51, 66] Namely,

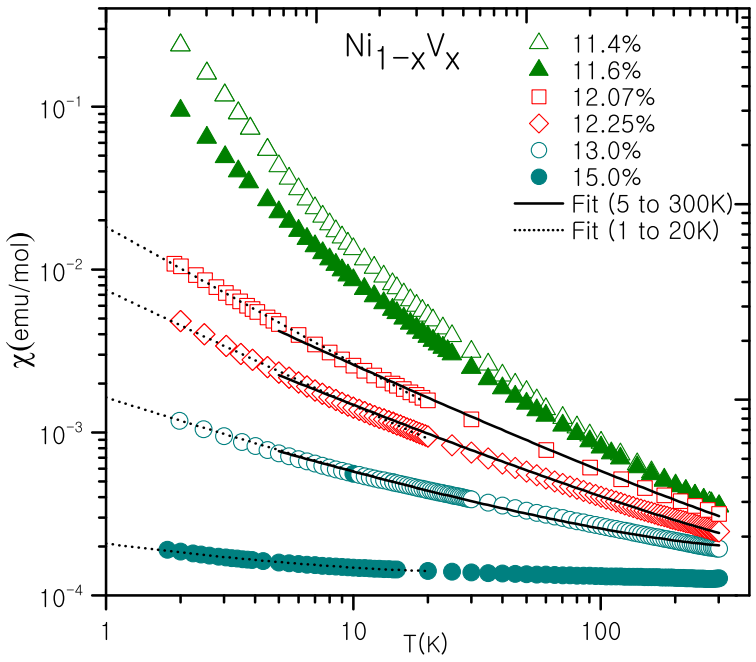

Figure 1: (Color online). Temperature dependence of the susceptibility of $Ni_{1-x}V_x$ for different Vanadium concentrations. Solid and dotted lines represent fits to Eq. (4.26) in the different temperature ranges 5 to 300 K and 1 to 20 K, respectively (data from Ref. [48]).

for Ising symmetry at low temperatures, the overdamping causes sufficiently large rare regions to stop tunneling. Instead, they behave classically, leading to superparamagnetic behavior and a smeared quantum phase transition. In contrast, at higher temperatures but below a microscopic cutoff scale, the damping is unimportant and quantum Griffiths singularities can be observed. In contrast to the Ising case, the itinerant Heisenberg ferromagnet displays quantum Griffiths singularities when damping is sufficiently strong, i.e., at low temperatures. Above a crossover temperature, conventional behavior is expected.

Although the phenomenologies of the ferro- and antiferromganetic cases are similar, the functional forms of the quantum Griffiths singularities are different. In ferromagnetic quantum Griffiths phases, the tunneling rate (or characteristic energy) of a rare region decays as $\exp[-\text{const.} \times \gamma L^{a+3}]$ with its linear size L, where a is

equal to 1 or 2 for ballistic and diffusive ferromagnets, respectively. This leads to the modified nonpower-law quantum Griffiths singularities in thermodynamic quantities, discussed in Sec. 5, in contrast to the power-law quantum Griffiths singularities in itinerant antiferromagnets. The reason is the following. Because of the order parameter conservation in the itinerant quantum ferromagnet, the damping effects are further enhanced as the dimensionless dissipation strength α for a rare region of linear size L is proportional to L^{a+3} rather than L^3.

In strongly disordered system, where our theory is most likely to apply, the motion of the electron is diffusive. Correspondingly, we expect $a = 2$. In hypothetical systems with rare regions, but ballistic dynamics of the electrons, a would take the value 1.

In our explicit calculations, we have used Hertz's form [14] of the order-parameter field theory of the itinerant ferromagnetic quantum phase transition. However, mode-coupling effects in the Fermi liquid lead to an effective long-range spatial interaction between the order parameter fluctuations. [98, 109, 110] In the order-parameter field theory, this leads to a nonanalytic momentum dependence of the static action Eq. (4.2). The effects of this long-range interaction on the existence and energetics of a locally ordered rare region were studied in detail in Ref. [106]. This work showed that the long-range interactions only produce subleading corrections to the droplet-free energy. Therefore, including these long-range interactions in the action Eq. (4.1) will not change the results of the present paper.

Let us now turn to the limitations of our theory. In our calculations, we assumed that the droplet maintains its shape while collapsing and reforming. Correspondingly, our calculation provides a variational upper bound for the instanton action. There could be faster relaxation processes; however, it is hard to image the droplet dynamics to avoid the restriction coming from the order parameter conservation. We treated the individual, locally ordered rare regions as independent. But,

in a real metallic magnet, they are weakly coupled by a Ruderman-Kittel-Kasuya-Yosida (RKKY), interaction which is not included in the Landau-Ginzburg-Wilson action Eq. (4.1). At the lowest temperatures, this RKKY interactions between the rare regions induces a cluster glass phase. [65] Finally, our theory does not take the feedback of the order parameter fluctuations on the fermions into account. It has been found that for some quantum phase transitions, the Landau-Ginzburg-Wilson theory breaks down sufficiently close to the transition point due to this feedback. [42, 111] For strongly disordered systems, this question has not been addressed yet, it remains a task for the future.

Turning to experiment, our theory does not significantly improve the description of the data of $Ni_{1-x}V_x$. [48, 49] We believe that the main reason is that our theory is valid for asymptomatically large rare regions where the order parameter transport plays an important role, whereas the experimental accessible rare regions in $Ni_{1-x}V_x$ are not large enough for the order parameter conservation to dominate their dynamics. We expect our theory can be applied in systems where one can observe Griffiths singularities at lower temperatures leading to larger rare regions.

7. APPENDIX: RENORMALIZATION GROUP THEORY

In this section, we show the derivation of Eqs. (4.19) and (4.21) by renormalization group (RG) analysis. At low temperatures, the action Eq. (4.18) is formally equivalent to a quantum non-linear sigma model [112] in imaginary time τ. We can set $\mathbf{n}(\tau) = (\pi(\tau), \sigma(\tau))$, where $\pi(\tau) = (\pi_1(\tau), \pi_2(\tau))$ represents transverse fluctuations. After expanding in π and keeping terms up to $\mathcal{O}(g^{-2})$, $\mathcal{O}(\alpha^{-2})$, we find [112]

$$S = \int \frac{d\omega}{2\pi} \left(g\omega^2 + \frac{\alpha}{4}|\omega| \right) |\tilde{\pi}(\omega)|^2 + \int \frac{d\omega_1 d\omega_2 d\omega_3}{(2\pi)^3} \left(\frac{\alpha}{8}|\omega_1| - g\omega_1\omega_3 \right) \tilde{\pi}_\beta(\omega_1)\tilde{\pi}_\beta(\omega_2)\tilde{\pi}_{\beta'}(\omega_3)\tilde{\pi}_{\beta'}(-\omega_1-\omega_2-\omega_3)\,. \tag{4.33}$$

We now consider the case of the small damping $\alpha \ll g$. Two different energy regimes can be distinguished: (i) ω larger than some crossover energy $\omega_c \sim \alpha/g$, implying that the undamped dynamics dominates the systems properties, and (ii) $\omega \ll \omega_c$, when the damping term is dominant.

(i) Because the contribution of the undamped dynamics is dominant in this regime, we neglect the damping term and renormalize g. To construct a perturbative renormalizaition group, consider a frequency region $[-\Lambda, \Lambda]$ (Λ is a high energy cut off), and divide the modes into slow and fast ones, $\tilde{\pi}(\omega) = \tilde{\pi}^<(\omega) + \tilde{\pi}^>(\omega)$. The modes $\tilde{\pi}^<(\omega)$ involve frequency $-\Lambda/b < \omega < \Lambda/b$, and are kept. We integrate out the short-wavelength fluctuations $\pi^>(\omega)$ (with frequencies in the region $-\Lambda < \omega < -\Lambda/b$ and $\Lambda/b < \omega < \Lambda$) in perturbation theory using the propagator $\langle \tilde{\pi}^>_\beta(\omega)\tilde{\pi}^>_{\beta'}(\omega')\rangle = \pi\delta_{\beta\beta'}\delta(\omega+\omega')/(g\omega^2)$.

After applying standard techniques, we find that this coarse graining changes the coupling constant g to $g_{\rm co} = g + I_g(b)$, where $I_g(b) = (2\pi\Lambda)^{-1}(b-1)$. After rescaling $\tau' = \tau/b$ and renormalizing $\pi'(\tau') = \pi^<(\tau)/\zeta_g$, we obtain the renormalized coupling constant in the form

$$g' = b^{-1}\zeta_g^2 g_{\rm co}\,. \tag{4.34}$$

To find the rescaling factor ζ_g, we average $\mathbf{n}$ over the short wavelength modes $\pi^>$ and obtain

$$\begin{aligned}\langle \mathbf{n} \rangle^> =& \langle (\pi_1^< + \pi_1^>, ..., \sqrt{1-(\pi^< + \pi^>)^2}) \rangle^> \\ =& (1 - \langle (\pi^>)^2 \rangle^>/2 + \mathcal{O}(g^{-2}))(\pi_1^<, ..., \sqrt{1-(\pi^<)^2}) \,. \end{aligned} \tag{4.35}$$

Thus, we identify

$$\zeta_g = 1 - \langle (\pi^>)^2 \rangle^>/2 + \mathcal{O}(g^{-2}) = 1 - \frac{I_g(b)}{g} + \mathcal{O}(g^{-2}) \,. \tag{4.36}$$

Correspondingly, the renormalized coupling constant given in Eq. (4.34) becomes

$$g' = b^{-1}(g - I_g(b)) \,. \tag{4.37}$$

Setting $b = 1 + \delta l$, and integrating Eq. (4.37) gives the recursion relation $g(l) = g(0)e^{-l}$. To find the relaxation time, we run the RG to $g(l) = 1$ and use $\xi^\tau \sim e^l$. This gives

$$\xi_g^\tau \sim L^3 \,. \tag{4.38}$$

(ii) In the same way, for low energies $\omega \ll \omega_c$, we neglect the term corresponding to the undamped dynamics and renormalize the α coefficient. We find that α is not modified by the perturbation, i.e., $\alpha_{\rm co} = \alpha$, and the field rescaling factor ζ_α is given by

$$\zeta_\alpha = 1 - \frac{I_\alpha(b)}{\alpha} + \mathcal{O}(\alpha^{-2}) \,, \tag{4.39}$$

where $I_\alpha(b) = 2\pi^{-1}\log(b)$. Then, we find the recursion relation $\alpha(l) = \alpha(0) - 4\pi^{-1}l$. This leads to the relaxation time

$$\xi_\gamma^\tau \sim \exp[\text{const.} \times \gamma L^{3+a}]\,. \tag{4.40}$$

8. ACKNOWLEDGEMENTS

This work has been supported by the NSF under Grant No. DMR-0906566.

V. NUMERICAL METHOD FOR DISORDERED QUANTUM PHASE TRANSITIONS IN THE LARGE$-N$ LIMIT

David Nozadze and Thomas Vojta

[1]*Department of Physics, Missouri University of Science & Technology, Rolla, MO 65409*

ABSTRACT*

We develop an efficient numerical method to study the quantum critical behavior of disordered systems with $\mathcal{O}(N)$ order-parameter symmetry in the large$-N$ limit. It is based on the iterative solution of the large$-N$ saddle-point equations combined with a fast algorithm for inverting the arising large sparse random matrices. As an example, we consider the superconductor-metal quantum phase transition in disordered nanowires. We study the behavior of various observables near the quantum phase transition. Our results agree with recent renormalization group predictions, i.e., the transition is governed by an infinite-randomness critical point, accompanied by quantum Griffiths singularities. Our method is highly efficient because the numerical effort for each iteration scales linearly with the system size. This allows us to study larger systems, with up to 1024 sites, than previous methods. We also discuss generalizations to higher dimensions and other systems including the itinerant antiferomagnetic transitions in disordered metals.

*Submitted to Computer Physics Communications (2013).

1. INTRODUCTION

Randomness can have much more dramatic effects at quantum phase transitions than at classical phase transitions because quenched disorder is perfectly correlated in the imaginary time direction which needs to be included at quantum phase transitions. Imaginary time acts as an additional coordinate with infinite extension at absolute zero temperature. Therefore, the impurities and defects are effectively very large which leads to strong-disorder phenomena including power-law quantum Griffiths singularities [30, 99, 100], infinite-randomness critical points characterized by exponential scaling [22, 101], and smeared phase transitions [51]. For example, the zero-temperature quantum phase transition in the random transverse-field Ising model is governed by an infinite-randomness critical point [22] featuring slow *activated* (exponential) rather than power-law dynamical scaling. It is accompanied by quantum Griffiths singularities. This means, observables are expected to be singular not just at criticality but in a whole parameter region near the critical point which is called the quantum Griffiths phase.

Quantum Griffiths singularities are caused by rare spatial configurations of the disorder. Due to statistical fluctuations, one can always find spatial regions (rare regions) which are impurity free. The probability $\mathcal{P}(V_{\mathrm{RR}})$ to find such a rare region is exponentially small in its volume V_{RR}, $\mathcal{P}(V_{\mathrm{RR}}) \sim \exp(-bV_{\mathrm{RR}})$ with b being a constant that depends on the disorder strength. Close to a magnetic phase transition, the rare region can be locally in the magnetic phase while the bulk system is still non-magnetic. When the characteristic energy ϵ of such a rare region decays exponentially with its volume, $\epsilon \sim \exp(-cV_{\mathrm{RR}})$ (as in the case of the transverse-field Ising model), the resulting rare-region density of states has power-law form, $\rho(\epsilon) \sim \epsilon^{\lambda-1}$, where $\lambda = b/c$ is the non-universal Griffiths exponent. λ takes the value zero at the quantum critical point and increases throughout the quantum Griffiths phase. The singular density of

states of the rare regions leads to quantum Griffiths singularities of several thermodynamic observables including order-parameter susceptibility, $\chi \sim T^{\lambda-1}$, specific heat, $C \sim T^{\lambda}$, entropy, $S \sim T^{\lambda}$, and zero-temperature magnetization-field curve $m \sim h^{\lambda}$ (for reviews see, e.g., Refs. [17, 18]).

Many interesting models in statistical mechanics and field theory contain some integer-valued parameter N and can be solved in the large$-N$ limit. Therefore, the large$-N$ method is a very useful tool to study classical and quantum phase transitions. An early example is the Berlin-Kac spherical model [113] which is equivalent to a classical $\mathcal{O}(N)$ order parameter field theory in the large$-N$ limit [114]. Analogously, the quantum spherical model [115, 116, 117] has been used to investigate quantum critical behavior. In both cases, N is the number of order parameter components. Another potential application of the large$-N$ method are $\mathcal{SU}(N)$ Kondo models [118] with spin-degeneracy N. In all of these cases, the partition function can be evaluated in saddle point approximation in the limit $N \gg 1$, leading to self-consistent equations. In clean systems, these equations can often be solved analytically. However, in the presence of disorder, one obtains a large number of coupled self-consistent equations which can be solved only numerically.

In this paper, we develop a new efficient numerical method to study critical behavior of disordered system with $\mathcal{O}(N)$ order-parameter symmetry in the large$-N$ limit. We apply this method to the superconductor-metal quantum phase transition in disordered nanowires. Using a strong-disorder renormalization group, it has recently been predicted that this transition is in the same universality class as the random transverse-field Ising model. We confirm these predictions numerically. We also find the behaviors of observables as a function of temperature and an external field. They follow the expected quantum Griffiths power laws. We consider up to 3000 disorder realizations for system sizes $L = 256$ and 1024. The paper is organized as follows: In Sec. 2 we introduce the model: a continuum Landau-Ginzburg-Wilson

order-parameter field theory in the presence of dissipation; and we generalize the theory to quenched disordered systems. Then, we discuss the predicted critical behavior of this model and derive the large$-N$ formulation. In Sec. 3, we review an existing numerical approach to this model. In Sec. 4, we present our numerical method to study the quantum critical behavior. We discuss the results in Sec. 5, and we compare them to the behavior predicted by the strong-disorder renormalization group. Sec. 6 is devoted to the computational performance of our method. Finally, we conclude in Sec. 7 by discussing and comparing our numerical method to the existing one. We also discuss generalizations to higher dimensions and other models.

2. THE MODEL

We start from the quantum Landau-Ginzburg-Wilson free-energy functional for an $N-$component vector order parameter φ in one space dimension. For a clean system with overdamped order parameter dynamics the Landau-Ginzburg-Wilson action reads,[†]

$$\begin{aligned} S =& \frac{1}{2}\int dx \int_0^{1/T} d\tau \Big[\alpha\varphi^2(x,\tau) + J[\partial_x\varphi(x,\tau)]^2 + \frac{u}{2N}\varphi^4(x,\tau)\Big] \\ &+ \frac{\gamma T}{2}\sum_{\omega_n} |\omega_n| \int dx |\tilde{\varphi}(x,\omega_n)|^2 - h\int dx \int_0^{1/T} d\tau \varphi(x,\tau)\,, \end{aligned} \tag{5.1}$$

where α is the bare distance from criticality. γ and J are the strength of dissipation and interaction, respectively. u is the standard quartic coefficient. h is a uniform external field conjugate to the order parameter. $\tilde{\varphi}(x,\omega_n)$ is the Fourier transform of the order parameter $\phi(x,\tau)$ with respect to imaginary time, and $\omega_n = 2\pi nT$ is a Matsubara frequency. The above action with $N = 2$ order parameter components

[†]We set Planck's constant and Boltzmann constant to unity ($\hbar = k_B = 1$) in what follows.

(equivalent to one complex order parameter) has been used to describe [119] the superconductor-metal transition in nanowires [120]. This transition is driven by pair-braking interactions, possibly due to random magnetic moments trapped on the wire surface [120], which also introduce quenched disorder in the nanowire. The action (5.1) can be generalized to $d = 3$ space dimensions and $N = 3$ order parameter components, in this case, it describes itinerant antiferromagnetic quantum phase transitions [14, 15].

In the presence of quenched disorder, the functional form of Eq. (5.1) does not change qualitatively. However, the coupling constants become random functions of position x. The full effect of disorder can be realized by setting $u = \gamma = 1$ while considering the couplings α and J to be randomly distributed in space [121]. The quantum phase transition in zero external field can be tuned by changing the mean of the α_i distribution, $\overline{\alpha}$.

Recently, the model (5.1) has been investigated by means of a strong-disorder renormalization group method [107, 122]. This theory predicts that the model falls in the same universality class as the one-dimensional random transverse-field Ising model which was studied extensively by Fisher [22]. Thus, the phase transition is characterized by an infinite-randomness critical point at which the dynamical scaling is exponential instead of power-law. Off criticality, the behaviors of observables are characterized by strong quantum Griffiths singularities.

Let us focus on the Griffiths phase on the disordered side of the transition, where the distance from criticality $\delta = \bar{\alpha} - \bar{\alpha}_c > 0$. The strong-disorder renormalization group predicts the disorder averaged equal-time correlation function $C(x)$ to behave as [22]

$$C(x) \sim \frac{\exp[-(x/\xi) - (27\pi^2/4)^{1/3}(x/\xi)^{1/3}]}{(x/\xi)^{5/6}} \tag{5.2}$$

for large distances x. Here, ξ is the correlation length which diverges as $\xi \sim |\delta|^{-\nu}$ with $\nu = 2$ as the critical point is approached. The disorder averaged order parameter as a function of the external field h in the Griffiths phase has the singular form [22]

$$\varphi(h) \sim h^{\lambda} \,. \tag{5.3}$$

Here, λ is the non-universal Griffiths exponent which vanishes at criticality as $\lambda \sim \delta^{\nu\psi}$ with critical exponent $\psi = 1/2$. Right at criticality, the theory predicts logarithmic behavior rather than a power law [22],

$$\varphi(h) \sim [\log(h_0/h)]^{\phi - 1/\psi} \,. \tag{5.4}$$

Here, the exponent $\phi = (1 + \sqrt{5})/2$ equals to the golden mean, and h_0 is some microscopic energy scale.

The average order parameter susceptibility as a function of temperature T in the disordered Griffiths phase is expected to have the form [22]

$$\chi(T) \sim T^{\lambda - 1} \tag{5.5}$$

with the same $\lambda-$exponent as in Eq. (5.3).

Our goal is to test the strong-disorder renormalization group predictions by means of a numerical method. As a first step, we discretize the continuum model (5.1) in space and Fourier-transform from imaginary time τ to Matsubara frequency ω_n. The discretized Landau-Ginzburg-Wilson action has the form

$$S = \frac{T}{2}\sum_{i=1}^{L}\sum_{\omega_n}\Big[\alpha_i|\tilde{\varphi}_i(\omega_n)|^2 + J_i|\tilde{\varphi}_i(\omega_n) - \tilde{\varphi}_{i+1}(\omega_n)|^2 + \frac{1}{2N}|\tilde{\varphi}_i(\omega_n)|^4\Big] + \sum_{i=1}^{L}\Big[\frac{T}{2}\sum_{\omega_n}|\omega_n||\tilde{\varphi}_i(\omega_n)|^2 - h\tilde{\varphi}_i(0)\Big]\,, \tag{5.6}$$

where L is the system size. The nearest-neighbor interactions $J_i > 0$ and the mass terms α_i (bare local distances from criticality) are random quantities. The critical behavior of the model (5.6) can be studied in the limit of a large number of order parameter components N. In this limit, the above action can be reduced to a Gaussian form. This can be done in several ways, for example by decomposing the square of each component of the order parameter $|\tilde{\varphi}_i^{(k)}(\omega_n)|^2$ into its average $\langle\varphi^2\rangle$ and fluctuation $\Delta|\tilde{\varphi}_i^{(k)}(\omega_n)|^2$: $|\tilde{\varphi}_i^{(k)}(\omega_n)|^2 = \langle\varphi^2\rangle + \Delta|\tilde{\varphi}_i^{(k)}(\omega_n)|^2$. Substituting this into the quartic term of the action (5.6) and using the central limit theorem, the quartic term can be replaced by $\langle\varphi^2\rangle|\tilde{\varphi}_i(\omega_n)|^2$. This leads to the Gaussian action

$$S = \frac{T}{2}\sum_{i,j=1}^{L}\sum_{\omega_n}\tilde{\varphi}_j^*(\omega_n)(M_{ij} + |\omega_n|\delta_{i,j})\tilde{\varphi}_j(\omega_n) + h\sum_{i=1}^{L}\tilde{\varphi}_i(0)\,. \tag{5.7}$$

The coupling matrix is given by

$$M_{ij} = -J_i\delta_{i,j+1} - J_j\delta_{i,j-1} + (r_i + 2J_i)\delta_{i,j}\,. \tag{5.8}$$

The renormalized local distance r_i from criticality at site i must be determined self-consistently from

$$r_i = \alpha_i + \langle\varphi^2\rangle\,, \tag{5.9}$$

where $\langle\varphi^2\rangle$ is given by

$$\langle\varphi^2\rangle = T\sum_{\omega_n}[M + |\omega_n|\mathbb{1}]^{-1}_{ii} + h^2\sum_{j,k=1}^{L} M^{-1}_{ij}M^{-1}_{ik}\,. \tag{5.10}$$

Here, $\mathbb{1}$ is the identity matrix. In the presence of disorder, the self-consistent equations (5.9) at different sites are not identical. We thus arrive at a large number of coupled non-linear self-consistent equations. Therefore, numerical techniques are required to solve them.

3. EXISTING NUMERICAL APPROACH

In this section, we review the numerical method proposed by Del Maestro *et al.* [123] to study the model (5.7) at zero temperature and in the absence of an external field ($h = 0$). The matrix M is spectral decomposed in terms of its orthogonal eigenvectors V_{ij} and eigenvalues ϵ_i as

$$\sum_{j=1}^{L} M_{ij}V_{jk} = V_{ik}\epsilon_k\,. \tag{5.11}$$

Using this decomposition, the inverse matrix in Eq. (5.10) can be written as

$$[M + |\omega_n|\mathbb{1}]^{-1}_{ij} = \sum_{k=1}^{L}\frac{V_{ik}V_{kj}}{\epsilon_k + |\omega_n|}\,. \tag{5.12}$$

At zero temperature the sum over Matsubara frequencies in Eq. (5.10) turns into an integral which can be performed analytically. This leads to the self-consistent equations (for $h = 0$),

$$\frac{1}{\pi}\sum_{j=1}^{L}(V_{ij})^2\log\left(1 + \frac{\Lambda_\omega}{\epsilon_j}\right) + \alpha_i - r_i = 0\,. \tag{5.13}$$

Here, for convergence of the frequency integral, an ultra violet cutoff Λ_ω is introduced. Numerical solutions to Eq. (5.13) were obtained by an iteration process using a modified Powell's hybrid method. The method works well for large distances from criticality and small system sizes, but it becomes computationally prohibitive near criticality where the correlation length ξ becomes of order of the system size. This problem can be partially overcome by implementing a clever iterative solve-join-patch procedure. However, the system size L is still limited because large matrices need to be fully diagonalized which requires $\mathcal{O}(L^3)$ operations per iteration. Therefore, for large L the method gets very slow.

As the result, the largest sizes studied in Ref. [123] were $L = 128$. The authors analyzed equal time correlations, energy gap statistics and dynamical susceptibilities and found them in agreement with the strong-disorder renormalization group predictions [107, 122]. The method was also used in Ref. [124] to study the conductivity.

4. METHOD

We now present a novel numerical method to study the model (5.7) at non-zero temperatures. Its numerical effort scales linearly with system size L (per iteration) compared with the L^3 scaling of the numerical method outlined in Sec. 3. The basic idea of our method is that, for $h = 0$, we only need the diagonal elements of the inverse matrix M^{-1} to iterate the self-consistent Eq. (5.9). The numerical effort for finding the diagonal elements of the inverse of a sparse matrix is much smaller than that of a full diagonalization. Combining Eqs. (5.9) and (5.10), the system of self-consistent equations at non-zero temperatures T, and in the presence of an external field h, reads

$$r_i = 2T\sum_{n=1}^{m}[M + 2\pi nT\mathbb{1}]^{-1}_{ii} + TM^{-1}_{ii} + h^2\sum_{j,k=1}^{L} M^{-1}_{ij}M^{-1}_{ik} + \alpha_i\,. \tag{5.14}$$

Here, $m = \Lambda_\omega(2\pi T)^{-1}$ with an ultra-violet cutoff frequency Λ_ω. To solve these equations (5.14) iteratively, we find the inverses of the tridiagonal[‡] matrices $[M_{ij} + 2\pi nT\mathbb{1}]$ and M_{ij} using the fast method proposed in Ref. [125]. This algorithm is summarized in Sec. 8. In zero external field, we only need the diagonal elements of $[M_{ij} + 2\pi nT\mathbb{1}]^{-1}$ and the number of operations per iteration scales linearly with system size L, while it scales quadratically in the presence of a field because for $h \neq 0$, full inversion of the matrix is required.

Once the full set of r_i has been obtained, we can compute observables from the quadratic action (5.7). Let us first consider observables in the absence of an external field. The equal-time correlation function $C(x) = \overline{\langle\varphi_x(\tau)\varphi_1(\tau)\rangle}$ averaged over disorder realizations can be obtained from Eq. (5.7),

$$C(x) = \frac{T}{L-x}\overline{\sum_{i=1}^{L-x}\left(\sum_{n=1}^{m} 2[M + 2\pi nT\mathbb{1}]^{-1}{}_{i,i+x} + M^{-1}_{i,i+x}\right)}\,, \tag{5.15}$$

where the overbar indicates the average over disorder configurations. Similarly, in the zero external field, we can calculate the order parameter susceptibility as a function of temperature. The disorder-averaged order parameter susceptibility $\chi(T)$ can be expressed as

$$\chi(T) = \frac{T}{L}\overline{\sum_{i=1}^{L}\sum_{k=1}^{L} M^{-1}_{ik}}\,. \tag{5.16}$$

[‡]We use open boundary conditions.

In the presence of an external field, we need to include h in the solution of Eq. (5.14). We can then compute the order-parameter *vs*. field curve. The disorder-averaged order parameter reads

$$\varphi(h) = \frac{h}{L}\overline{\sum_{i=1}^{L}\sum_{k=1}^{L} M_{ik}^{-1}}\,. \tag{5.17}$$

We note that the number of operations to calculate observables for one disorder configuration scales quadratically with the system size L. However, this needs to be done only once, outside the loop that iterates the self-consistent equations. At low temperatures, according to Eq. (5.14), we need to invert a huge number of matrices $[M_{ij} + 2\pi nT\mathbb{1}]$ per iteration (one for each Matsubara frequency). Naively, one might therefore expect the numerical effort to scale linearly in $1/T$. However, these matrices are not very different. We can therefore accelerate the method by combining them appropriately. This is explained in Sec. 9.

5. RESULTS

In this section, we report results of our numerical calculations of the model (5.7). We consider the interactions J_i to be uniformly distributed on $(0, 1)$ with mean $\overline{J} = 0.5$ and the bare local distances from criticality α_i to be Gaussian distributed with mean $\overline{\alpha}$ and variance 0.25.

An advantage of our method is that it gives direct access to the temperature dependencies of observables. For example, we calculate the zero-field order parameter susceptibility as a function of temperature for various values of the control parameter $\bar{\alpha}$ according to Eq. (5.16). At low temperatures, the Griffiths power law (5.5) describes the data very well (see Figure 1). The non-universal Griffiths exponent λ can be determined from fits in the temperature range $T = 10^{-3} - 1.5 \times 10^{-2}$. Figure 2(a) shows how λ varies as the distance from criticality $\delta = \bar{\alpha} - \bar{\alpha}_c$ changes. The power law

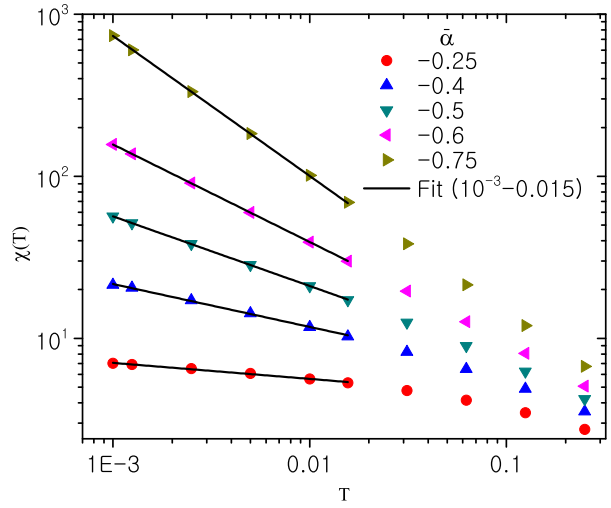

Figure 1: (Color online) Order-parameter susceptibility χ versus temperature T for various distances from criticality $\bar{\alpha}$ in the Griffiths phase. All data are averaged over 3000 disorder configurations with system size $L = 256$. The solid lines represent fits to the Griffiths power law (5.5), $\chi(T) \sim T^{\lambda-1}$, over the temperature range $T = 10^{-3} - 1.5 \times 10^{-2}$.

$\lambda \sim \delta^{\nu\psi}$ describes the data well with the critical point $\bar{\alpha}_c = -0.85(3)$, and exponents $\nu = 2.0(2)$ and $\psi = 0.51(2)$. Here, the number in brackets indicates the uncertainty in the last digit. These results are consistent with the predictions of Refs. [107, 122].

We also compute the order parameter as a function of an external field at $T = 10^{-3}$ for various $\bar{\alpha}$ (Figure 3). The off-critical data ($\delta > 0$) are described by the Griffiths power law (5.3) with an exponent λ. At the critical point, the $\varphi(h)$ curve follows the logarithmic dependence (5.4) with exponents $\psi = 0.51(2)$ and $\phi = 1.61(2)$. The value for exponent ϕ is in agreement with the predicted one [107, 122]. The values of the Griffiths exponent λ match those extracted from susceptibility data (see Figure 2 (a)). The deviation near the critical point may be due to the fact that the correlation length becomes comparable to the system size and correspondingly causes finite-size effects in the data.

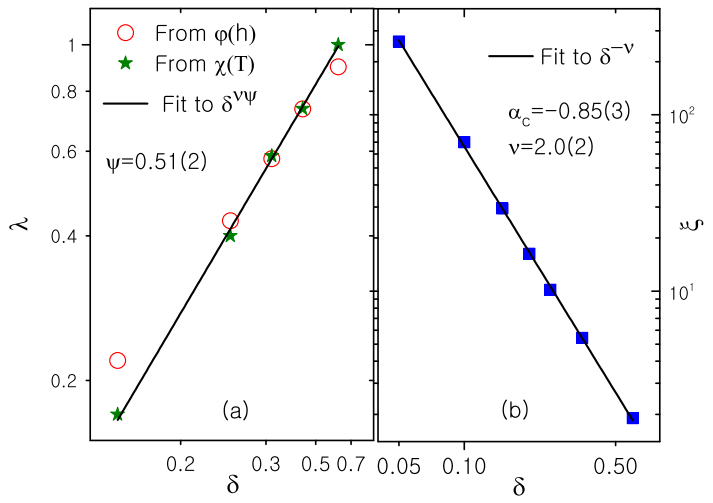

Figure 2: (Color online) a) The Griffiths exponent λ versus distance from criticality δ. The solid line is a fit to the power law $\lambda \sim \delta^{\psi\nu}$. b) The correlation length ξ obtained by analyzing correlation function data versus distance δ from criticality. The solid line is a fit to a power law, resulting in a critical point of $\bar{\alpha}_c = -0.85(3)$ and the correlation length exponent $\nu = 2.0(2)$.

In addition, in the absence of an external field h, for system size $L = 1024$, we compute the disorder-averaged correlation functions (5.15) at temperature $T = 10^{-3}$ for various values of $\bar{\alpha}$ (see Figure 4). The values of correlation length ξ can be extracted by fitting the data to Eq. (5.2). We find good agreement of the data with Eq. (5.2) for distances between $x = 5$ and some cutoff at which the curves start to deviate from the zero-temperature behaviors due to temperature effects and where curves start to become noisy because correlations become dominated by very rare large clusters.

Figure 2(b) shows how the correlation length ξ changes with distance from criticality δ. The data can be fitted to the power law $\xi \sim |\delta|^{-\nu}$, as expected [22]. By fitting, we extract the critical point $\bar{\alpha}_c = -0.85(3)$ and exponent $\nu = 2.0(2)$. The

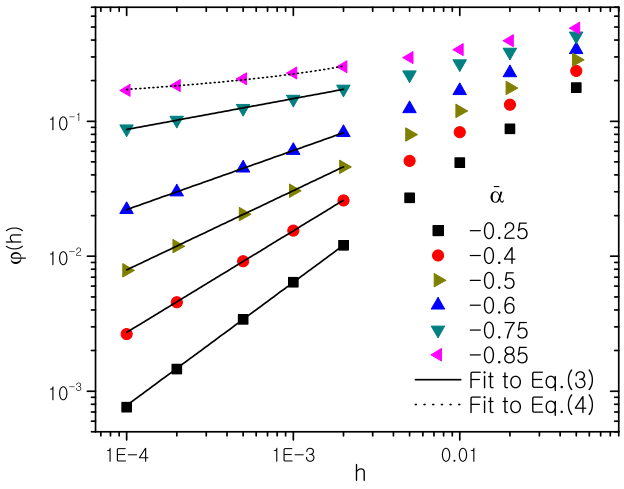

Figure 3: (Color online) Order parameter ϕ versus external field h for various $\bar{\alpha}$. The data are averaged over 3000 disorder configurations of system size $L = 256$. In the field range $h = 10^{-4}$ to 2×10^{-3}, the dotted and solid lines represent fits to Eq. (5.4) and the Griffiths power law (5.3), respectively.

values of exponent ν and critical point $\bar{\alpha}_c$ are in agreement with those obtained from $\chi(T)$ and $\varphi(h)$.

6. COMPUTATIONAL PERFORMANCE

In this section, we discuss the execution time of our method for solving the self-consistent Eqs. (5.14) iteratively (*i.e.*, the time needed to get a full set of renormalized distances from criticality r_i). In our method, the time per iteration scales linearly with the system size L in the absence of an external field because the operation count is dominated by the matrix inversion. Thus, the disorder-averaged execution time $\bar{t} \sim n_{\rm it} L$ for a single disorder configuration, where $n_{\rm it}$ is the number of iterations needed for convergence of the self-consistent Eqs. (5.14). The number of iterations $n_{\rm it}$ depends on the disorder configuration, it is larger for a disorder realization which has locally ordered rare regions with smaller α. In the conventional paramagnetic phase,

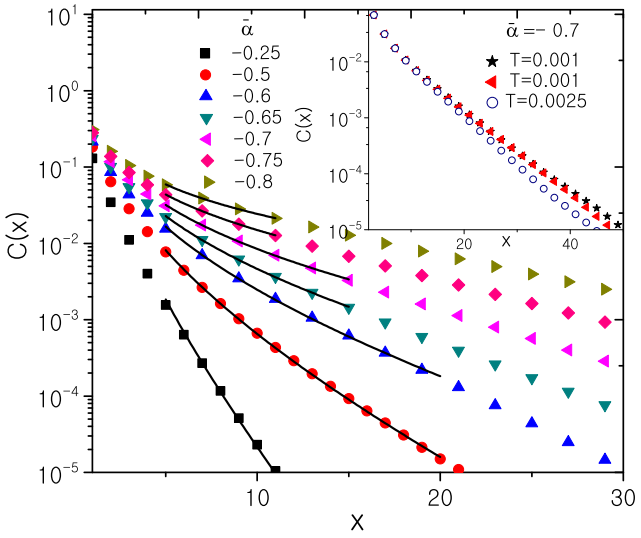

Figure 4: (Color online) The equal-time correlation functions for several values of $\bar{\alpha}$. All data are averaged over 3000 samples of size $L = 1024$ at $T = 10^{-3}$. The solid lines are fits to Eq. (5.2). Inset: Deviations of correlation function at fixed value of $\bar{\alpha} = -0.7$ due to temperature effects and statistical error of an average over disorder configurations. The data represented by circles and stars are averaged over the same 1000 disorder configurations at $T = 0.0025$ and $T = 10^{-3}$, respectively. The curves represented by triangles are averaged over different set of 1000 disorder configurations at $T = 10^{-3}$.

i.e., for larger values of $\bar{\alpha}$ away from criticality, locally ordered rare regions are almost absent, therefore the number of iterations $n_{\rm it}$ is a constant. Thus, in the conventional paramagnetic phase, the execution time is expected to scale linearly with the system size, $\bar{t} \sim L$. Figure 5 shows that it indeed scales linearly with the system size for $\bar{\alpha} = 1$. In contrast, in the quantum Griffiths phase, where locally ordered rare regions are present, $n_{\rm it}$ is expected to be large and to become larger close to criticality. If we compare two different system sizes in the quantum Griffiths phase, the larger system is expected to have locally ordered rare region with higher probability. Thus, in the quantum Griffiths phase the number of iterations $n_{\rm it}$ is expected to be a function of system size L, which we model as $n_{\rm it} \sim L^y$ with some non-negative exponent y. Therefore, in the quantum Griffiths phase the execution time does not scale linearly

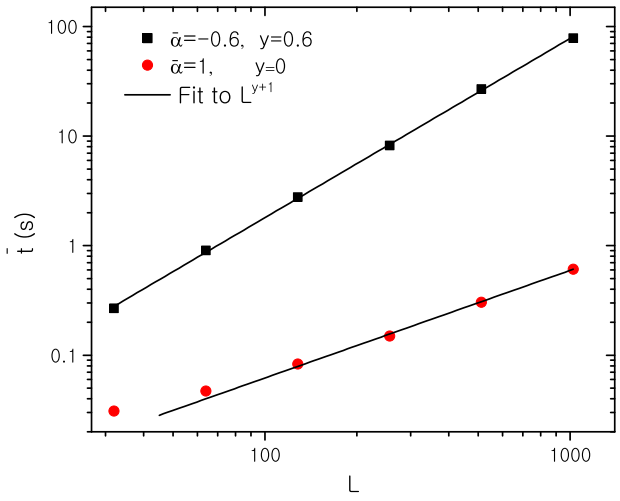

Figure 5: (Color online) At the temperature $T = 10^{-3}$ and in the zero field $h = 0$, execution time for a single disorder configuration $\bar{t}$ versus system size L for $\bar{\alpha} = -0.6$ and $\bar{\alpha} = 1$. All data are averaged over 1000 disorder realizations. The solid lines represent fits to the power-law. (times measured on an Intel Core i5 CPU)

with the system size but it behaves as $\bar{t} \sim L^{y+1}$. Figure 5 shows that for $\bar{\alpha} = -0.6$ in the quantum Griffihts phase, the disorder averaged execution time $\bar{t}$ does not scales linearly with L but behaves as power law $\bar{t} \sim L^{y+1}$ with $y = 0.6$.

Because our method performs the Matsubara sums numerically, the effort increases with decreasing temperature T. As shown in Sec. 9, this increase is only logarithmic in $1/T$ if we approximately combine higher Matsubara frequencies.

7. CONCLUSIONS

In summary, we have developed an efficient numerical method for studying quantum phase transitions in disordered systems with $\mathcal{O}(N)$ order parameter symmetry in the large$-N$ limit. Our algorithm solves iteratively the large$-N$ self-consistent equations for the renormalized distances from criticality using the fast method of

Ref. [125] for the necessary matrix inversions. We have applied our method to the superconductor-metal quantum phase transition in nanowires and studied the critical behavior of various observables near the transition. Our results are in agreement with strong-disorder renormalization predictions [107, 122] that the quantum phase transition is governed by infinite-randomness critical point accompanied by quantum Griffiths singularities.

Let us compare the performance of our method with that of the method proposed in Ref. [123] and outlined in Sec. 3. The main difference is how the sums over the Matsubara frequencies in the self-consistent equations (5.9) are handled. The method of Ref. [123] works at $T = 0$ where the Matsubara sum becomes an integral. This integral is performed analytically which saves computation time. However, the price is a complete diagonalization of the coupling matrix M which is very costly ($\mathcal{O}(L^3)$ operations per iteration). Moreover, observables at $T \neq 0$ are not directly accessible.

In contrast, our method performs the Matsubara sum numerically which allows us to use the fast matrix inversion of Ref. [125] (which needs just $\mathcal{O}(L)$ operations per iteration) instead of a full diagonalization. Furthermore, we can calculate observables at $T \neq 0$. However, our effort increases with decreasing T. Thus, the two methods are in some sense complimentary. The method of Ref. [123] is favourable for small systems when true $T = 0$ results are desired. Our method works better for larger systems at moderately low temperatures.

We also emphasize that all our results have been obtained by converging the self-consistent equations (5.9) by means of a simple mixing scheme. Even better performance could be obtained by combining our matrix inversion scheme with the solve-join-patch algorithm [123] for convergence acceleration.

Our method can be generalized to higher-dimensional problems. The self-consistent equations can be solved in the same way, using a fast method for inverting

the arising sparse matrices. For two dimensional systems, one could use the methods given in Refs. [126, 127] for which the cost of inversion is $\mathcal{O}(N^{3/2})$, where N is a total number of sites. We therefore expect the cost of our method to scale as $N^{y+3/2}$ or $N^{3/2}$ in the quantum Griffiths and quantum paramagnetic phases, respectively. For three dimensional systems, sparse matrices can be inverted in $\mathcal{O}(N^2)$ operations [127], correspondingly the cost of our method is expected to behave as N^{y+2} (N is number of sites) in the quantum Griffiths phase. In the quantum paramagnetic phase it should scale as N^2.

A possible application of our method in three dimensions is the disordered itinerant antiferromagnetic quantum phase transitions [107, 122]. The clean transition is described by a Landau-Ginzburg-Wilson theory which is generalization of the action (5.1) to $d = 3$ space dimensions and $N = 3$ order parameter components [14, 15]. Introducing disorder leads to random mass terms as in the case of the superconductor-metal quantum phase transition in nanowires.

8. APPENDIX: INVERSION OF TRIDIAGONAL MATRIX

In this section we sketch the fast method for the inversion of a tridiagonal matrix outlined in Ref. [125]. The cost of finding the diagonal elements of the inverse matrix is $\mathcal{O}(L)$ operations while inverting the full matrix costs $\mathcal{O}(L^2)$ operations. The basic idea is that the inverse matrix of the tridiagonal matrix M_{ij} can be represented by two sets of vectors v_j and u_j: $M_{ij}^{-1} = u_i v_j$. Let diagonal and offdiagonal elements of matrix M_{ij} be $M_{ii} = a_i$ and $M_{i,i+1} = M_{i,i+1} = -b_i$, respectively. By combining a UL decomposition of the linear system for v and a UL decomposition of M_{ij}, one can determine the set of vectors

$$v_1 = \frac{1}{d_1}\,, \qquad v_i = \frac{b_2 \cdots b_i}{d_1 \cdots d_{i-1} d_i}\,, \qquad i = 2, \cdots, n\,, \tag{5.18}$$

where

$$d_n = a_n\,, \qquad d_i = a_i - \frac{b_{i+1}^2}{d_{i+1}}\,, \qquad i = n-1, \cdots, 1\,. \tag{5.19}$$

The set of vectors u_j can be found by combining a LU decomposition of the linear system for u and a LU decomposition of M_{ij}, yielding

$$u_n = \frac{1}{\delta_n v_n}\,, \qquad u_{n-i} = \frac{b_{n-i+1}\cdots b_n}{\delta_{n-i}\cdots\delta_n v_n}\,, \qquad i = 1, \cdots, n-1\,, \tag{5.20}$$

where

$$\delta_1 = a_1\,, \qquad \delta_i = a_i - \frac{b_i^2}{\delta_{i-1}}\,, \qquad i = 2, \cdots, n\,. \tag{5.21}$$

Finding both sets of vectors needs $\mathcal{O}(L)$ operations, consequently the number of operations to extract the diagonal elements $M_{ii}^{-1} = u_i v_i$ of inverse matrix scales linearly with L while the cost of finding the full inverse matrix $M_{ij}^{-1} = u_i v_j$ is $\mathcal{O}(L^2)$.

9. APPENDIX: ACCELERATION OF METHOD

In this section we propose an approach to accelerate the summation over the Matsubara frequencies in our method. The idea is based on the fact that the critical behaviors are dominated by low-frequencies, correspondingly only matrices associated with low Matsubara frequencies ω_n have dominant contributions in Eq. (5.14). At higher ω_n, consecutive matrices change very little. Therefore, instead of finding diagonal elements of $[M_{ij}+2\pi T n\mathbb{1}]^{-1}$ for each Matsubara frequencies ω_n, we invert matrices corresponding to $n = 1, ..., 100$ and correspondingly calculating the sum of first 100 terms in Eq. (5.14) exactly. Then, we approximate sum of the remaining terms corresponding to $n > 100$ (higher Matsubara frequencies) in the following way: we find

diagonal elements of $[M_{ij}+2\pi Tn\not{k}]^{-1}$ corresponding to the midpoints of subintervales obtained by dividing interval $n = 10^{l+1}+1, ..., 10^{l+2}$ $(l = 1, ..., \log_{10}(m/100))$ into 90 subintervales of width 10^l. Then, we approximate appropriate sum in Eq. (5.14) by summing over terms calculated at midpoints multiplied by 10^l. In this case, numerical effort scales logarithmically as $\log_{10}(1/T)$ compared with $1/T$ scaling in the case of exact summation. To check the magnitude of errors arising due to this approximation, we have compared observables calculated exactly and using acceleration method for the system with size $L = 256$ and control parameter $\bar{\alpha}_c = -0.6$ at the temperature $T = 10^{-3}$. We have found that arising errors are less than 0.1%.

10. ACKNOWLEDGEMENTS

This work has been supported by the NSF under Grant Nos. DMR-0906566 and DMR-1205803.

VI. TRANSPORT PROPERTIES IN ANTIFERROMAGNETIC QUANTUM GRIFFITHS PHASES

David Nozadze and Thomas Vojta

[1] *Department of Physics, Missouri University of Science & Technology, Rolla, MO 65409*

ABSTRACT*

We study the electrical resistivity in the quantum Griffiths phase associated with the antiferromagnetic quantum phase transition in a metal. The resistivity is calculated by means of the semi-classical Boltzmann equation. We show that the scattering of electrons by locally ordered rare regions leads to a singular temperature dependence. The rare-region contribution to the resistivity varies as T^{λ} with temperature T, where λ is the usual Griffiths exponent which takes the value zero at the critical point and increases with distance from criticality. We find similar singular contributions to other transport properties such as thermal resistivity, thermopower and the Peltier coefficient. We also compare our results with existing experimental data and suggest new experiments.

*Published in Europhysics Letters **95**, 57010 (2011).

1. INTRODUCTION

Quantum phase transitions [12] occur at zero temperature when an external parameter such as magnetic field, pressure or chemical composition is varied. They are driven by quantum rather than thermal fluctuations. At continuous quantum phase transitions, i.e., quantum critical points, the quantum fluctuations driving the transition diverge and become scale invariant in space and time. These fluctuations dominate the material's properties in the vicinity of the quantum critical point at low but non-zero temperatures. In metallic systems, they can cause strong deviations from the conventional Fermi-Liquid behavior of normal metals [13].

Impurities, defects or other kinds of quenched disorder can significantly modify the low temperature behavior of quantum many-particle systems. The interplay between dynamic quantum fluctuations and static disorder fluctuations leads to much more dramatic effects at quantum phase transitions than at classical thermal phase transitions, including quantum Griffiths singularities [30, 99, 100], infinite randomness critical points featuring exponential instead of power-law scaling [22, 101] and the smearing of the phase transition [51]. These unconventional phenomena are caused by large spatial regions (rare regions) that are devoid of impurities and can show local order even if the bulk system is in the disordered phase. The fluctuations of these rare regions are very slow because they require changing the order parameter in a large volume. Griffiths showed that this leads to a singular free energy in a whole parameter region which is now known as the Griffiths phase. The probability $\mathcal{P}(L^d)$ for finding an impurity-free rare region with linear size L in a disordered system is exponentially small in its volume L^d, $\mathcal{P}(L^d) \sim \exp(-cL^d)$ with c being a constant that depends on the disorder strength. In systems in which the characteristic energy ϵ of such a rare region decays exponentially with its volume, $\epsilon \sim \exp(-bL^d)$, the resulting density of states is of power-law type, $\rho(\epsilon) \propto \epsilon^{\lambda-1}$, where $\lambda = c/b$ is the

non-universal Griffiths exponent. It varies systematically within the Griffiths phase and vanishes at the critical point. The power-law density of states $\rho(\epsilon)$ leads to non-universal power-law quantum Griffiths singularities of several thermodynamical observables including the specific heat, $C \sim T^{\lambda}$, and the magnetic susceptibility, $\chi \sim T^{\lambda-1}$. The zero-temperature magnetization-field curve behaves as $M \sim H^{\lambda}$ (for reviews, see Refs. [17, 18]).

Quantum Griffiths phases have been predicted to occur not only in localized magnets but also in metallic systems [31, 66, 122], but clear-cut experimental verifications have been absent for a long time. Only recently, quantum Griffiths phases have been observed in experiment in a number of systems such as magnetic semiconductors [43, 44, 45], Kondo lattice ferromagnets [46, 47] and transition metal ferromagnets [48]. The lack of experimental evidence for quantum Griffiths phases in metals may be (at least partially) due to the theories being incomplete: while the thermodynamics in quantum Griffiths phases is comparatively well understood, very little is known about the experimentally important and easily accessible transport properties.

In this Letter we therefore study the electrical resistivity in the quantum Griffiths phase of an antiferromagnetic metal by means of the semi-classical Boltzmann equation approach. In the same manner, we also investigate other transport properties such as the thermal resistivity, the thermopower and the Peltier coefficient. We find that the scattering of the electrons by spin-fluctuations in the rare regions leads to singular temperature dependencies not just at the quantum critical point but in the entire antiferromagnetic quantum Griffiths phase. The rare region contribution to the resistivity varies as $\Delta\rho \propto T^{\lambda}$ with temperature T, the contribution to thermal resistivity behaves as $\Delta W \propto T^{\lambda-1}$, and the thermopower and the Peltier coefficient behave as $\Delta S \propto T^{\lambda+1}$ and $\Delta\Pi \propto T^{\lambda+2}$, respectively.

2. MODEL AND METHOD OF SOLUTION

Let us now sketch the derivation of these results. The transport properties of the itinerant antiferromagnetic systems we are interested in can be described by a two-band model consisting of s and d electrons [128, 129]. The Hamiltonian has the form $H = H_s + H_d + H_{s-d}$, where H_s and H_d are the Hamiltonians of s and d electrons, respectively. H_{s-d} corresponds to the exchange interaction between s and d electrons. Only the s electrons contribute to the transport properties. They are scattered by the spin-fluctuations of the d electrons which are assumed to be in the antiferromagnetic quantum Griffiths phase. The contribution to the resistivity from the scattering by the spin-fluctuations stems from the $s-d$ exchange interaction term of the Hamiltonian

$$H_{s-d} = g \int d\mathbf{r}\ \mathbf{s}(\mathbf{r}) \cdot \mathbf{S}(\mathbf{r})\,, \tag{6.1}$$

where g is the coupling between s and d electrons. $\mathbf{s}$ and $\mathbf{S}$ are the spin densities of the s and d electrons, respectively.

Close to an antiferromagnetic transition in three-dimensional space, transport properties can be treated within a semi-classical approach using the Boltzmann equation because quasiparticles are still (marginally) well defined. For simplicity, we also assume that the spin-fluctuations are in equilibrium, i.e., we neglect drag effects. This approximation is valid if the system can lose momentum efficiently by Umklapp or impurity scattering as is the case in a dirty antiferromagnetic system. The linearized Boltzmann equation in the presence of an electric field $\mathbf{E}$ and a temperature gradient ∇T, but zero magnetic field can be written as [58]

$$-\mathbf{v_k}\frac{\partial f^0_{\mathbf{k}}}{\partial T}\nabla T - \mathbf{v_k}\frac{\partial f^0_{\mathbf{k}}}{\partial \varepsilon_{\mathbf{k}}}\mathbf{E} = \left(\frac{\partial f_{\mathbf{k}}}{\partial t}\right)_{scatt}, \tag{6.2}$$

where $f^0_{\mathbf{k}}$ is the equilibrium Fermi-Dirac distribution function. The first and second terms correspond to the rate changes of the electron distribution function $f_{\mathbf{k}}$ due to the diffusion and electric field $\mathbf{E}$, respectively. The last one is the collision term. Let the stationary solution of the Boltzmann equation be $f_{\mathbf{k}} = f^0_{\mathbf{k}} - \Phi_{\mathbf{k}}(\partial f^0_{\mathbf{k}}/\partial\varepsilon_{\mathbf{k}})$, where $\Phi_{\mathbf{k}}$ is a measure of the deviation of the electron distribution from equilibrium. Then the linearized scattering term due to the spin-fluctuations has the form [129, 130]

$$\begin{aligned}\left(\frac{\partial f_{\mathbf{k}}}{\partial t}\right)_{scatt} &= \frac{2g^2}{T}\sum_{\mathbf{k}'} f^0_{\mathbf{k}'}(1-f^0_{\mathbf{k}})n(\varepsilon_{\mathbf{k}}-\varepsilon_{\mathbf{k}'})\mathrm{Im}\chi(\mathbf{k}-\mathbf{k}',\varepsilon_{\mathbf{k}}-\varepsilon_{\mathbf{k}'})(\Phi_{\mathbf{k}}-\Phi_{\mathbf{k}'}) \\ &= \frac{1}{T}\sum_{\mathbf{k}'}\mathcal{P}_{\mathbf{k}'}(\varepsilon_{\mathbf{k}}-\varepsilon_{\mathbf{k}'})(\Phi_{\mathbf{k}}-\Phi_{\mathbf{k}'})\,, \qquad (6.3)\end{aligned}$$

where $n(\varepsilon_{\mathbf{k}}-\varepsilon_{\mathbf{k}'})$ is the Bose-Einstein distribution function and χ is the total dynamical susceptibility of the spin-fluctuations of the d electrons.

3. ELECTRICAL RESISTIVITY

In order to calculate the electrical resistivity we consider Ziman's variational principle [58]. The resistivity ρ is given as the minimum of a functional of $\Phi_{\mathbf{k}}$ [58] †

$$\rho[\Phi_{\mathbf{k}}] = \min\left[\frac{1}{2\mathrm{T}}\frac{\int\int(\Phi_{\mathbf{k}}-\Phi_{\mathbf{k}'})^2\Gamma^{\mathbf{k}'}_{\mathbf{k}}\mathrm{d}\mathbf{k}\mathrm{d}\mathbf{k}'}{\left(\int \mathrm{v}_{\mathbf{k}}\Phi_{\mathbf{k}}\frac{\partial \mathrm{f}^0_{\mathbf{k}}}{\partial\varepsilon_{\mathbf{k}}}\mathrm{d}\mathbf{k}\right)^2}\right], \qquad (6.4)$$

where

$$\Gamma^{\mathbf{k}'}_{\mathbf{k}} = \int_0^\infty d\omega\ \mathcal{P}_{\mathbf{k}'}(\omega)\delta(\varepsilon_{\mathbf{k}'}-\varepsilon_{\mathbf{k}}+\omega)\,. \qquad (6.5)$$

†We set Plank's constant, electron's charge and Boltzmann constant $\hbar = e = k_B = 1$ in what follows.

Quantum Griffiths effects in disordered metallic systems are realized both in Heisenberg magnets [31, 43] and in Ising magnets. In the latter case, they occur in a transient temperature range where the damping is unimportant [66]. In the following, we consider both cases.

As we are interested in the rare-region contribution to the resistivity in the Griffiths phase, we need to find the rare region dynamical susceptibility which is simply the sum over the susceptibilities of the individual rare regions. The imaginary part of the dynamical susceptibility of a single cluster (rare region) of characteristic energy ϵ in the quantum Griffiths phase of a disordered itinerant quantum Heisenberg antiferromagnet is given by

$$\mathrm{Im}\chi_{\mathrm{cl}}(\mathbf{q},\omega;\epsilon) = \frac{\mu^2\gamma\omega}{\epsilon^2(\mathrm{T})+\gamma^2\omega^2}\mathrm{F}_\epsilon^2(\mathbf{q})\,, \tag{6.6}$$

where μ is the moment of the cluster and γ is the damping coefficient which results from the coupling of the spin-fluctuations and the electrons. $\epsilon(T)$ plays the role of the local distance from criticality. For high temperatures $\gamma T \gg \epsilon$, $\epsilon(T) \approx T$ and for low temperatures $\gamma T \ll \epsilon$, $\epsilon(T) \approx \epsilon$. $F_\epsilon(\mathbf{q})$ is the form factor of the cluster which encodes the spatial magnetization profile. For random quantum Ising models the imaginary part of the dynamical magnetic susceptibility of a single cluster (rare region) is given by

$$\mathrm{Im}\chi_{\mathrm{cl}}(\mathbf{q},\omega;\epsilon) \;=\; \pi\frac{\mu^2}{4}\tanh\left(\frac{\epsilon}{2T}\right)[\delta(\epsilon-\omega)-\delta(\epsilon+\omega)]F_\epsilon^2(\mathbf{q})\,. \tag{6.7}$$

To get the total rare-region susceptibility, we integrate over all rare regions using the density of states $\rho(\epsilon)$,

$$\mathrm{Im}\chi(\mathbf{q},\omega) = \int_0^\Lambda \mathrm{d}\epsilon\rho(\epsilon)\mathrm{Im}\chi_{\mathrm{cl}}(\mathbf{q},\omega;\epsilon)\,, \tag{6.8}$$

where Λ is an energy cut-off. The precise functional form of $F_\epsilon(\mathbf{q})$ is not known, since every cluster has a different shape and size. However, we can find it approximately by analyzing the Fourier transform of a typical local magnetization profile of the rare region. Consider a rare region of linear size L (located at the origin). Following Millis *et al.* [36], the order parameter is approximately constant for $r < L$, while for large $r > L$, it decays as $e^{-r/\xi}/r$, where ξ is the bulk correlation length. Taking the Fourier transform we find that $F_\epsilon(\mathbf{q})$ depends on ε via the combination $|\mathbf{Q}-\mathbf{q}|^3 \log(\epsilon^{-1})$ only, where $\mathbf{Q}$ is the ordering wave vector. Correspondingly, from Eq. (6.8), we find that the rare region contribution to the zero-temperature susceptibility in the quantum Griffiths phase can be expressed as

$$\mathrm{Im}\chi(\mathbf{q},\omega) \propto |\omega|^{\lambda-1}\mathrm{sgn}(\omega)\,\mathrm{X}[(\mathbf{q}-\mathbf{Q})^3 \log(\omega^{-1})]\,, \tag{6.9}$$

where X is a scaling function. The precise form of the logarithmic correction is difficult to find and beyond the scope of this paper. For random quantum Ising models, the susceptibility has the same structure as Eq. (6.9) [66]. It is clear that the scaling function X will give only logarithmic corrections to the temperature dependence of the resistivity ρ in our further calculations.

To minimize the resistivity functional (6.4), we need to make an ansatz for the distribution Φ. Close to an antiferromagnetic quantum phase transition, the magnetic scattering is highly anisotropic because $\chi(\mathbf{q},\omega)$ peaks around the ordering wave vector $\mathbf{Q}$. However, since we are interested in a strongly disordered system, the low-temperature resistivity will be dominated by the elastic impurity scattering which is isotropic and redistributes the electrons over the Fermi surface. Correspondingly, we can use the standard ansatz

$$\Phi_{\mathbf{k}} \propto \mathbf{n}\cdot\mathbf{k}\,. \tag{6.10}$$

where $\mathbf{n}$ is a unit vector parallel to the electric filed. Note that any constant prefactor in $\Phi_{\mathbf{k}}$ is unimportant because it drops out in the resistivity functional (6.4) and in the corresponding thermal resistivity functional (6.13). Then, after applying standard techniques [58] the magnetic part of the resistivity given in Eq. (6.4) becomes

$$\Delta\rho \propto T \int d^3\mathbf{q} \frac{(\mathbf{n}\cdot\mathbf{q})^2}{q} \int_0^\infty d\omega \frac{\partial n(\omega)}{\partial T} \mathrm{Im}\chi(\mathbf{q},\omega)\,. \tag{6.11}$$

Inserting the susceptibility (6.9) yields the rare-region contribution to the resistivity in the antiferromagnetic quantum Griffiths phase as

$$\Delta\rho \propto T^\lambda\,. \tag{6.12}$$

Thus, the temperature-dependence of the resistivity follows a non-universal power-law governed by the Griffiths exponent λ.

4. OTHER TRANSPORT PROPERTIES

In the same way, we study other transport properties such as the thermal resistivity, the thermopower, and the Peltier coefficient. The variational principle for the thermal resistivity has the form [58]

$$W[\Phi_{\mathbf{k}}] = \min\left[\frac{\int\int(\Phi_{\mathbf{k}}-\Phi_{\mathbf{k}'})^2\Gamma_{\mathbf{k}}^{\mathbf{k}'}\mathrm{d}\mathbf{k}\mathrm{d}\mathbf{k}'}{\left(\int \mathrm{v}_{\mathbf{k}}(\varepsilon_{\mathbf{k}}-\mu)\Phi_{\mathbf{k}}\frac{\partial \mathrm{f}^0_{\mathbf{k}}}{\partial\varepsilon_{\mathbf{k}}}\mathrm{d}\mathbf{k}\right)^2}\right], \tag{6.13}$$

where μ is the chemical potential of the s-electrons. As long as impurity scattering dominates, we can use the standard ansatz for the variational function,

$$\Phi_{\mathbf{k}} \propto (\varepsilon_{\mathbf{k}}-\mu)\mathbf{n}\cdot\mathbf{k}\,. \tag{6.14}$$

Then, following the calculation for the thermal resistivity outlined in Ref. [58] we obtain

$$\begin{aligned} \Delta W &\propto \frac{1}{T^2}\int d^3\mathbf{q}\int d\omega \frac{\partial n(\omega)}{\partial T}\mathrm{Im}\chi(\mathbf{q},\omega) \\ &\times \left[\omega^2\left(\frac{1}{q}-\frac{q}{6{k_F}^2}\right)+\frac{\pi^2 q}{3{k_F}^2}T^2\right]. \end{aligned} \tag{6.15}$$

where k_F is Fermi momentum of the s-electrons [‡]. Inserting the susceptibility (6.9) into (6.15), the temperature dependence of the thermal resistivity due to the spin-fluctuations in the Griffiths phase from the above equation is given by

$$\Delta W \propto T^{\lambda-1}. \tag{6.16}$$

The existence of an electric field $\mathbf{E}$ in a metal subject to a thermal gradient ∇T is called Seebeck effect and is characterized by the thermopower S which is defined via $\mathbf{E} = S\ \nabla T$. To calculate the thermopower, we analyze the Boltzmann equation (6.2) in the presence of both $\mathbf{E}$ and ∇T using the trial function

$$\phi_{\mathbf{k}} \propto \eta_1 \mathbf{n}\cdot\mathbf{k} + \eta_2(\varepsilon_{\mathbf{k}}-\mu)\mathbf{n}\cdot\mathbf{k}. \tag{6.17}$$

where η_1 and η_2 are variational parameters. Elastic impurity scattering leads to the usual linear temperature dependence $S_{imp} \propto T$ while the contribution due to the magnetic scattering by the rare regions in the Griffiths phase reads

$$\Delta S \propto T^{\lambda+1}. \tag{6.18}$$

Another transport coefficient called the Peltier coefficient Π characterizes the flow of a thermal current in a metal in the absence of a thermal gradient. It is related

[‡]Here, we have averaged over all directions of the vector $\mathbf{n}$; this is sufficient to get the temperature dependence.

to the thermopower by $\Pi = S\ T$. Correspondingly, the rare-region contribution to the Peltier coefficient has the form

$$\Delta\Pi \propto\ T^{\lambda+2}\,. \tag{6.19}$$

5. DISCUSSION AND CONCLUSIONS

In summary, we have investigated the transport properties in the quantum Griffiths phase close to an antiferromagnetic quantum phase transition in a metallic system (see Fig. (1)). The rare-region contributions to electrical resistivity, thermal resistivity, thermopower, and the Peltier coefficient are characterized by non-universal power-laws in T which are controlled by the Griffiths exponent λ.

Our results have been obtained using the semi-classical Boltzmann equation approach. This approach is valid in Griffiths phase in which the system consists of a few locally ordered rare regions in a non-magnetic bulk where the quasiparticles are well-defined. Sufficiently close to the actual quantum critical point (which is of infinite-randomness type) the quasiparticle description may break down, invalidating our results. A detailed analysis of this question hinges on the fate of the fermionic degrees of freedom at the infinite-randomness quantum critical point. This difficult problem remains a task for the future.

We have used the standard isotropic ansatz (6.10, 6.14) for the deviation of the electron distribution from equilibrium. This is justified as long as the rare-region part $\Delta\rho(T)$ of the resistivity is small compared to the impurity part ρ_0. When $\Delta\rho$ becomes larger, the anisotropy of the scattering needs to be taken into account. This can be done by adapting the methods of Rosch [131] to the situation at hand.

We emphasize that our results have been derived for antiferromagnetic quantum Griffiths phases and may not be valid for ferromagnetic systems. The problem is that a complete theory of the ferromagnetic quantum Griffiths phase in a metal does

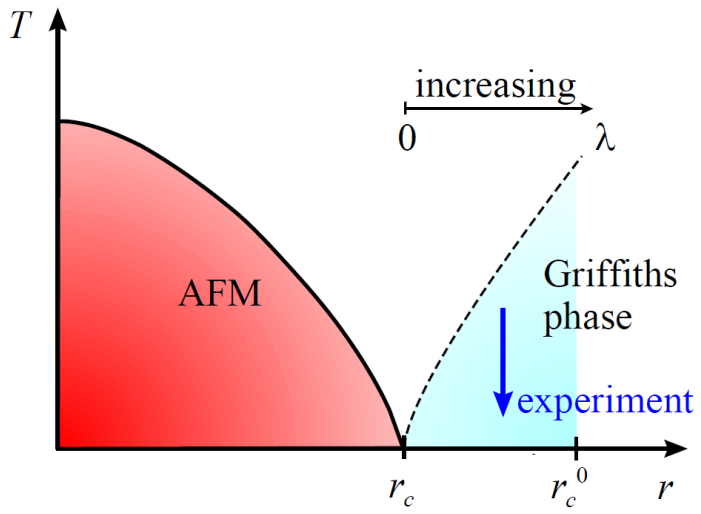

Figure 1: (Color online) Schematic temperature-control parameter phase diagram of an itinerant antiferromagnet close to the quantum critical point. Our results apply in the Griffiths phase at low temperatures.

not exist. In particular, the dynamical susceptibility still is not known. Correspondingly, the transport properties in ferromagnetic quantum Griffiths phases remain an open problem.

Non-universal power-laws in a variety of observables including transport properties can also arise from a different physical mechanism far away from the magnetic quantum phase transition. In Kondo-disordered systems, the existence of a wide distribution of local single-ion Kondo temperatures is assumed, this leads to the power-law singularities [132, 133]. This model was used to explain experimental results in some heavy fermion compounds such as UCu_4Pd and $UCu_{3.5}Pd_{1.5}$ [134, 135].

Let us now turn to experiment. Unfortunately and somewhat ironically, all clear-cut experimental observations of quantum Griffiths phases are in itinerant ferromagnets rather than in antiferromagnets. However, quantum Griffiths effects have been discussed in the context of the antiferromagnetic quantum phase transition in

heavy fermion systems [136, 137]. One of the most striking predictions following from our theory is that the exponent characterizing the electrical resistivity should be less than one sufficiently close to the quantum phase transition. There are several antiferromagnetic systems such as $CeCo_{1.2}Cu_{0.8}Ge_2$ and $Ce(Ru_{0.6}Rh_{0.4})_2Si_2$ [136, 137] that show unusual power-law behaviour of the electrical resistivity with an exponent less than unity. The first system's resistivity increases with decreasing temperature. This is incompatible with our prediction and described by the Kondo model. The resistivity of the second compound decreases with decreasing temperature in agreement with our prediction. However, it is not clear whether this behaviour is indeed caused by the quantum Griffiths phase. To establish this, one should measure various thermodynamics quantities as well as the transport properties and relate their low-temperature behavior.

6. ACKNOWLEDGMENT

This work has been supported by the NSF under Grant No. DMR-0906566.

SECTION

2. CONCLUSIONS

In this thesis, reprints of six papers have been presented that studied various aspects of quenched disorder effects on phase transitions. In papers I, II, and III, we investigated smeared phase transitions in binary alloys $A_{1-x}B_x$, in which the transition is tuned by changing the composition x. We considered both spatially correlated and uncorrelated disorder. This theory was put to a test in experiments on the $Sr_{1-x}Ca_xRuO_3$ compound in paper III.

Paper IV studied quantum Griffiths singularities associated with the ferromagnetic quantum phase transition in a disordered metal for Ising and Heisenberg order parameter symmetries. The resulting quantum Griffiths singularities are even stronger than usual quantum Griffiths singularities.

Paper V was devoted to an efficient numerical method to study the quantum critical behavior of disordered systems with $\mathcal{O}(N)$ order-parameter symmetry in the large-N limit. The method is based on the iterative solution of the large$-N$ saddle-point equations combined with a fast algorithm for inverting the arising large sparse random matrices.

In paper VI, we studied transport properties in the quantum Griffiths phase associated with the antiferromagnetic quantum phase transition in a metal by means of the semi-classical Boltzmann transport theory.

In summary, we explained how quenched disorder can affect a variety of phase transitions and modify the behavior of observable quantities close to the transition

point. We thus took a step towards a better understanding of the interplay between randomness and phase transitions. However, many interesting open questions remain. The complete theories of smeared phase transitions and quantum Griffiths phases are not obtained yet. It would be interesting, for example, to study effects of spatial long-range correlations of the disorder on smeared phase transitions. Moreover, theories of quantum Griffiths phases in metals neglect weak localization effects. Because the system is strongly disordered in the quantum Griffiths phase, it would be interesting to study weak localization effects and other quantum effects on observable quantities in quantum Griffiths phases.

BIBLIOGRAPHY

[1] Q. Bitko, T. F. Rosenbaum, and G. Aeppli. *Phys. Rev. Lett.*, 77:940, 1996.

[2] N. Goldenfeld. *Lectures on Phase Transitions and the Renormalization Group.* Westview Press, 1992.

[3] V. L. Ginzburg. *Sov. Phys. Sol. State*, 2:1824, 1960.

[4] K. G. Wilson. *Phys. Rev. B*, 4:3174, 1971.

[5] K. G. Wilson. *Phys. Rev. B*, 4:3184, 1971.

[6] M. Kardar. *Statistical physics of fields.* 2007.

[7] L. P. Kadanoff, W. Ǵotze, D. Hamblen, R. Hecht, E. A. S. Lewis, V. V. Palciauskas, M. Rayl, and J. Swif. *Rev. Mod. Phys.*, 39:395, 1967.

[8] B. Widom. *J. Chem. Phys.*, 43:3892, 1965.

[9] M. E. Fisher. *Phys. Rev.*, 180:594, 1969.

[10] B. D. Josephson. *Proc. Phys. Soc.*, 92:269, 1967.

[11] G. S. Rushbrooke. *J. Chem. Phys.*, 39:842, 1963.

[12] S. Sachdev. *Quantum Phase Transitions.* Cambridge University Press, Cambridge, England, 1999.

[13] H. V. Löhneysen, T. Pietrus, G. Portisch, H. G. Schlager, A. Schörder, M. Sieck, and T. Trappmann. *Phys. Rev. Lett.*, 72:3262, 1994.

[14] J. Hertz. *Phys. Rev. B*, 14:1165, 1976.

[15] A. J. Millis. *Phys. Rev. B*, 48:7183, 1993.

[16] H. V. Löhneysen, A. Rosch, M. Vojta, and P. Wölfle. *Rev. Mod. Phys.*, 79, 2007.

[17] T. Vojta. *J. Phys. A*, 39:R143, 2006.

[18] T. Vojta. *J. Low Temp. Phys.*, 161:299, 2010.

[19] G. Grinstein. *Fundamental problems in statistical mechanics.* 1985.

[20] A. B. Harris. *J. Phys. C: Solid State Phys.*, 7:1671, 1974.

[21] S. K. Ma, C. Dasgupta, and C. K. Hu. *Phys. Rev. Lett.*, 43:1434, 1979.

[22] D. S. Fisher. *Phys. Rev. B*, 51:6411–6461, 1995.

[23] O. Motrunich, S. C. Mau, D. A. Huse, and D. S. Fisher. *Phys. Rev. B*, 61:1160, 2000.

[24] C. Holm and W. Janke. *Phys. Rev. B*, 48:936, 1993.

[25] A. M. Ferrenberg and D. P. Landau. *Phys. Rev. B*, 44:5081, 1991.

[26] H. G. Ballesteros, L. A. Fernandez, V. Martin-Mayer, A. M. Sedupe, G. Parisi, and J. J. Ruiz-Lorenzo. *Phys. Rev. B*, 58:2740, 1998.

[27] R. N. Bhatt and P. A. Lee. *Phys. Rev. Lett.*, 48:344, 1982.

[28] A. P. Young and H. Rieger. *Phys. Rev. B*, 53:8486, 1996.

[29] C. Pich, A. P. Young, H. Rieger, and N. Kawashima. *Phys. Rev. Lett.*, 81:5916, 1998.

[30] R. B. Griffiths. *Phys. Rev. Lett.*, 23:17–19, 1969.

[31] T. Vojta and J. Schmalian. *Phys. Rev. B*, 72:045438, 2005.

[32] N. Read, S. Sachdev, and J. Ye. *Phys. Rev. B*, 52:384, 1995.

[33] R. Sknepnek, T. Vojta, and M. Vojta. *Phys. Rev. Lett.*, 93:097201, 2004.

[34] B. M. McCoy and T. T. Wu. *Phys. Rev.*, 176:631, 1968.

[35] R. Sknepnek and T. Vojta. *Phys. Rev. B*, 69:174410, 2004.

[36] A. J. Millis, D. K. Morr, and J. Schmalian. *Phys. Rev. Lett.*, 87:167202, 2001.

[37] A. J. Millis, D. K. Morr, and J. Schmalian. *Phys. Rev. B*, 66:174433, 2002.

[38] I. M. Lifshitz. *Zh. Eksp. Teor. Fiz.*, 53:743, 1967.

[39] I. M. Lifshitz. *Sov. Phys.—JETP*, 26:462, 1968.

[40] A. B. Harris. *Phys. Rev. B*, 12:203, 1975.

[41] T. Senthil and S. Sachdev. *Phys. Rev. Lett.*, 77:5292, 1996.

[42] D. Belitz, T. R. Kirkpatrick, and T. Vojta. *Rev. Mod. Phys.*, 77:579, 2005.

[43] S. Guo, D. P. Young, R. T. Macaluso, D. A. Browne, N. L. Henderson, J. Y. Chan, L. L. Henry, and J. F. DiTusa. *Phys. Rev. Lett.*, 100:017209, 2008.

[44] S. Guo, D. P. Young, R. T. Macaluso, D. A. Browne, N. L. Henderson, J. Y. Chan, L. L. Henry, and J. F. DiTusa. *Phys. Rev. B*, 81:144423, 2010.

[45] S. Guo, D. P. Young, R. T. Macaluso, D. A. Browne, N. L. Henderson, J. Y. Chan, L. L. Henry, and J. F. DiTusa. *Phys. Rev. B*, 81:144424, 2010.

[46] J. G. Sereni, T. Westerkamp, R. Küchler, N. Caroca-Canales, P. Gegenwart, and C. Geibel. *Phys. Rev. B*, 75:024432, 2007.

[47] T. Westerkamp, M. Deppe, R. Küchler, M. Brando, C. Geibel, P. Gegenwart, A. P. Pikul, and F. Steglich. *Phys. Rev. Lett.*, 102:206404, 2009.

[48] S. Ubaid-Kassis, T. Vojta, and A. Schroeder. *Phys. Rev. Lett.*, 104:066402, 2010.

[49] A. Schroeder, S. Ubaid-Kassis, and T. Vojta. *J. Phys. Condens. Matter*, 23:094205, 2011.

[50] D. J. Thouless. *Phys. Rev.*, 187:732, 1969.

[51] T. Vojta. *Phys. Rev. Lett.*, 90:107202, 2003.

[52] M. N. Barber. Finite-size scaling. In C. Domb and J. L. Lebowitz, editors, *Phase Transitions and Critical Phenomena*, volume 8, pages 145–266. Academic, New York, 1983.

[53] J. Cardy, editor. *Finite-size scaling*. North Holland, Amsterdam, 1988.

[54] H. Bruus and K. Flensberg. *Many-body quantum theory in condensed matter physics*. 2004.

[55] A. A. Abrikosov. *Fundamentals of the Theory of Metals*. 1988.

[56] G D. Mahan. *Many Particle Physics*. Kluwer, New York, 2000.

[57] H. V. Löhneysen. *J. Phys. Condens. Matter*, 8:9689, 1996.

[58] J. Ziman. *Electrons and Phonons*. Clarendon, Oxford, 1960.

[59] J. A.. Hoyos and T. Vojta. *Phys. Rev. Lett.*, 100:240601, 2008.

[60] T. Vojta. *J. Phys. A*, 36:10921, 2003.

[61] A. J. Legget, S. Chakravarty, A. T. Dorsey, M. P. A. Fisher, A. Garg, and W. Zwerger. *Rev. Mod. Phys.*, 59:1, 1987.

[62] I. M. Lifshitz. *Usp. Fiz. Nauk*, 83:617, 1964.

[63] I. M. Lifshitz. *Sov. Phys. Usp*, 7:549, 1965.

[64] B. I. Halperin and M. Lax. *Phys. Rev.*, 148:722, 1966.

[65] V. Dobrosavljević and E. Miranda. *Phys. Rev. Lett.*, 94:187203, 2005.

[66] A. H. Castro Neto and B. A. Jones. *Phys. Rev. B*, 62:14975, 2000.

[67] J. A. Hoyos and T. Vojta. *Phys. Rev. B*, 74:140401(R), 2006.

[68] G. Cao, S. McCall, M. Shepard, J. E. Crow, and R. P. Guertin. *Phys. Rev. B*, 56:321, 1997.

[69] K. Yoshimura, T. Imai, T. Kiyama, K. R. Thurber, A. W. Hunt, and K. Kosuge. *Phys. Rev. Lett.*, 83:4397, 1999.

[70] T. Kiyama, K. Yoshimura, K. Kosuge, H. Mitamura, and T. Goto. *J. Phys. Soc. Jpn.*, 68:3372, 1999.

[71] A. B. Harris and T. C. Lubensky. *Phys. Rev. Lett.*, 33:1540, 1974.

[72] G. Grinstein and A. Luther. *Phys. Rev. B*, 19:3580, 1976.

[73] Y. Imry and M. Wortis. *Phys. Rev. B*, 19:3580, 1979.

[74] M. Aizenman and J. Wehr. *Phys. Rev. Lett*, 62:2503, 1989.

[75] K. Hui and A. N. Berker. *Phys. Rev. Lett.*, 62:2507, 1989.

[76] J. A. Hoyos, N. Laflorencie, A. P Vieira, and T. Vojta. *Europhys. Lett.*, 93:30004, 2011.

[77] A. Weinrib and B. I. Halperin. *Phys. Rev. B*, 27:413, 1983.

[78] F. Hrahsheh, D. Nozadze, and T. Vojta. *Phys. Rev. B*, 83:224402, 2011.

[79] H. A. Makse, S. Havlin, M. Schwartz, and H. E. Stanley. *Phys. Rev. E*, 53:5445, 1996.

[80] H. Rieger and F. Igloi. *Phys. Rev. Lett.*, 83:3741, 1999.

[81] C. Svoboda and et al. unpublished.

[82] M. Wissinger, D. Fuchs, L. Dieterle, H. Leiste, R. Schneider, D. Gerthsen, and H. V. Löhneysen. *Phys. Rev. B*, 83:144430, 2011.

[83] N. Hosaka, H. Yamada, Y. Shimada, J. Fujioka, S. Bordács, I. Kézsmárki, M. Kawasaki, and Y. Tokura. *Appl. Phys. Express*, 1:113001, 2008.

[84] M. Schneider, V. Moshnyaga, and P. Gegenwart. *Phys. Status Solidi B*, 247:577, 2010.

[85] P. Khalifah, I. Ohkubo, H. M. Christen, and D. G. Mandrus. *Phys. Rev. B*, 70:134426, 2004.

[86] G. Schehr and H. Rieger. *Phys. Rev. Lett.*, 96:227201, 2006.

[87] G. Schehr and H. Rieger. *J. Stat. Mech.*, page P04012, 2008.

[88] T. Vojta. *Phys. Rev. E*, 70:026108, 2004.

[89] S. L. Sondhi, S. M. Girvin, J. P. Carini, and D. Shahar. *Rev. Mod. Phys.*, 69:315, 1997.

[90] N. Kolev, C. L. Chen, M. Gospodinov, R. P. Bontchev, V. N. Popov, A. P. Litvinchuk, M. V. Abrashev, V. G. Hadjiev, and M. N. Iliev. *Phys. Rev. B*, 66:014101, 2002.

[91] Y. Bréad, V. Hardy, B. Raveau, A. Maignan, H-J. Lin, L-Y. Jang, H. H. Hsieh, and C. T. Chen. *J. Phys. Condens. Matter*, 19:216212, 2007.

[92] J. Okamoto, T. Okane, Y. Saitoh, K. Terai, S. I. Fujimori, Y. Muramatsu, K. Yoshii, K. Mamiya, T. Koide, A. Fujimori, Z. Fang, Y. Takeda, and M. Takano. *Phys. Rev. B*, 76:184441, 2007.

[93] I. Ohkubo, H. M. Christen, P. Khalifah, S. Sathyamurthy, H. Y. Zhai, C. M. Rouleau aand D. G. Mandrus, and D. H. Lowndes. *Appl. Surf. Sci.*, 223:35, 2004.

[94] M. Ohtani, M. Lippmaa, T. Ohnishi, and M. kawasaki. *Rev. Sci. Instrum.*, 76:062218, 2005.

[95] C. U. Jung, H. Yamada, M. Kawasaki, and Y. Tokura. *Appl. Phys. Lett.*, 84:2590, 2004.

[96] G. Herranz, N. Dix, F. Sánchez, B. Martínez, J. Fontcuberta, M. V. García-Cuenca, C. Ferrater, M. Varela, D. Hrabovsky, and A. R. Fert. *J. Appl. Phys.*, 97:10M321, 2005.

[97] See supplemental material at http://link.aps.org/supplemental/10.1103 /physrevlett.108. 185701 for details on the sample preparation, characterization, and on the experimental methodology.

[98] T. R. Kirkpatrick and D. Belitz. *Phys. Rev. B*, 53:14364, 1996.

[99] M. Thill and D .A. Huse. *Physica A*, 214:321–355, 1995.

[100] H. Rieger and A. P. Young. *Phys. Rev. B*, 54:3328, 1996.

[101] D. S. Fisher. *Phys. Rev. Lett.*, 69:534–537, 1992.

[102] A. Rogachev and A. Bezryadin. *Appl. Phys. Lett.*, 83:512, 2003.

[103] S. A. Grigera, R. S. Perry, A. J. Schofield, M. Chiao, S. R. Julian, G. G. Lonzarich, S. I. Ikeda, Y. Maeno, A. J. Millis, and A P. Mackenzie. *Science*, 294:329, 2001.

[104] C. Pfleiderer, G. J. McMullan, S. R. Julian, and G. G. Lonzarich. *Phys. Rev. B*, 55:8330, 1997.

[105] M. C. de Andrade, R Chau, R. P. Dickey, N. R. Dilley, E. J. Freeman, D. A. Gajewski, M B. Maple, R. Movshovich, A. H. Castro Neto, G. Castilla, and B. A. Jones. *Phys. Rev. Lett.*, 81:5620, 1998.

[106] J. A. Hoyos and T. Vojta. *Phys. Rev. B*, 75:104418, 2007.

[107] T. Vojta, C. Kotabage, and J. A. Hoyos. *Phys. Rev. B*, 79:024401, 2009.

[108] T. Moriya. *J. Phys. Soc. Jpn.*, 18:516, 1963.

[109] T. Vojta, D. Belitz, R. Narayanan, and T. R Kirkpatrick. *Europhys. Lett.*, 36:191, 1996.

[110] T. Vojta, D. Belitz, R. Narayanan, and T. R. Kirkpatrick. *Z. Phys. B*, 103:451, 1997.

[111] Ar. Abanov, A. V. Chubukov, and J. Schmalian. *Adv. Phys.*, 52:119, 2003.

[112] David R. Nelson and Robert. A. Pelcovits. *Phys. Rev. B*, 16:2191, 1977.

[113] T. H. Berlin and M. Kac. *Phys. Rev.*, 86:821, 1952.

[114] H. E. Stanley. *Phys. Rev.*, 176:718, 1968.

[115] T. Vojta and M. Schreiber. *Phys. Rev. B*, 50:1272, 1994.

[116] Th. M. Nieuwenhuizen. *Phys. Rev. Lett.*, 74:4293, 1995.

[117] T. Vojta and M. Schreiber. *Phys. Rev. B*, 53:8211, 1996.

[118] N. E. Bickers. *Rev. Mod. Phys.*, 59:845, 1987.

[119] S. Sachdev, P. Werner, and M. Troyer. *Phys. Rev. Lett.*, 92:237003, 2004.

[120] A. Rogachev, T.-C. Wei, D. Pekker, A. T. Bollinger, P. M. Goldbart, and A. Bezryadin. *Phys. Rev. Lett.*, 97:137001, 2006.

[121] J. Tucker and B. Halperin. *Phys. Rev. B*, 3:3768, 1971.

[122] J. A. Hoyos, C. Kotabage, and T. Vojta. *Phys. Rev. Lett.*, 99:230601, 2007.

[123] A. Del Maestro, B. Rosenow, M. Müller, and S. Sachdev. *Phys. Rev. Lett.*, 101:035701, 2008.

[124] A. Del Maestro, B. Rosenow, J. A.. Hoyos, and T. Vojta. *Phys. Rev. Lett.*, 105:145702, 2010.

[125] G. Meurant. *Siam J. Matrix Anal. Appl.*, 13:707, 1992.

[126] S. Li, S. Ahmed, G. Klimeck, and E. Darve. *Journal of Computational Physics*, 227:9408, 2008.

[127] L. Lin, J. Lu, L. Ying, R. Car, and W. E. *Commun. Math. Sci.*, 7:755, 2009.

[128] D. L. Mills and P. Lederer. *J. Phys. Chem. Solids*, 27:1805, 1966.

[129] K. Ueda and T. Moriya. *J. Phys. Soc. Jpn.*, 39:605, 1975.

[130] R. Hlubina and T. M. Rice. *Phys. Rev. B*, 51:9253, 1995.

[131] A. Rosch. *Phys. Rev. Lett.*, 82:4280, 1999.

[132] E. Miranda, V. Dobrosavljević, and G. Kotliar. *Phys. Rev. Lett.*, 78:290, 1997.

[133] E. Miranda, V. Dobrosavljević, and G. Kotliar. *J. Phys.: Condens. Matter*, 8:9871, 1996.

[134] O. O. Bernal, D. E. MacLaughlin, H. G. Lukefahr, and B. Andraka. *Phys. Rev. Lett.*, 75:2023, 1995.

[135] M. C. Aronson, M. B. Maple, R. Chau, A. Georges, A. M. Tsvelik, and R. Osborn. *J. Phys.: Condens. Matter*, 8:9815, 1996.

[136] G. R. Stewart. *Rev. Mod. Phys.*, 73:797, 2001.

[137] G. R. Stewart. *Rev. Mod. Phys.*, 78:743, 2006.

VITA

David Nozadze was born in Tbilisi, Gerogia. He received his bachelor in theoretical physics from the Faculty of Exact and Natural Sciences, Ivane Javakhishvili Tbilisi State University (TSU) in May 2007. He received his Master in theoretical condensed matter physics from TSU. At TSU during his Master, he was working on Master thesis under supervison of Dr. George Japaridze. After finishing his Masters, he moved to The Abdus Salam International Center for Theoretical Physics (ICTP) in Italy, where he got a Diploma in Condensed Matter Theory in 2010. At the ICTP, he did his Diploma thesis under the supervision of Dr. Alessandro Silva. In 2010, he joined the group of Dr. Thomas Vojta at Missouri University of Science and Technology to work on his PhD in Condensed Matter Theory.